Article:

Scotese, CR, Song, H, Mills, BJW orcid.org/0000-0002-9141-0931 et al. (1 more author) (2021) Phanerozoic Paleotemperatures: The Earth's Changing Climate during the Last 540 million years. Earth-Science Reviews, 215. 103503. ISSN 0012-8252

https://doi.org/10.1016/j.earscirev.2021.103503

Phanerozoic Paleotemperatures: The Earth's Changing Climate during the Last 540 million years

by

Christopher R. Scotese, Department of Earth and Planetary Sciences, Northwestern University, Evanston, IL, 60208, cscotese@gmail.com

Haijun Song, State Key Laboratory of Biogeology and Environmental Geology, School of Earth Sciences, China University of Geosciences, Wuhan, 430074, China, haijunsong@cug.edu.cn

Benjamin J.W. Mills, School of Earth and Environment, University of Leeds, Leeds, LS2 9JT, UK,

and Douwe G. van der Meer, CNOOC International, 945 Bunker Hill Road, Houston, Tx 77024, USA

11/25/2020

Version 17c

Abstract

This study provides a comprehensive and quantitative estimate of how global temperatures have changed during the last 540 million years. It combines paleotemperature measurements determined from oxygen isotopes with broader insights obtained from the changing distribution of lithologic indicators of climate, such as coals, evaporites, calcretes, reefs, and bauxite deposits. The waxing and waning of the Earth's great polar icecaps have been mapped using the past distribution of tillites, dropstones, and glendonites. The global temperature model presented here includes estimates of average global temperate (GAT), changing tropical temperatures (ΔT˚ tropical), deep ocean temperatures, and polar temperatures. Though similar, in many respects, to the temperature history deduced directly from the study of oxygen isotopes, our model does not predict the extreme high temperatures for the Early Paleozoic required by isotopic investigations. The history of global changes in temperature during the Phanerozoic has been summarized in a "paleotemperature timescale" that subdivides the many past climatic events into 8 major climate modes; each climate mode is made up of 3-4 pairs of warming and cooling episodes (chronotemps). A detailed narrative describes how these past temperature events have been affected by geological processes such as the eruption of Large Igneous Provinces (LIPS) (warming) and bolide impacts (cooling). The paleotemperature model presented here allows for a deeper understanding of the interconnected geologic, tectonic, paleoclimatic, paleoceanographic, and evolutionary events that have shaped our planet, and we make explicit predictions about the Earth's past temperature that can be tested and evaluated. By quantitatively describing the pattern of paleotemperature change through time, we may be able to gain important insights into the history of the Earth System and the fundamental causes of climate change on geological timescales. These insights can help us better understand the problems and challenges that we face as a result of Future Global Warming.

Keywords: paleoclimate, paleotemperature, Phanerozoic, climate change, climate history, ice age, icehouse, hothouse, Hirnantian Ice Age, Permo-Carboniferous Ice Age, End Triassic Extinction, K/T Extinction, K/T Impact Winter, PETM, Pleistocene Ice Age, Future Global Warming, $\partial^{18}O$, $\partial^{13}C$

Part I. Introduction, Methods, and Discussion

1. Introduction

There have been several recent studies of the Earth's changing temperature during the Phanerozoic, e.g. Grossman (2012a&b); Veizer and Prokoph, (2015); Scotese (2016); Mills et al. (2019); Henkes et al. (2018); Wing and Huber (2019); Verard and Veizer (2019); Song et al. (2019); Grossman and Joachimski, 2020). All of these studies are based on oxygen isotope measurements of $\delta^{18}O$ in carbonate or apatite microfossils. The first extensive compilation of oxygen isotope data assembled by Veizer and Hoefs (1976) and Veizer et al. (1986, 1999, 2000) has been used by other researchers to characterize temperature change at a variety of temporal and geographic scales (Royer et al., 2004; Prokoph et al., 2008; Grossman, 2012 a&b). Recently, two comprehensive, global Phanerozoic compilations of oxygen isotope paleotemperatures have been assembled (Song et al., 2019 and the PALects database, Grossman et al., 2018).

Urey (1951) and Emiliani (1955) were the first scientists to appreciate the utility of oxygen isotopes. For every 4.3˚C increase in temperature, there is a 0.1% decrease in the amount of ^{18}O (Epstein and Mayeda, 1953) used to produce the calcium carbonate of the foraminifera's shell. By measuring the ratio of ^{18}O to ^{16}O, also referred to as $\delta^{18}O$, it is possible to estimate the temperature at which the calcium carbonate was produced. Savin et al. (1975), Savin (1977), Miller et al. (1987), Zachos et al., (2001, 2008) and Cramer et al. (2009) used the changing ratios of ^{18}O /^{16}O in benthic foraminifera to describe the changing temperature of the world's oceans and the growth of the polar icecaps. For an excellent summary of the science of oxygen isotopes see Grossman (2012a).

The oxygen isotope record is strongly biased towards tropical regions and measurements of temperature derived from localities above 40˚ N or S are sparse; therefore, paleotemperature curves that exclusively use $\delta^{18}O$ data (Song et al., 2019; Verard and Veizer, 2019; Veizer and Prokoph, 2015; Grossman, 2012a&b; Royer et al. 2004) are measurements of tropical temperature, not global temperature. Only the Phanerozoic paleotemperature curves of Scotese (2016), Mills et al., (2019, 2020), Wing and Huber (2019), and Valdes et al. (2018) (Figure 1), either adjust the isotopic temperatures to compensate for the difference between tropical and global temperatures or use non-isotopic temperature information (e.g., HadCM3 paleoclimate model simulations, Valdes et al., 2020).

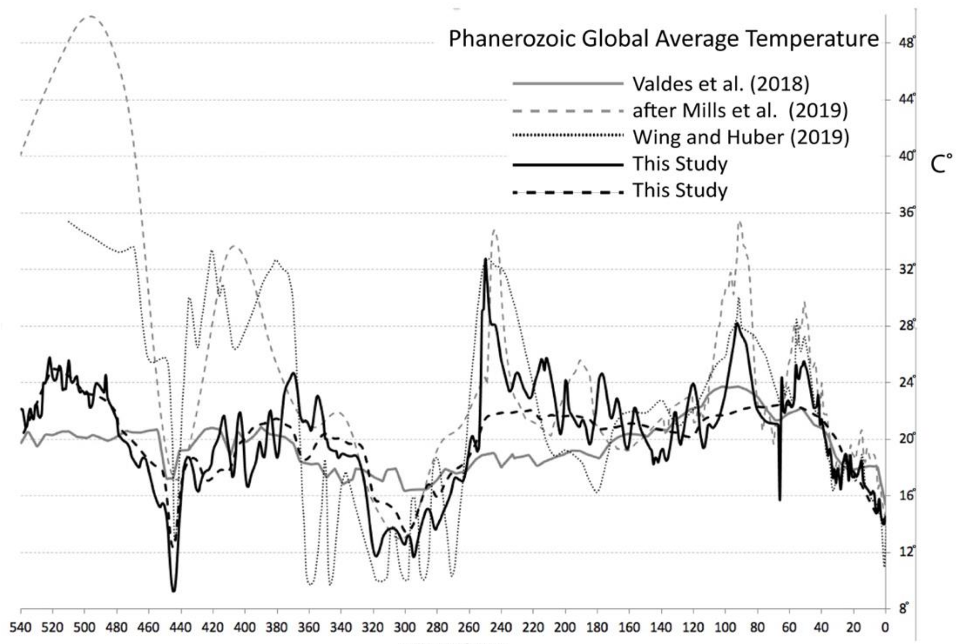

Figure 1. Estimates of Phanerozoic Global Average Temperature (GAT). Sources: Wing and Huber (2019), Valdes et al. (2018), Mills et al. (2019), and This study.

These curves are in good agreement and show the classic "double hump" Phanerozoic temperature history shown in Figure 2 (Fischer, 1981, 1982, 1984; Frakes, et al., 1992, fig. 11.1; Scotese et al., 1999; Summerhayes, 2015). Temperatures are high during the Early Paleozoic. Cooler temperatures prevail during the Late Paleozoic, followed by warmer Mesozoic and early Cenozoic temperatures, finally returning to cooler temperatures in the Late Cenozoic. This pattern is linked to the "Wegener Supercontinent" cycle (Nance et al., 2014; Van der Meer et al., 2014; 2017), namely: the breakup of the supercontinent, Pannotia, during the latest Precambrian (Powell et al., 1993; Powell, 1995; Scotese, 2009; Nance and Murphy, 2018), the formation of Pangea during the late Paleozoic (~300 Ma), its subsequent breakup (~200 Ma), and the assembly of the modern continental configuration.

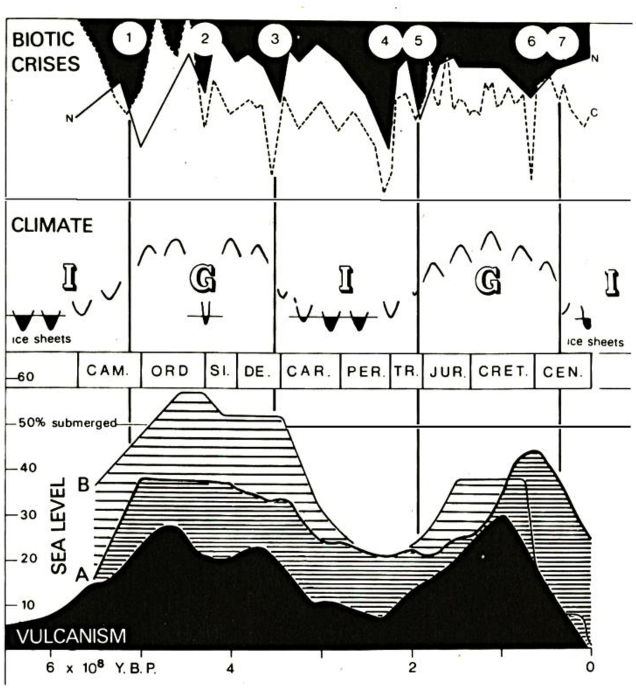

Figure 2. "Double Hump" pattern of Phanerozoic Climate (Fischer, 1981; 1982), I = Icehouse, G = Greenhouse .

Specific features that the curves in Figure 1 share in common are:

1) A broad sinusoidal pattern with peaks near 20 Ma, 50 Ma, 90 Ma, 245 Ma, 370 Ma, 420 Ma, and 500 Ma, with the highest peaks occurring at, 90 Ma, and 245 Ma.

2) Broad troughs link the 370 Ma and 245 Ma peaks and the 245 Ma and 90 Ma peaks.

3) The three youngest peaks (i.e. 90 Ma, 50 Ma, and 20 Ma) decrease, stepwise, in height.

4) The coherence of the curves breaks down during the middle and early Paleozoic. Some curves rapidly trend toward higher isotopic temperatures.

5) The temperatures between 330 Ma and 290 Ma (Permo-Carboniferous Ice Age), are ~14˚C on average, but fluctuate 6˚C with a period of ~10 million years.

6) A sharp “dip” occurs at in all curves at 445 Ma (Hirnantian Ice Age).

The pre-Carboniferous portions of these temperature curves can be divided into two groups: the “hothouse” middle and early Paleozoic versions (Valdes et al., 2018; this study), and the “extreme hothouse” middle and early Paleozoic versions (Mills et al., 2019; Wing and Huber, 2019).

It should be emphasized that the paleotemperature curve that we will present here is a “model” of Phanerozoic temperature change. No one line of evidence, such as, lithologic indicators of climate, oxygen isotopic measurements, or CO_2 proxy information (Foster et al., 2017) is sufficient to estimate past temperatures. We combine multiple, independent lines of evidence to produce a synthetic, multi-disciplinary model that describes how global temperature may have varied during the last 540 million years. The temperature predictions made by this model can be used to form hypotheses that can be tested by the acquisition of new $\delta^{18}O$ temperature data, by other independent measurements of paleotemperature (e.g.,Tex 86 or clumped isotope data), as well as the expected effects of temperature on the evolution of life and the environment.

2. Methods

2.1 Derivation of the Phanerozoic Global Average Temperature Curve

Our Phanerozoic Global Average Temperature Curve has been produced by combining: 1) estimates of the changing pole-to-Equator temperature gradient obtained from lithologic indicators of climate (i.e. paleo-Köppen belts), and 2) estimates of tropical changes in temperature obtained from oxygen isotopes. The temperatures obtained from oxygen isotope measurements have been summarized and sometimes temperatures have been modified to better agree with the geological and paleontological record.

We only schematically illustrate the extremely rapid (<1 million years), high amplitude temperature fluctuations that occurred during the coldest intervals. These dramatic temperature fluctuations are triggered by variations in insolation due to changes in the three Milankovitch parameters (obliquity, precession, and eccentricity). The effect of on short term climate are discussed in more detail in Kump et al. (1999c), Ruddiman (2001), and Hay (2016).

2.2 Estimates of Pole-to-Equator Temperature gradients derived by mapping Köppen Climate Belts

Long-term global temperature (>50 million years) is controlled by multiple tectonic and environmental processes that drive the Earth's climate from icehouse to hothouse conditions and vice-versa. The dominant factors are the level of greenhouse gases (principally CO_2), which are regulated by volcanic outgassing and the draw down of CO_2 due to weathering (van der Meer et al. 2014, Torsvik et al., 2020) the geographic configuration of the continents and ocean basins (paleogeography and paleoceanography), and the reflectivity of the Earth's surface (albedo). Many of these factors are interconnected by a complex network of positive and negative feedback loops that can accelerate or slowdown changes in long-term global temperature (Hay, 2016; Ruddiman, 2001).

In this paper we use the geologic record, specifically the paleogeographic distribution of lithologic indicators of climate to map how the Earth's Pole-to-Equator temperature gradient has changed through time. The expansion, contraction, and shifting position of the Earth's climatic belts provides important insights into the changes in the Earth's long-term climate history.

Using modern temperature and rainfall records, we can map five very distinct climatic regions called "Köppen Climate Belts" (Figure 3). The Köppen Climate Belts are defined by seasonal variations in temperature and precipitation (Köppen, 1918). These variations give rise to regional climates and create the mosaic of diverse environments that cover the Earth. These environments include: (A) tropical rainforests near the Equator, (B) desert belts at subtropical latitudes that transition into (C) warm temperate grasslands and forests. In the modern world, as we move poleward, warm-temperate regions are replaced by (D) seasonally warm/cold temperate regions and (E) finally frigid polar regions. These climatic zones extend over the oceans where they are primarily zonal. Each of these climatic zones is characterized by a distinctive, flora, fauna, land-cover, and geology.

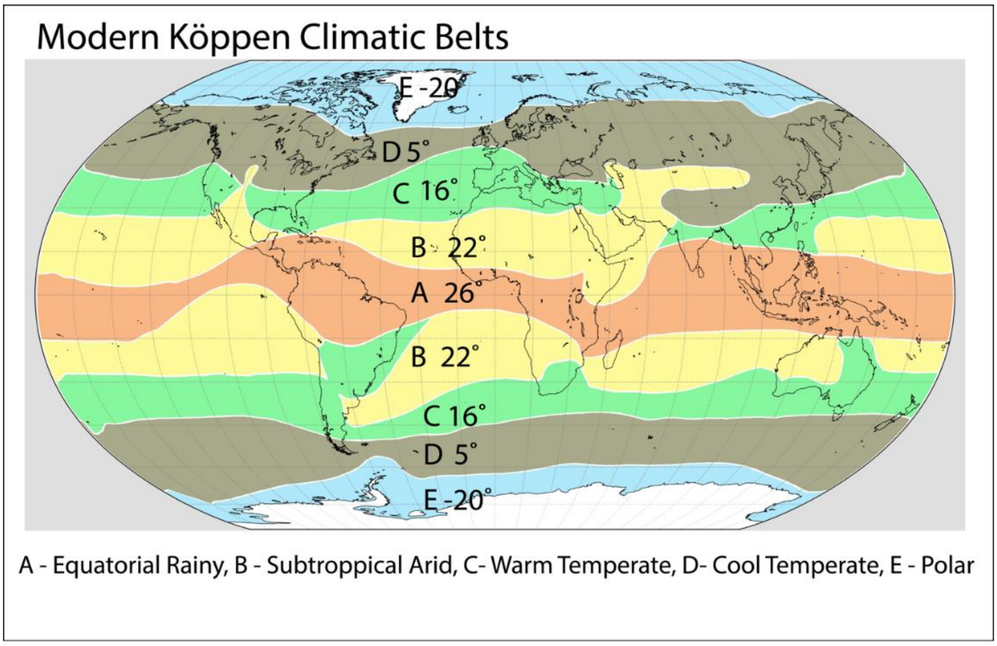

Figure 3. Modern Köppen belts and the average temperature of each belt.

Using lithologic indicators of climate such as coals, evaporites, and glacial deposits, it is possible to map “paleo”– Köppen Climate Belts for ancient time periods (Ziegler et al., 2003; Boucot et al., 2013; Figures 4 and 5). Over the past 20 years, a global database of over 15,000 lithologic indicators of climate was assembled (Boucot et al., 2013). For a thorough discussion of both lithologic and biological indicators of climate, see Parrish, 1998; Boucot et al., 2013; and Cao et al., 2019. Other important lithologic indicators of climate are: soil minerals such as bauxite, an aluminum ore which forms in warm, wet climates; calcrete, or caliche, which forms in semi-arid regions; and kaolinite which forms in regions with climates that are sometimes wet and sometimes dry (warm temperate climate belt). Dropstones, like tillites, are important indicators of frozen lakes or sea ice. A glendonite it is a pseudomorph of ikaite, a low temperature, hydrated polymorph of $CaCO_3$ that forms at temperatures <4˚ C. Recent experimental data suggests that it may also form at higher temperatures under special conditions (Tollefsen et, 2020). The legend inset on Figures 4 and 5 summarizes the association of the various lithologic indicators of climate with warm/cool and wet/dry environmental conditions.

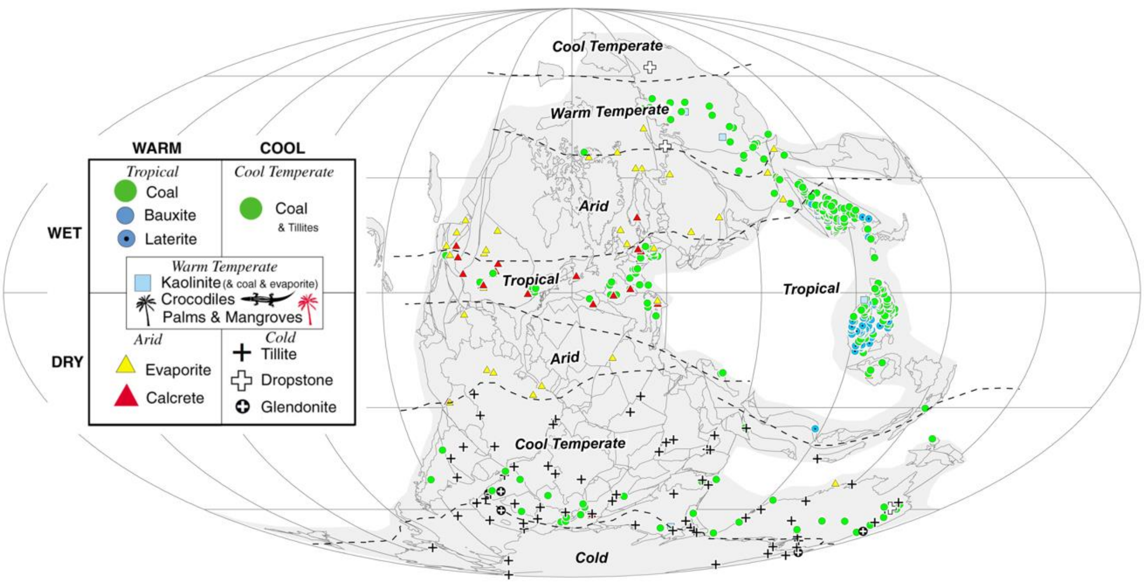

Figure 4. Early Permian (280 Ma) lithologic indicators of climate and continental paleo-Köppen Belts (Boucot et al., 2013).

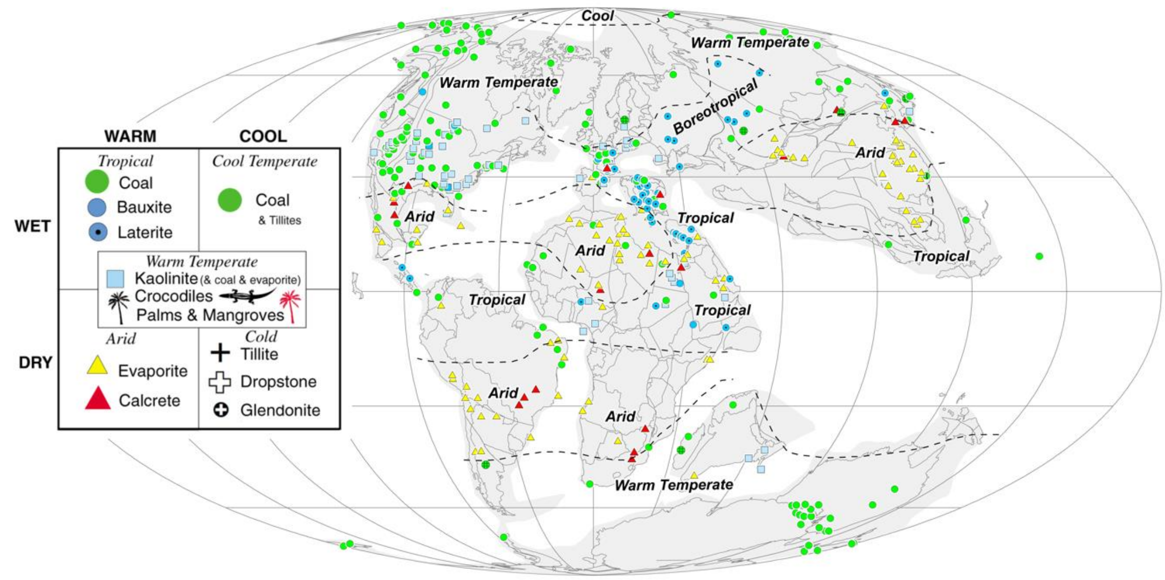

Figure 5. Mid-Cretaceous (100 Ma) lithologic indicators of climate and continental paleo-Köppen Belts (Boucot et al., 2013).

Bauxites, as a general rule, reflect tropical-subtropical humid, monsoonal conditions. Their modern occurrence is almost entirely restricted to the Equatorial Wet Belt. The occurrence of bauxite deposits in northern Europe and Siberia during the late Jurassic, Cretaceous, Paleocene, and Eocene times (Boucot et al., 2013), is one of the strongest geological indications of warm and wet conditions at high latitudes.

When we plot these lithologic indicators of climate on a set of paleogeographic maps we find that there have been times (e.g., Early Permian, Figure 4) when the Earth's climate was much like the present-day "icehouse" world. An icehouse world is simply defined as a time when the Earth is covered by permanent ice at either pole. For permanent ice to accumulate in the polar regions (>67˚ N & S) the temperatures must remain below freezing during the summer months. In other words, the global average temperature (GAT) must be less than around 18˚C and the average annual temperature of the polar region must be below -5 ˚C. Though the tropics remain relatively warm (26˚C) in an icehouse world, the polar regions are frigid (-5˚C to - 50˚C).

There are also have been times when there was no ice above the polar circle – even during the winter (e.g., Late Cretaceous, Figure 4). During these "hothouse" times, the average temperature of the Earth was generally above 20˚C (68˚F) and the polar regions were relatively warm (5˚C to 15˚C) and no ice could accumulate. It is a well-established fact that no polar ice existed during the Paleocene-Eocene Thermal Maximum (55.6 Ma; McInerney and Wing, 2011) or the Cenomanian-Turonian Thermal Maximum (93 Ma; Ziegler et al., 1985).

The long-term temperature curve (Figure 6) was calculated by mapping past extent of the five major Köppen belts using lithologic indicators of climate (tillites, dropstones, glendonites, high latitude mangroves, palms, and crocodiles; temperate coal, evaporites, calcretes, tropical coals, bauxites, and laterites (Boucot et al., 2013)). These paleoclimatic reconstructions, spaced at intervals of 5 million years, were used to characterize changes in global temperature along a spectrum of climatic states ranging from Severe Icehouse (GAT = 10˚ - 14˚C) to Extreme Hothouse (GAT = 22˚ - 26˚C; Figure 5). The complete set of more than 100 paleo-Köppen maps illustrating the distribution of lithologic indicators of climate are provided in the Supplemental Materials (Part 3).

Figure 6. Long-Term Phanerozoic temperature trend calculated by estimating the changing area of paleo-Köppen belts (see Supplementary Materials for data and details of calculations).

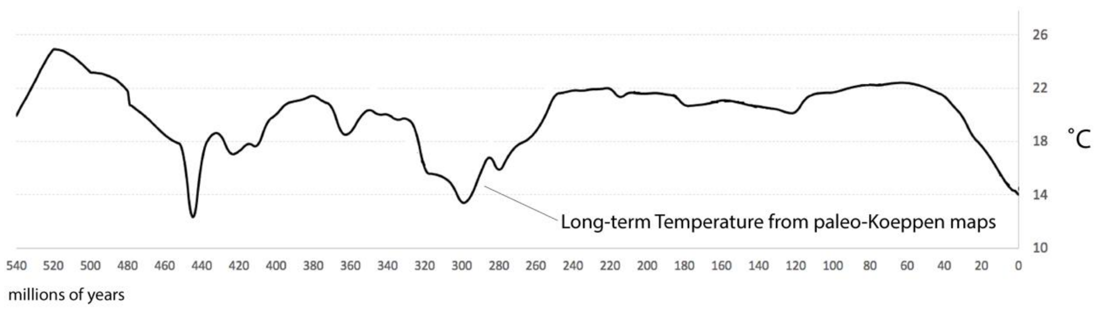

The average temperatures of the modern Köppen belts was calculated using the global temperature model of Legates and Wilmott (1990). The Equatorial Rainy Belt has a Mean Annual Temperature (MAT) of 26˚C; the Subtropical Arid Belt's MAT is 22˚C; the Warm Temperate Belt's MAT is 16˚; the Cool Temperate Belt's MAT is 5 ˚C; and the North & South Cold Polar Belts' MAT average -20˚C. The Global Average Temperature (GAT) was then estimated by summing the areas of the 5 major Köppen climatic belts on each of the paleoclimatic reconstruction and then multiplying that area by the MAT of that Köppen belt. For example, for the modern world (Figure 3): the Equatorial Rainy Belt (A) covers 23% of the Earth's surface, the Arid Belt (B) covers 28%, the Warm Temperate Belt (C) covers 20%, the Cool Temperate Belt (D) covers 20%, and the Polar Belt (E) covers 9%. The present-day global average temperature (GAT) = $.23*(26^\circ C) + .28*(22^\circ C) + .20*(16^\circ C) + .20*(5^\circ C) + .09*(-20^\circ C)$, which simplifies to $(5.98^\circ C + 6.16 + 3.2 + 1.0 – 1.8)\ ^\circ C = 14.5^\circ C$.

On the mid-Cretaceous paleoclimatic reconstruction (Figure 5): the Equatorial Rainy Belt covers 25% of the Earth's surface, the Subtropical Arid belt covers 29%, the Warm Temperate Belt covers 44%, the Cool Temperate Belt covers 2%, and the Cold Polar Belt covers 0%. The GAT = $.25*(26^\circ C) + .29*(22^\circ C) + .44*(16^\circ C) + .02*(5^\circ C) + 0.0$, which gives $20^\circ C$. The Boreotropical belt, which is strictly a climatic feature of hothouse worlds is assigned the same average temperature as the Arid Belt.

In a similar fashion, the global average temperature for the Early Permian (280 Ma, Figure 4) was calculated as follows: GAT = $.20*(26^\circ C)+.29*(22^\circ C)+.16*(16^\circ C)+.30*(5^\circ C)+.05*(-20^\circ C)$, which equals $14.6^\circ C$. The global average temperature during the early Permian icehouse was similar to the present-day icehouse.

Global temperatures were calculated in this manner for 100 Phanerozoic reconstructions of paleo-Köppen belts (one map ~ 5 million years). For an in-depth discussion of the data and methodology used see the Supplementary Materials. The resulting long-term global temperature curve is shown in Figure 6.

The estimates of global temperature obtained in this manner, do not provide a precise or detailed measurement of how the Earth's temperature has changed though time. The width of the Köppen belts are only approximate and are poorly known for older time periods, especially the Early Paleozoic. Though we assume a zonal pattern for the oceans, there are certainly major distortions caused by ocean currents and upwelling (Figure 3). Most importantly, the temperatures assigned to each of the Köppen belts are based on modern icehouse values and may not reflect temperatures in past hothouse worlds.

Despite these limitations, the Köppen approach does provide one important bit of information. This procedure tells how the Pole-to-Equator temperature gradient has changed through time. The relative widths of the equatorial wet and the subtropical arid belt do not change significantly through time because they are controlled by Hadley Cell Circulation. The changing in Pole-to-Equator temperature gradient is due nearly exclusively due to the changing width of the Warm Temperate, Cool Temperate and Polar Belts.

In icehouse worlds, like the present-day, Pole-to-Equator temperature gradient is very steep. The temperature falls .75˚ - 1˚ C per degree of latitude as we move towards the Pole (e.g., if we start at 30˚C at the Equator, we end up with temperatures of -40C˚ to -60˚C at the pole). During hothouse worlds (e.g., Cenomanian-Turonian Thermal Maximum, 93 Ma), the pole-to-Equator temperature gradient was much shallower, approximately .20˚ - .33˚ C per degree of latitude. That means that if we start out at 30˚C at the Equator, the temperature at the Pole would still be well above freezing (0˚ to 12˚C).

Figure 7 illustrates the possible range of ancient Pole-to-Equator gradients. The plus signs lie along the modern Pole-to-Equator gradient and describe how temperatures change as a function of latitude. In the present-day world, the temperature near the Equator is 26˚C. The temperature remains nearly constant in the subtropics (0˚ - 15˚ latitude), and then begins to decrease rapidly. Freezing temperatures are reached at 60˚ latitude; falling to -35˚ C at the Poles.

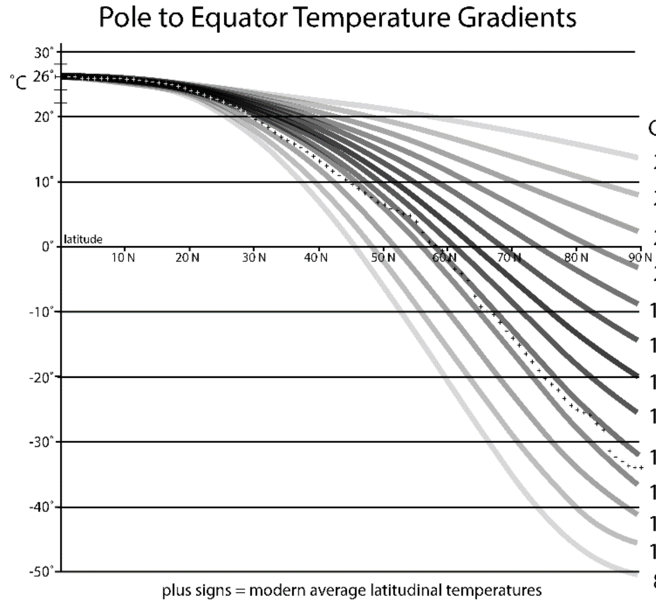

Temperatures			Gradient	Frequency
GAT	Polar	Deep Sea	°C / latitude	% Phanerozoic
23°	17°	20°	.15	0%
22°	12°	18°	.22	0%
21°	8°	16°	.30	4%
20°	4°	14°	.37	29%
19°	-1°	12°	.45	30%
18°	-5°	10°	.52	11%
17°	-9°	8°	.60	11%
16°	-14°	6°	.67	5%
15°	-18°	4°	.74	6%
14°	-22°	2°	.82	3%
12°	-29°	2°	.96	1%
10°	-35°	1°	1.1	0%
8°	-42°	1°	1.25	0%

Figure 7. The polar temperature and the Pole to Equator temperature gradient for different Global Average Temperatures (GAT). Polar Temperature = average temperature above 67° latitude (N&S), Deep Sea = the average temperature at the bottom of the oceans (after Valdes et al., 2020). Pole to Equator Gradient = the average change in temperature for every one degree of latitude measured between 30° and 60° latitude. The Pole to Equator temperature gradient is shallow near the Equator and steepens rapidly near the Pole. The plus signs are the combined average temperatures for the present-day northern and southern hemispheres. Frequency % Phanerozoic = the percent of the time during the Phanerozoic characterized by this specific Pole-to-Equator temperature gradient. All of these calculations are based on an average tropical temperature of 26°C (15° N – 15° S).

The first column labelled "GAT" is the global average temperature obtained by the Köppen technique. The adjacent curve is the Pole-to-Equator temperature gradient associated with that GAT. The modern world (GAT = 14.5°C) falls between the 14°C and 15°C curves. The other columns describe how the polar temperature, the temperature of the deep ocean and the latitudinal gradient (between 30° - 60° latitude), change with each "GAT" curve. These topics will be discussed later. The final column labelled, "Frequency % Phanerozoic", records the frequency of these various GATs during the Phanerozoic. Past hothouse worlds with global temperatures ranging between 19° - 20°C have been the most frequent (~60%). Icehouse worlds with global temperatures similar to the modern world (>15°C) are relatively rare (~10%). It should be noted that some very shallow Pole-to-Equator gradients (GAT > 21°C), though theoretically possible, have probably not been achieved. Conversely, Pole-to-Equator gradients associated with GATs below 10° C, have only been seen in the Snowball Earth worlds of the late Precambrian (Hoffman and Schrag, 1998; 2000; 2002 ; 2009).

Though these estimates of Global Average Temperature are based on a methodology rooted in the modern icehouse world, it is possible to make adjustments to these GATs so that they also reflect temperature changes in past hothouse worlds. As can be seen in Figure 7, all of the Pole-to-Equator temperature gradient curves are set to 26˚C at the Equator. This equatorial temperature is certainly lower than the equatorial temperatures during hothouse times. In the next section we describe how we used oxygen isotopic data to estimate the change in tropical temperatures through time.

2.3 Global Temperature Change (~10 - 20 million years) derived from Oxygen Isotopic Data

In addition to the gradual change in global temperature recorded by the changing pole-to-Equator gradient, we know that the Earth's temperature has varied significantly over periods of 10 – 20 million years. The evidence for these temperature changes comes from the measurements of the ratio of ^{18}O /^{16}O (also referred to as $\delta^{18}O$) in the shells and bones secreted by marine organisms (Figure 8).

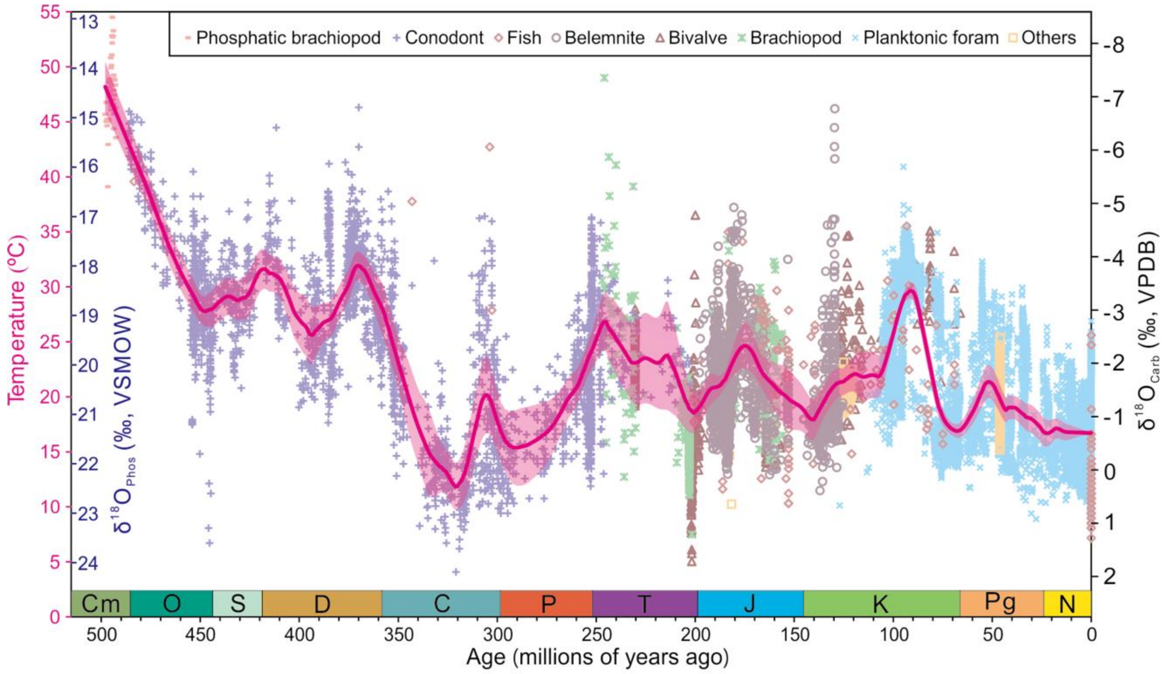

Figure 8. Raw and mean values of oxygen isotopes from phosphatic and carbonate fossils for reconstructing sea surface temperatures over the past 500 million years (modified after Song et al., 2019). The scale of δ18OPhos is used for phosphatic fossils, i.e., phosphatic brachiopod, conodont, and fish. The scale of δ18OCarb is used for carbonate fossils, i.e., belemnite, bivalve, brachiopod, planktonic foraminifer, and others. Magenta curve represents the mean values of sea surface temperatures per million years. Shaded area represents 95% confidence intervals.

The solid black line in Figure 9A illustrates the isotopic temperature of seawater for the last 500 million years based on a compilation of >22,000 oxygen isotope measurements (Song et al., 2019). Isotopic values were converted to temperature using the equation of Lécuyer (2013) for phosphate fossils and by using the equation of Hays and Grossman (1991) for carbonate fossils. Because the samples upon which this curve is based come entirely from tropical and subtropical latitudes (< 40˚ N&S), this curve is essentially an estimate of tropical temperatures through time.

Each dot in Figure 9A represents the average of all isotopic estimates of temperature that fall within a one million year interval. Error estimates of the average temperature calculation are given in Song et al. (2019). The best-fit curve in Figure 9A was obtained using the Savitsky-Golay smoothing technique which fits successive sub-sets of adjacent data points with a low-degree polynomial by the method of linear least squares (Savitsky and Glay, 1964). We found the Savitsky-Golay method did a better job honoring the data points than either the high-order polynomial or LOESS techniques traditionally employed.

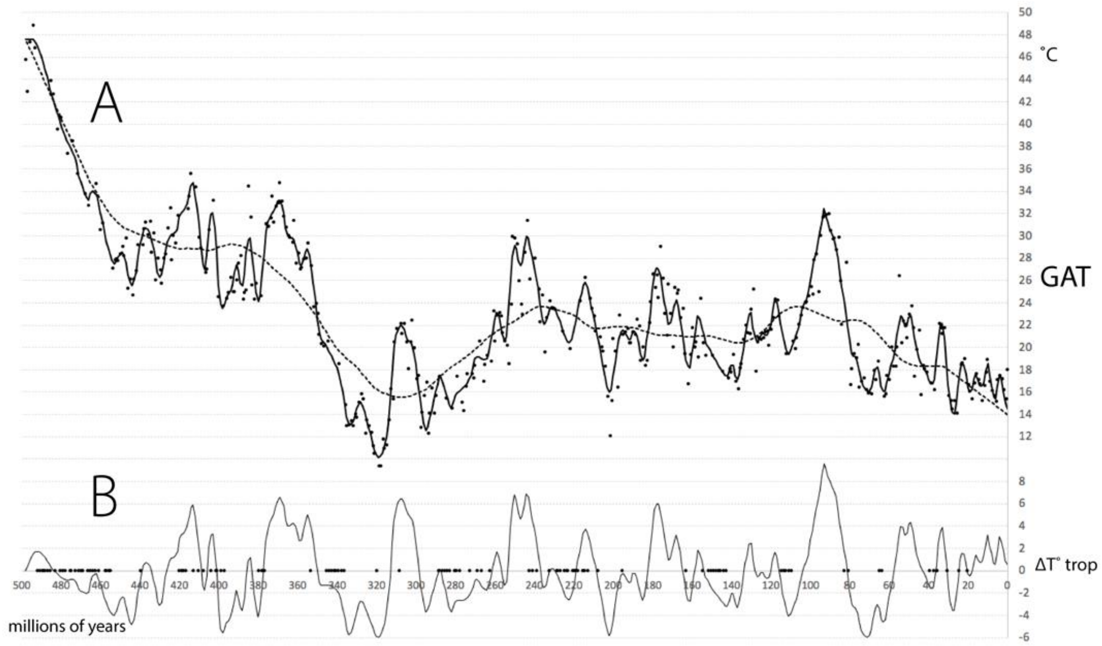

Figure 9. Phanerozoic Isotopic Temperature (Song et al., 2019). A. = Each dot represents the average of all temperatures that fall within a given one million year interval. The best-fit curve was obtained using the Savitsky-Golay smoothing technique (window 11-15, degree 4). B. Change in Tropical Temperature (ΔT˚trop). The black dots along the x-axis are the times when no data are available.

Though the isotopic temperature curve is relatively flat for much of the Mesozoic and Cenozoic, the curve has a steep, linear negative slope during the early Paleozoic. The isotopic estimates of temperature for these times appear to be much higher (up to +24˚C difference at 500Ma) than the temperatures obtained from lithologic indicators of climate.

It should be noted that the isotopic temperatures illustrated in this curve do not take into account regional variations in the isotopic composition of seawater, or proposed Phanerozoic changes in the ^{18}O ^{16}O ratio of seawater. Some researchers believe that there is a long-term trend in the average isotopic composition of seawater (Veizer, 2000; Prokoph et al., 2008; Verard and Veizer, 2019). Others vehemently disagree (Grossman, 2012 a&b). This debate has been going on for more than 30 years. It seems incredible that the average temperature of the tropical oceans could have been as high as 50˚C (122˚ F) during the early Paleozoic and late Precambrian. This implies that diurnal or seasonal temperatures were much higher. Even in extreme cases, modern organisms cannot survive when seawater temperatures reach 40˚C (104˚F) (Fraenkel, 1960). Verard and Veizer (2019) propose that a systematic decrease in plate tectonic activity during the last 540 million years may have systematically increased the ratio of ^{18}O to ^{16}O in seawater; however, they admit that the details of the correlation are poor and that tectonic activity prior to the formation of Pangea is not well-known. It may be possible that the $\delta^{18}O$ composition of seawater has not remained constant, nor has it gradually changed in a quasi-linear fashion. Rather the $\delta^{18}O$ could have varied non-monotonically through time.

Upon reflection, what may be important is not the "absolute" temperature provided by the isotopic data, but rather the "relative" change in temperature at shorter timescales. For our purposes, the most useful information that can be gleaned from the isotopic temperature record is the change in the tropical temperatures through time (i.e., the ΔT°_{trop}), Figure 9B. In order to calculate the ΔT°_{trop}, we first estimated the long-term isotopic temperature signal by averaging the isotopic data using a 60 million year running-average. We chose 60 million years because it best approximated the long-term temperature signal from the Köppen analysis. The 60 million year running average was then subtracted from the best-fit isotopic tropical temperature estimates (Figure 9A, black line) to obtain the ΔT°_{trop} value (Figure 9B).

2.4 Modifying the Isotopic Estimates of Changing Tropical Temperatures Using Geological and Paleontological Constraints

The isotopic temperature of seawater can be affected by multiple environmental conditions: hypersalinity or hyposalinity, the presence of continental ice caps, or the water depth at which sampled organisms originally resided (Grossman2012a,b). In this section we review the isotopic estimate of tropical temperature described in the previous section and make modifications based on geological and paleontological constraints.

Figure 10 illustrates the changing temperature of the Tropics (ΔT˚ trop) based on isotopic measurements (dotted line). Superimposed on the dotted line are colored lines that represent seven time intervals when the "raw" isotopic estimates of tropical temperature that do not agree with geological or paleontological information and therefore, must be adjusted or modified. These seven intervals are: the Cambrian, 540 – 485 Ma; the latest Ordovician, 445 -443 Ma; parts of the Permo-Carboniferous, 340 – 275 Ma; the Triassic, 252 – 200 Ma; the Early Cretaceous, 125 Ma – 95 Ma; the latest Cretaceous, 80 – 65 Ma; and the Cenozoic (65 – 0 Ma).

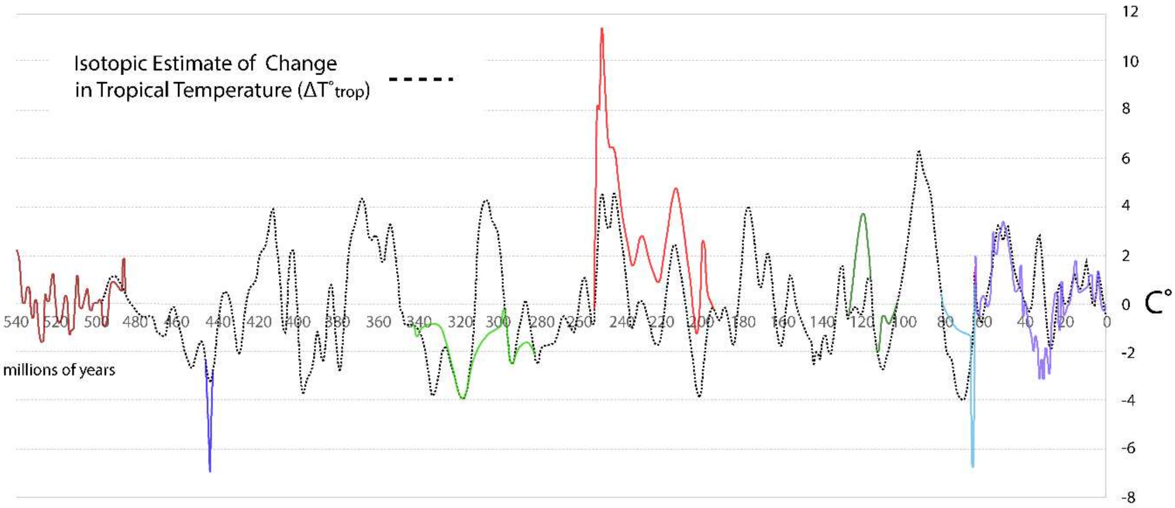

Figure 10. Modifications to the Phanerozoic Isotopic Temperature Curve. The dashed line is the isotopic temperature curve (see Figure 8). The colored lines represent modifications and adjustments made to that curve based on geological and paleontological constraints.

The procedure that we used to determine whether in isotopic measurements require modification was initially developed at a workshop convened by Scott Wing and Brian Huber at the Smithsonian National Museum of Natural History (April, 2017 & 2018). At those meetings a multidisciplinary group of more than 20 earth scientists convened at the Museum to refine a Phanerozoic paleotemperature curve that eventually became part of an exhibit on Global Warming in the Museum's Earth History Hall (Wing and Huber, 2019). During that meeting participants were invited, based on their geological and paleontological knowledge and expertise, to make additions and revisions to the proposed Phanerozoic temperature curve which was posted as a wall-sized display. The results of that collaborative effort are illustrated in Figure 1 (Wing and Huber, 2019). The criteria used to modify or adjust the isotopic estimate of temperature included the addition of ephemeral events which have not been sampled in the isotopic record (e.g., KT Impact Winter, Permo-Triassic Thermal Maximum), the elimination of spurious thermal maxima during times of icehouse conditions (e.g., late Pennsylvanian thermal maximum), and the elimination of cooling events that would require large, permanent ice caps during times of hothouse conditions (e.g., latest Cretaceous cooling). This same basic procedure was used by the authors to modify and adjust the raw isotopic estimates of temperature so that they better agreed with geological and paleontological constraints. In the following section, we describe the changes that have been made to the raw isotopic estimates and the reasons for these changes.

2.4.1 Cambrian, 540 485 Ma.

There is sparse isotopic data older than 500 million years (Bergmann et al., 2018b; Hearing et al., 2018; Henkes et al., 2018). The data that is available indicates that tropical temperatures were in excess of 40˚C; as noted previously, this is problematic (Fraenkel, 1960). For a more detailed discussion of global temperatures during the Cambrian, see section 5.2.

The dark red curve in Figure 10 is a speculative estimate of temperature changes based on the carbon isotope record. They coincide with 10 proposed Cambrian $\partial^{13}C$ isotopic excursions (Zhu et al., 2006). The covariance of $\partial^{13}C$ and $\partial^{18}O$ trends has long been noted (Wenzel and Joachimski, 1996; Jenkyns et al., 2002). Approximately 80% of the positive $\partial^{13}C$ excursions are correlated with warmer temperatures (hyperthermals). The correlation is generally attributed to the causal relationship between higher ocean temperatures, the formation of deep water anoxia, and the subsequent preservation of organic carbon.

2.4.2 Latest Ordovician (Hirnatian, 445-443 Ma)

The isotopic estimates of tropical temperatures during the Hirnantian Ice Age (see section 5.3), show a notable dip of 3˚ C. We have exaggerated the dip in temperature to help explain the growth of the massive, Hirnantian south polar ice cap that extended well into the Ordovician tropics (~35˚ S).

2.4.3 Permo-Carboniferous Icehouse

Evaporitic anomalies are known to affect the isotopic measurements made in the great subtropical epeiric seas of the Paleozoic (Mii et al., 1999). Because evaporation preferentially removed the lighter isotope of oxygen (^{16}O), the observed isotopic temperature measurements obtained from organisms living in these evaporitic seas are erroneously too cool. Conversely, freshwater is rich in ^{16}O, so isotopic estimates of temperature made in areas that receive a large influx of freshwater are erroneously too warm.

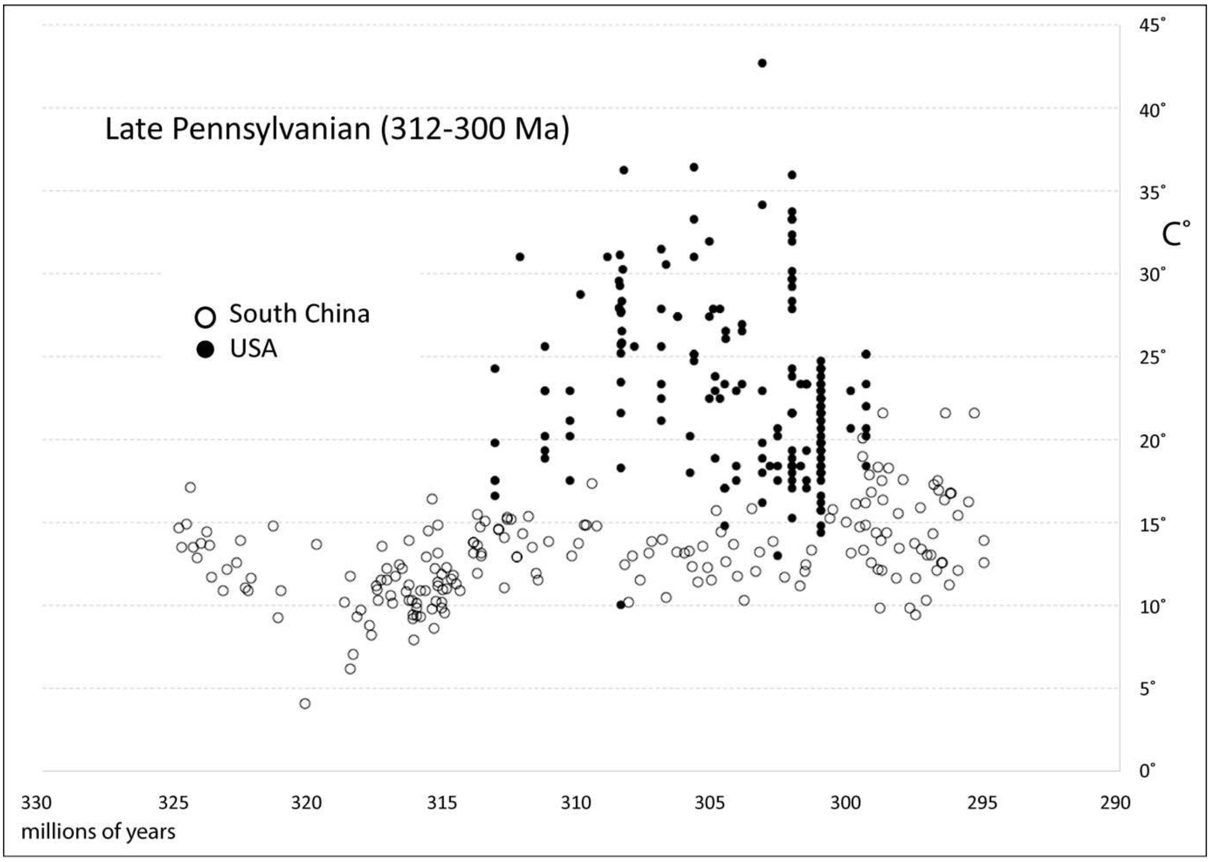

Figure 11. Comparison of isotopic temperature data from the late Pennsylvanian of South China (open dots) and the USA (black dots) (Song et al., 2019).

As Figure 10 shows, a broad temperature peak (dotted line) sits in the middle of the Permo-Carboniferous Ice Age. A closer examination of the isotopic temperature record reveals that the isotopic data for the late Pennsylvanian come primarily from South China and the USA (Figure 11). The isotopic temperatures for China (Chen et al., 2013; 2016) and the USA (Luz et al., 1984;

Joachimski et al., 2006; Elrick and Scott, 2010; Rosenau et al., 2014) are very different. The average temperature for the USA data is ~ 25˚C, whereas the average temperature for South China is ~13˚C. This difference in temperature cannot be explained in terms of latitudinal position. 310 million years ago, both of these regions straddled the paleo-Equator (Scotese, 2014). The difference in isotopic temperatures is more likely due to environmental differences. In the USA, the influx of fresh water rich in ^{16}O from the rising Central Pangean mountain ranges may have altered the ^{18}O / ^{16}O ratio, making the seawater "lighter", giving a false, warmer isotopic temperature. We invoke a similar explanation to explain the much smaller thermal anomaly in the early Permian (~285 Ma).

As described above, evaporitic anomalies may cause isotopic temperatures to appear "too cool". We can speculate that this phenomenon may explain the cooler than expected temperatures during the early Carboniferous (~335 Ma).

We have applied an ad hoc correction of 4-5˚C to the mid-Pennsylvanian isotopic measurements to bring them into line with the geological observations. This adjustment keeps temperatures below the global temperature required to form permanent polar ice caps (see section 3.2). A more modest adjustment of 2-3˚C was applied to the earliest Permian (295 – 285 Ma) because extensive south polar glacial deposits indicate the Permo-Carboniferous glacial maximum occurred during the latest Carboniferous – earliest Permian (see section 5.5). Conversely, the isotopic temperatures for the Visean appear to be much too cold suggesting that the Visean represented the depths of the Permo-Carboniferous Ice Age. This is not the case, the Visean was one of the warmest intervals of the Carboniferous (Mii et al., 1999). Consequently, isotopic temperatures have been increased a modest 2-3 ˚C.

2.4.1 Triassic and early Jurassic (252 – 200 Ma)

Three adjustments to the average isotopic temperature were made for the Triassic. The Permo-Triassic Extinction was the greatest mass extinction of the Phanerozoic (see section 5.6). The kill mechanism was massive, global warming (see section 3.1.2). It is likely that average global temperatures reached 40˚C (Sun et al., 2012). The sharp spike in temperatures at the Permo-Triassic have been adjusted accordingly.

Global temperatures peaked during the earliest Triassic, fell sharply during the early Triassic (Sun et al., 2012), and extreme hothouse conditions did not ameliorate until the mid-Triassic (Ladinian; see section 5.6). The averaged isotopic temperatures for the late Triassic and early Jurassic are far too low and erroneously suggest possible icehouse conditions. This anomaly is probably due to the fact that some of the isotopic measurements come from belemnites and clams that once inhabited deeper, cooler waters (Dera et al., 2011; Wierzbowski and Joachimski, 2007). To remedy this mismatch between isotopic and geologic evidence, global temperatures were increased by 2-3 ˚C.

Finally, the end of the Triassic was marked by a major extinction event that was most likely triggered by the eruption of the Central Atlantic Magmatic Province (see sections 3.2 and 5.6). There is no oxygen isotope record of this relatively brief event (1-2 million years; Ernst, 2014). To explain the extinction event and other paleontological evidence of global warming, we have added a narrow thermal spike at 200-201 Ma.

2.4.5 Early Cretaceous (130 – 105 Ma) and latest Cretaceous (80 – 65 Ma).

The Late Jurassic – earliest Cretaceous is generally considered to be a relatively cool period with evidence of intermittent polar ice. Towards the end of this interval (~120 Ma), massive volcanic eruptions took place in the Central Pacific (Greater Ontong Java Plateau), along the southern margin of Africa, and forming the Kerguelen Plateau (see section 3.2 for details). The oldest Cretaceous oceanic anoxic event, OAE1a, the Selli/Goguel Thermal Maximum is coincident with these LIP events. Because this oceanic anoxic event is thought to have been triggered by significant global warming, we have added a thermal peak at ~120 Ma. This early Aptian warming was followed by a “cold snap” in the late Aptian – early Albian (see section 5.8). The little “bump” that precedes the Cenomanian-Turonian Thermal Maximum represents the Paquier/Urbino Thermal Maximum (OAE1b) (see Table 6).

2.4.6 Cenozoic (65 – 0 Ma)

The classic record of deep ocean temperatures based on benthic foraminifera assembled by James Zachos (Figure 12, Zachos et al., 2001, 2008; Westerhold et al., 2020) provides a framework for describing the temperature fluctuations during the Paleocene-Eocene Hothouse and the Late Cenozoic Icehouse (Koeberl and Montanari, 2009).

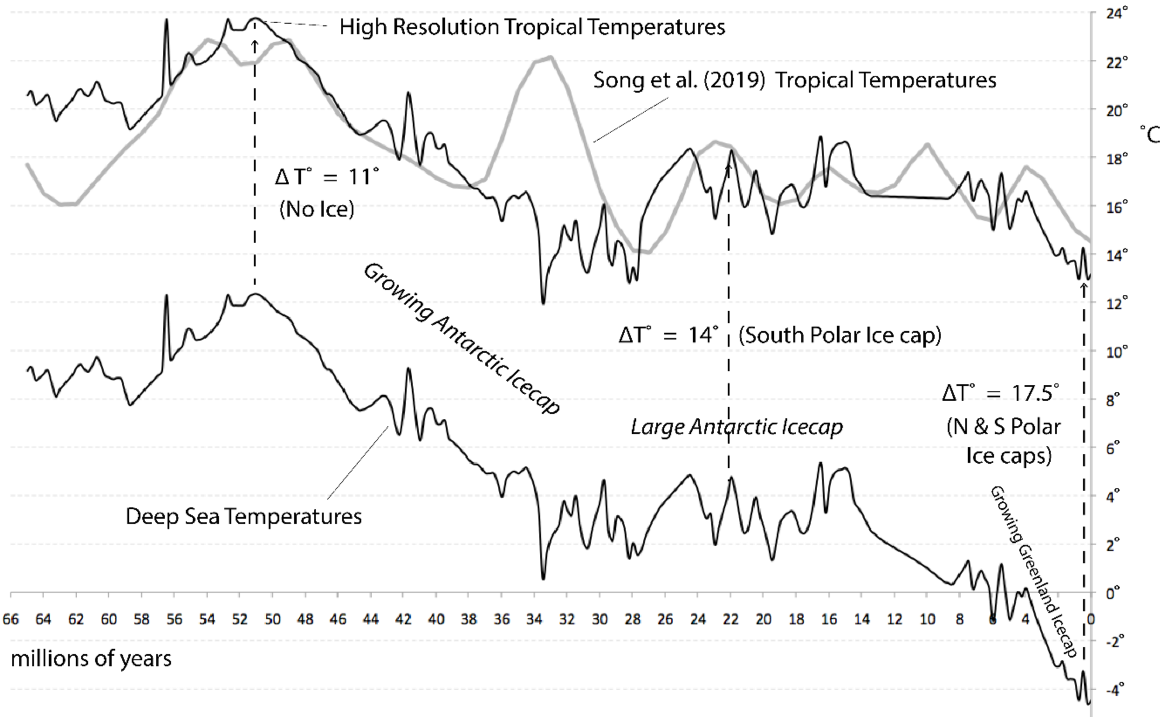

Figure 12. Comparison of Cenozoic deep ocean isotopic temperatures and tropical temperatures A. gray line = low resolution Tropical Temperatures (this study), and the black line = high resolution Δ Tropical Temperatures for the Cenozoic. B. isotopic temperatures from deep ocean, benthic foraminifera (Zachos et al., 2001, 2008; Westerhold et al., 2020).

The temporal resolution of the Phanerozoic isotopic temperature record from the tropics (Figure 9A) is one control point per million years. While this resolution is adequate for older geological periods, it does not permit a detailed description of Cenozoic temperature changes. We can improve the Cenozoic portion of the temperature curve if isotopic information from deep ocean, benthic foraminifera are used (Zachos et al., 2001, 2008; Westerhold, 2020). The isotopic record from benthic foraminifera provides a nearly continuous record of deep sea temperature changes from beginning of the Cenozoic to the present-day and has a temporal resolution of ~ 100,000 years.

As illustrated in Figure 12, we have converted the Cenozoic deep ocean temperatures to a high resolution estimate of global average temperatures by superimposing the high-resolution deep ocean temperature curve on our low-resolution estimate of tropical temperatures. This was done by adding ~11˚C to the pre-ice, Paleogene- early Oligocene portion of the deep ocean temperature curve (65 Ma – 28 Ma), as well as adding ~14˚C to the early and mid-Miocene portion of the deep ocean temperature curve (28 – 14 Ma). The late Miocene to Recent portions of the temperature curve (14 – 0 Ma) were transposed using linear approximation.

The overall shape and amplitudes of the superimposed curves are in remarkable agreement (Figure 12). The only significant mismatch is the late Eocene – early Oligocene (33 – 38 Ma) portion of the curve. The Oligocene portions of the transposed deep ocean temperature are 6˚ - 8˚ C cooler than isotopic tropical temperatures, which is certainly anomalous. We have chosen to use the updated high resolution Cenozoic tropical temperatures when building our model of Cenozoic global average temperatures.

It should be noted that the methods that Hansen et al. (2013) have used to estimate global average temperatures from deep sea temperatures were not used. Though the results he obtained for the Neogene are identical to our estimates, his methodology overestimates global temperatures when applied to hothouse climates.

2.4.7 Summary of Modifications to the Isotopic Temperature Curve

In summary, ~30% of the Phanerozoic isotopic paleotemperature curve was modified using geological and paleontological criteria. In most cases, 2-3˚C were added to or subtracted from the isotopic temperatures. Three notable exceptions are the Hirnantian Ice Age (-4˚C), the Permo-Triassic Extinction Event (+7 ˚C), and the KT Impact Winter (-6˚C). Two new thermal maxima were added (200Ma, CAMP; 124 Ma, OAE1a), three problematic apparent thermal maxima were removed (315-295 Ma; 285-275Ma, and 40-30 Ma), and two anomalous apparent cool episodes were either reduced (80-65Ma) or eliminated (340-330 Ma).

In addition, a high-resolution isotopic curve was used to represent Cenozoic temperatures (see section 5.9) and Cambrian carbon isotope excursions were used as a proxy for temperature (see section 5.2).

2.5 Combining the Estimates of the Changes in the Pole-to-Equator temperature gradient with the Revised Δ T°_{trop} curve derived from Oxygen Isotope Data

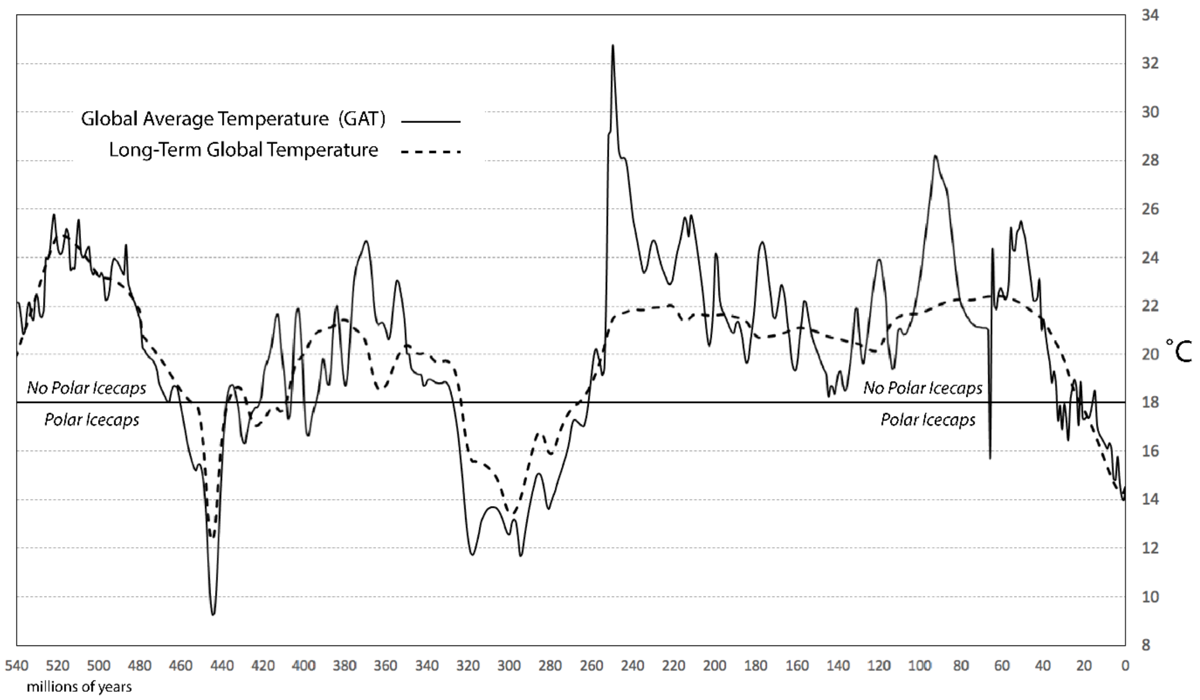

Figure 13. Phanerozoic Global Average Temperature (GAT), blackline = Global Average Temperature, dashed line = Long-term temperature change derived from changes in the pole-to-Equator temperature gradient calculated from the changing area of Köppen Climatic Belt (see Figure 6). When the Global Average Temperature is below 18˚C large polar icecaps can form. When the Global Average Temperature is above 18˚C large polar icecaps are unlikely to form.

In the final step of our methodology, we combine the estimates of Global Average Temperature obtained from the changes in the Pole-to-Equator temperature gradient (Figure 6) with the revised changing temperature of the Tropics (ΔT˚ trop) (Figure 10). The combined geological and isotopic temperature curve (Figure 13) is similar in many respects to the curve derived solely from isotopic data (Figure 9A), but also differs in several important ways.

1. The Paleogene portion of the isotopic temperature curve is ~ 1.5˚C cooler than the geologic temperature curve.

2. The isotopic temperature curve, overall, tends to indicate slightly warmer temperatures (e.g peak of the Cenomanian-Turonian thermal high).

3. The late Carboniferous through Triassic, and the late Jurassic - early Cretaceous portions of the isotopic temperature curve are 1.5˚ - 2˚C warmer than the geologic temperature curve.

4. The mid-Ordovician through Devonian portion of the isotopic temperature curve is significantly warmer than the geologic temperature curve (> 6˚ - 8˚C).

5. The Cambrian and early Ordovician temperatures indicated by the isotopic temperature curve are nearly double the geologically-inferred (~ 50˚C versus ~ 25˚C, respectively).

3. Discussion

A central thesis of this paper is that changes in the Earth's temperature during the Phanerozoic have been caused by factors that act on different time scales. This is not a new idea but rather goes back to the archetypical insights of Alfred Fischer (Fischer, 1981, 1982, 1984), who recognized climatic oscillations and cycles in the biosphere. We recognize three major timescales of temperature change. Long-term changes in temperature (>50 million years) are due to global changes in the rates of volcanic CO_2 degassing associated with seafloor spreading and subduction, as well as long-term changes in the weathering of continents. Long-term changes in temperature (>50 million years) are modeled by mapping the extent of ancient climatic belts (Köppen belts) which vary in response to changes in the Pole-to-Equator temperature gradient. Medium-term changes in temperature (10 – 20 million years) can be deduced from changes in the isotopic temperature of the tropical seas.

How well does our Phanerozoic temperature model (Figure 13) match the geological record? In the next section we compare the composite Phanerozoic temperature curve with a variety of geological phenomena including: LIP eruptions, bolide impacts, the formation of permanent ice caps, and changes in tropical, deep ocen, and polar temperatures during the Phanerozoic. We also discuss top priorities for future research.

3.1 Short-Term Global Temperature Excursions (< 1 to several million years) due to LIP Eruptions and Bolide Impacts

We know that very rapid excursions in temperature can be caused by a variety of tectonic and geological phenomena. For example, global temperatures can rise rapidly due to the release of vast amounts of CO_2 into the atmosphere by eruptions from Large Igneous Provinces (LIP) (Clapham and Renee, 2019). In Figure 14, the black rectangles represent the timing and relative magnitude of 21 major LIP eruptions (Ernst, 2014; Ernst and Youbi, 2017). Conversely, temperatures can fall rapidly, creating short-lived icehouse worlds, due to major bolide impact events (e.g., K/T boundary Impact Winter or possibly the Hirnantian Ice Age). Very large impact events (crater size > 150 km) may also trigger large igneous eruptions that create a period of global warming that follows impact-related cooling (e.g., Chicxulub impact event). In Figure 14, the circles illustrate the timing and crater size of the largest, well-established impact events (Spray, 2020).

3.2 Large Igneous Provinces (LIPs)

The slow and steady release of CO_2 from the volcanism that accompanies subduction and seafloor spreading is one of the major factors that determine the Earth's thermal equilibrium. This thermal equilibrium changes slowly because the plates move slowly and the continents erode slowly. In contrast, LIPs erupt rapidly, release tremendous amounts of CO_2 and consequently warm the Earth rapidly. The amount of global warming depends on the volume of CO_2 released and the amount of CO_2 in the atmosphere (i.e., climate sensitivity; Royer, 2016). A major LIP eruption during a period of icehouse climate will have a much greater effect than the same LIP eruption during a period of hothouse climate. The warming effects of LIPs will continue as long as voluminous eruptions continue, often for several million years. Beginning soon after eruption, the weathering of subaerial basalts may remove CO_2 from the atmosphere reducing global temperatures to near pre-eruption levels. The rate at which this occurs depends, in part, on the climatic setting of the LIP (Walker et al., 1981; Berner et al. 1983; Marshall et al. 1988; Raymo et al. 1988; Worsley & Kidder 1991; Bluth & Kump 1991; Otto-Bliesner 1995; Gibbs et al. 1999; Berner 2004; Nardin et al. 2011; Goddéris et al. 2012, 2014)

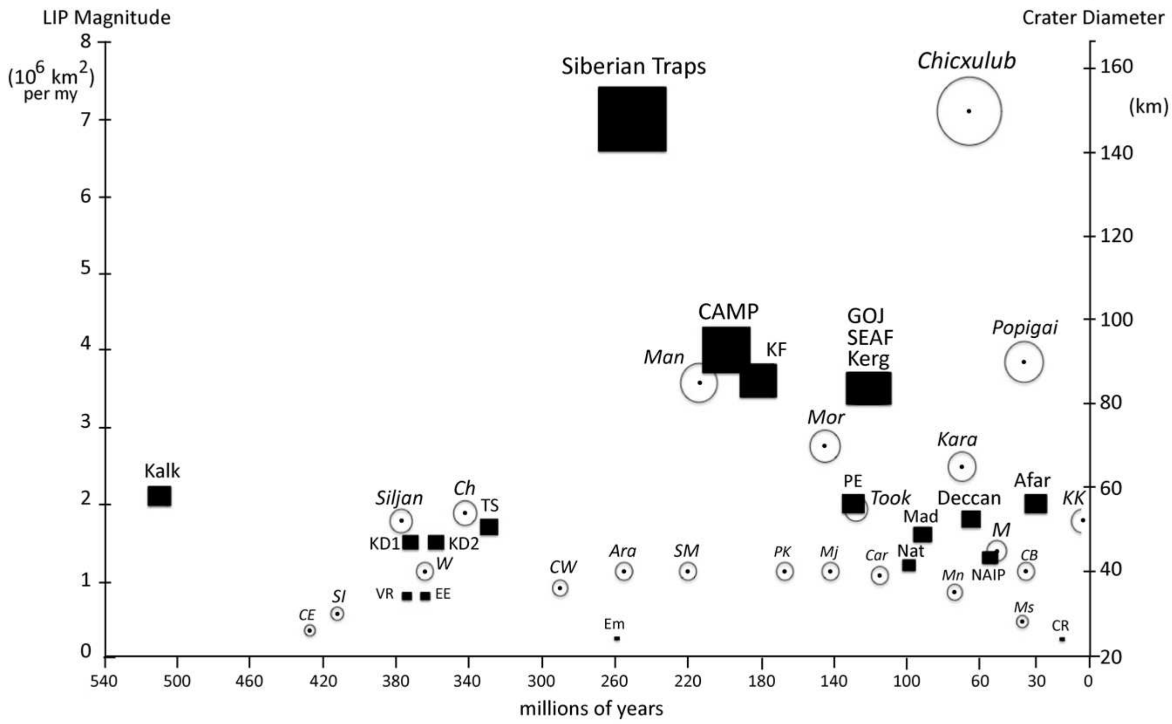

Figure 14. Timing and magnitude of Large Igneous Provinces (rectangles) eruptions and bolide impacts (circles). The size of the rectangles indicates the relative eruptive intensity (106 km2/my) (left-hand scale). See Table 1 and 2 for abbreviations. Sources: Ernst (2014), Spray (2020).

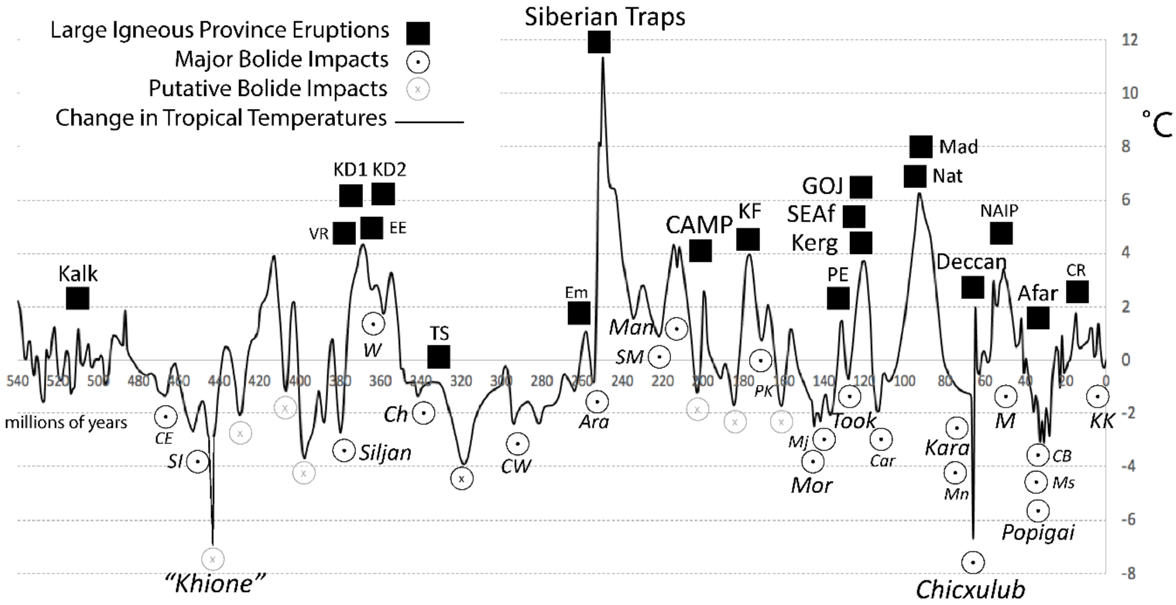

Figure 15. Comparison of the timing of LIPS (black squares, Table 1), large bolide impacts (circles with dots, Table 2), and putative large impact events (light gray circles with x's) with the changes in Tropical Temperature (ΔT°trop). The size of the lettering is roughly proportional to the size of the LIP or bolide imapact. See Table 1 and 2 for abbreviations. Sources: Ernst (2014), Spray (2020).

Table 1 lists 21 of the largest Phanerozoic Large Igneous Provinces (Ernst, 2014; Ernst and Youbi, 2017). They are also plotted as black squares in Figure 15. It is clear from a cursory look at Figure 15 that there is a strong correlation between warm periods and the eruption of LIPs. 19 of the 21 major LIPS fall within periods of global warming. Most notable are the correlation between: 1) the West Siberian Traps and the Permo-Triassic Thermal Maximum (252 Ma); 2) the correlation between the Barremian-early Aptian Warm Period (125 – 116 Ma) and the synchronous eruptions that formed the Greater Ontong Java plateau (Taylor, 2006), the Southeast African oceanic plateaus, and the Kerguelen Plateau; 3) the Viluy rift and the mid-late Devonian Hangenberg Thermal Maximum (375 – 355 Ma); 4) the Karoo-Ferrar LIP and the Toarcian Thermal Maximum (180 Ma) and; 5) the late Paleocene early Eocene Warm Period (58 – 55 Ma) and the eruption of the North Atlantic Igneous Province (NAIP). The one major exception was the East Africa eruptions (Afar LIP) which took place during the period of intense of late Eocene -early Oligocene cooling. Reluctantly, we have excluded the Caribbean LIP (Sullivan et al., 2020) from consideration because the origin of the underlying lithosphere is certainly older (Jurassic?) than the purported age of the LIP (90 Ma), and the age of the surfacing volcanics is not well-constrained.

As has been noted by numerous authors, (Kidder and Worsley, 2010; Wignall, 2001, 2015; Rampino and Self, 2015; Bond and Grasby, 2017; Ernst and Youbi, 2017; Clapham and Renne, 2019; Rampino et al., 2019; McKenzie and Jiang, 2019; Schobben et al., 2019; Suarez et al., 2019), the global warming caused by the eruption of large LIPS has often resulted in mass extinctions. LIP eruptions correlate with extinction events during the middle Cambrian (Kalkarindji, 510 Ma); at the Frasnian-Famennian boundary (Kellwasser extinction, 373-372 Ma); during the latest Devonian (Hangenberg extinction, 359-358 Ma); at the Triassic-Jurassic boundary (CAMP, 201 – 200 Ma); the Toarcian extinction (Karroo – Ferrar LIP, 183 – 181 Ma); the Eocene-Oligocene boundary extinction (Afar- E. African Rift, 31 – 29 Ma); not to mention the two greatest extinction events of all time, the Permo-Triassic Mass Extinction (West Siberian Traps, 252 Ma – 251 Ma) and the K/T Extinction (Deccan Traps, 66 Ma – 65 Ma).

Though the geochemistry of LIP lavas indicate that most LIPS are derived from deep mantle sources, there remains the possibility that a few of the largest LIPS (e.g., West Siberian Traps, CAMP, and the Greater Ontong Java Plateau ; Ernst, 2014; Ernst and Youbi, 2017) may have been produced by extremely large impact events (crater size > 200 km). Any craters produced by these gigantic impact events would probably have been obscured by the subsequent voluminous volcanic eruptions.

3.3 Bolide Impacts

Table 2 lists 29 bolide impact events that generated craters greater than 25 km in diameter (Spray, 2020). Figure 14 illustrates the relative size of these craters and the timing of the impact events.

The amount of energy generated by an impact event is described by the equation (Hughes, 2003; Rampino, 2020):

$E = 9.1 \times 10^{24} D^{a}$, where E = is the kinetic energy of the bolide impact in ergs, and D = the diameter of the resulting crater.

Proposed values for the exponent, a, range from 2.59 (Hughes, 2003) to 3.89 (Melosh, 1989). In either case, it is clear that the energy associated with an impact event correlates with the cube of the impact crater diameter.

The amount of aerosols, SO_4, and particulate matter injected into the atmosphere is primarily a function of the energy associated with the impact event. Whether a bolide lands on continental crust or oceanic crust may also affect the character of the impact event. In either case, the cooling effect of impact events drops off rapidly as the size of the bolide decreases. It has been suggested that after the impact of the bolide that formed the Chicxulub crater (150 km), the global mean temperature would have dropped 7˚ - 12˚ C (Vellekoop et al., 2014). By comparison, the impact event that formed the Manicouagan crater in Quebec, which is approximately half the size of the Chicxulub crater, would have generated only 2.5 ˚C of cooling. Impact events that produce craters that are less than 25 km in diameter cause negligible amounts of global cooling (< 1˚C).

As illustrated in Figure 15, there are remarkable number of Phanerozoic bolide impacts (circles) that coincidentally occurred during periods of major global cooling (18 of 22). The most notable are the Puchezh-Katunki impact (167 Ma, Middle Jurassic Cool Interval), the Morokweng, Mjolnir and Tookoonooka impacts (145 - 128 Ma, Tithonian- early Barremian Cool Interval), and the Carswell impact (115 Ma, Aptian – Albian Cold Snap). Though the timing of these impact events and the periods of cooling appears to be entirely coincidental, we cannot rule out the possibility that these intense, short-lived cooling events may have triggered ice-albedo feedbacks (Park and Royer, 2011) that accelerated cooling processes already underway.

A quick scan of Figure 15 reveals that there are several relatively brief periods of rapid global cooling (-2˚C to -12˚C) that may have been triggered by a bolide impact, but no crater has been associated with these cooling events. This, of course, is not surprising due to the incompleteness of the geological record. The craters that formed during these impact events may have been eroded, tectonically destroyed, or buried beneath a thick pile of sediments. There are no positively identified impact craters in the oceanic basins (Gersonde et al. 1997). Impact events older than 180 million years would have taken place on oceanic crust that has been subducted. Given the proportion of the area of continental crust versus the area of oceanic crust, we would expect that, during the last 540, million years the deep oceans of the Earth were hit by > 20 bolides that could have generated impact craters >50 km in diameter. One or two of these oceanic impacts could have been as large, or larger, than the Chicxulub crater (>150 km).

It is possible that as yet unknown bolide impacts may have caused some of the cooling events shown in Figure 15. The most notable putative impact is the “Khione” impact event which could have triggered the latest Ordovician ice age (444 Ma) and mass extinction (Brenchley et al., 1994; Kump et al., 1999a; Sheehan, 2001; Finnegan et al., 2011). The “Khione” (key-OH-nay) impact event is named after the daughter of the Greek god, Boreas, god of winter. Khione is the goddess of snow. The Hirnantian icehouse is especially interesting because it was very short-lived, yet very intense. Ice sheets extended from the South Pole to a paleolatitude of nearly 35˚S (Boucot et al., 2013). The Hirnantian Ice Age is anomalous because it occurred during a time of relatively high global temperatures (GAT = 20˚ - 22˚ C).

Other putative oceanic impact events may have caused the rapid drops in global temperature that are observed during the early Devonian (Pragian, 407 Ma), latest Triassic (Rhaetian, 203 Ma), early Jurassic (Pliensbachian, 184 Ma), and mid-Oligocene (28 Ma). These speculative impacts are indicated by the gray circles with x’s in Figure 15.

As noted earlier, Figure 15 compares the chronology of LIP eruptions (squares) and bolide impacts (circles) with the changes in global temperature. In Tables 1 and 2 we have estimated the magnitude of the warming and cooling effects of these LIP eruptions and bolide impacts, respectively (Black and Gibson, 2019; Vellekoop et al., 2014; Kamber and Petrus, 2019; Suarez et al., 2019). Large LIP eruptions nearly all have significant warming effects (i.e. several degrees centigrade). The cooling effects of most impacts are negligible. Several impacts were large enough that they should have had a noticeable effect on global temperatures (Sudbury, Popigai, Acraman, and Manicouagan). The Chicxulub impact (K/T boundary) and the putative Khione-type impacts undoubtedly had profound effects on global climate, extinction, and the evolution of life.

3.4 Icehouse Worlds

During the past 720 million years, the Earth's climate has transitioned from a frigid icehouse to a steaming hothouse seven times. Three of these icehouse periods took place during the late Precambrian (the Sturtian icehouse, 720 – 660 Ma; the Marinoan icehouse, 635 Ma; and the Gaskiers icehouse, 585 Ma (Ogg et al., 2016). During icehouse intervals, large permanent icecaps occupied either the northern or southern polar regions, or both. These times of icehouse conditions are recorded by glacial debris and tillites on land, dropstones in adjacent deep sea sediments that were released by melting icebergs, and glendonites in shallow marine environments where the temperature of the bottom waters is within a few degrees of freezing (Boucot et al., 2013).

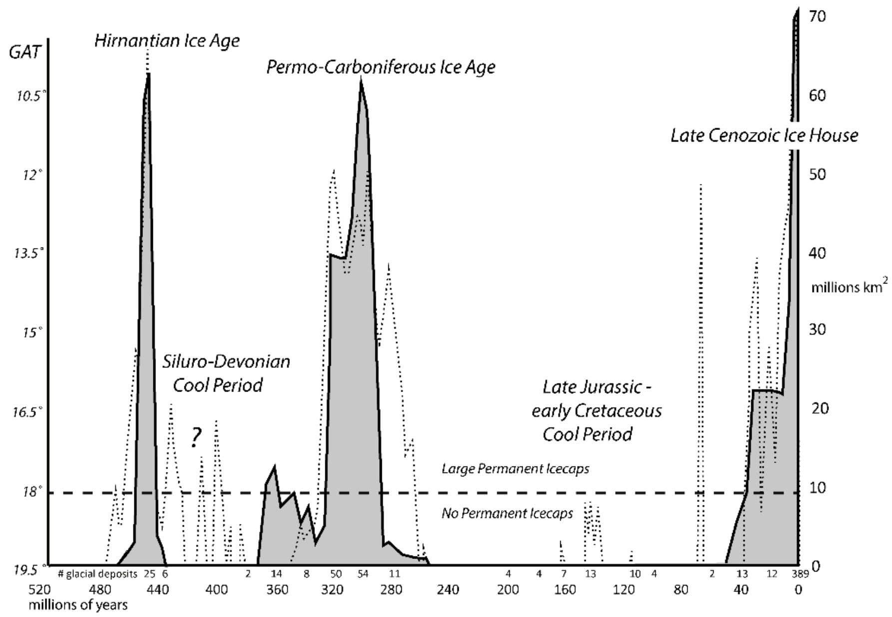

Figure 16. Phanerozoic Ice Ages. gray = global area of snow and ice cover (106 km2), dotted line = snow and ice predicted by Global Average Temperatures (GAT < 18˚C, Figure 12), numbers = number of glacial deposits (tillites, dropstones, and glendonites, Boucot et al., 2013). Note inverted temperature scale (left side).

Figure 16 plots the geological record of tillites, dropstones, and glendonites, as well as the area of permanent ice cover during the Phanerozoic (gray shading). Figure 16 also plots the global average surface temperature (GAT) during these icehouse intervals (dotted line). As expected, there is a good correspondence between the times when there is geological evidence for icehouse conditions and the times when the GAT is below 18˚C (dashed line). Permanent polar ice caps can only form if the global average temperature is less than 18˚C. At that global temperature, the average annual temperature of the polar region (>67 ˚ N&S) is not warm enough during the summer months to melt the winter snow and ice. Without a complete summer thaw, snow and ice can accumulate and large ice caps can grow rapidly. Conversely, a large, permanent polar ice cap cannot form if the average global temperature is greater than 20˚C (68˚F). At that temperature, the average annual temperature of the polar regions is ~7˚C, too warm for a permanent ice cap to form. A transition zone exists when global temperature ranges between 18˚C and 20˚C. Snow and ice will be present during the winter months and patches of permanent ice may develop close to the Pole or at high elevations (>500 m).

The last three major icehouse intervals (Hirnantian Ice Age (450-444 Ma), Late Paleozoic Icehouse (360 – 285 Ma), and the Late Cenozoic Icehouse (45 – 0 Ma) represent 23% of Phanerozoic time. However, the paleotemperature model presented here predicts that there may have been additional time intervals when icecaps may have existed, albeit briefly. If we accept the correlation of temperature and area shown in Figure 16 at face value, then the largest of these icecaps may have been the half the area of East Antarctica (434 – 385 Ma), the smallest icecaps may have been twice the area of Greenland (150 - 111 Ma). Several of these brief icehouse interludes are plausible because they occur during cool (but not frigid) intervals: 1) the Wenlock Cool Interval (434-326 Ma, 2) the Pragian Cool Event (411-406 Ma), (3) the Early-Middle Devonian Cool Interval (401-385 Ma), and 4) the Callovian Cool Event (166-164 Ma), Tithonian-Early Barremian Cool Interval (150-128 Ma). There are sparse, high latitude tillites, dropstones, and glendonites supporting the Jurassic-Cretaceous, and Aptian - Albian cool periods (Boucot et al., 2013). Much of the Siluro-Devonian is considered to be a cool period, but there are no known glacial deposits from this time interval (Boucot et al., 2013).

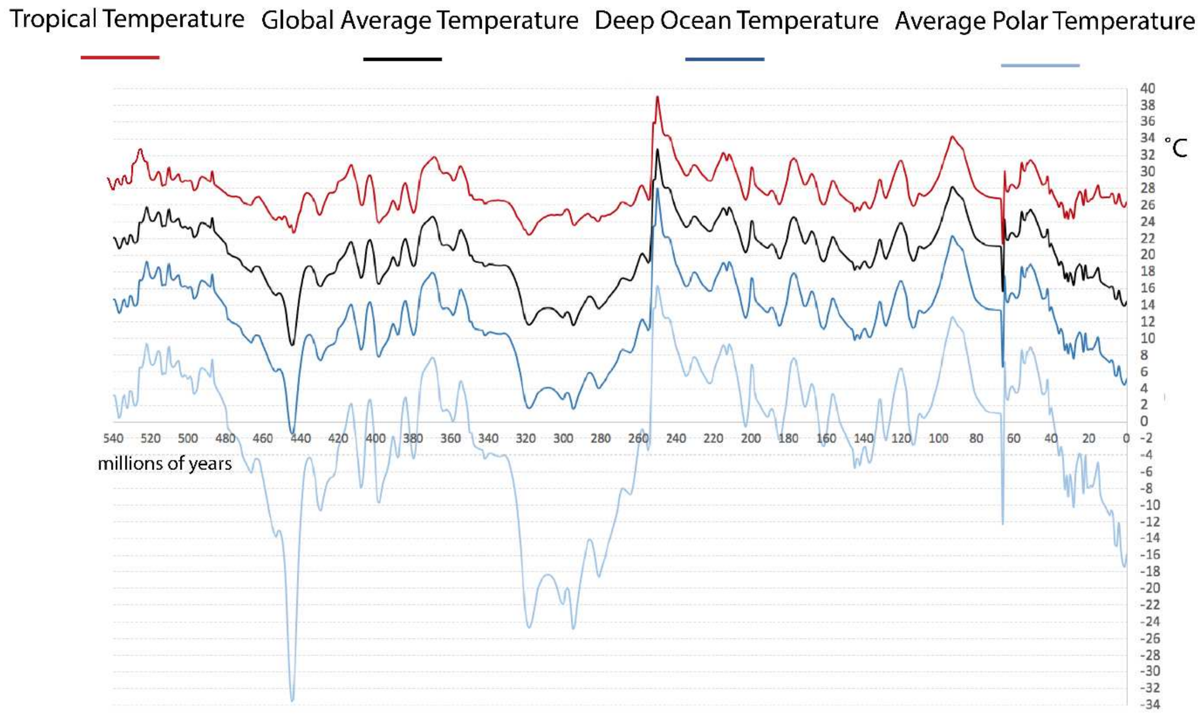

Figure 17. Tropical, Global Average, Deep Ocean, and Polar Temperatures. (a) red line = tropical temperature (15 N - 15 S), (b) black line = global average temperature (GAT), (c) blue line = deep ocean temperatures (after Valdes et al., 2020), (d) light blue line = polar temperature (> 67 N&S).

3.5 Tropical Temperatures

Estimating the Phanerozoic history of tropical temperature is straight-forward. Since we know the change in tropical temperature (ΔT°_{trop}, Figure 10), and the present-day average tropical temperature (26˚C ; Legates and Wilmott, 1990), then the ancient tropical temperature is simply the sum of the present-day tropical temperature (26˚C) and the change in tropical temperature ($\Delta_{trop}T^{\circ}$).

Tropical Temperature = 26˚C + ΔT°_{trop}

For example, the predicted average temperature of the tropical seas during the Paleocene-Eocene Thermal Maximum (55.6 Ma) was 26˚C + 5˚C = 31˚C.

The predicted mean temperature of the tropical seas back to 540 Million years is 28˚C. Tropical temperatures, for the most part, are modeled to have fluctuated between 25˚C and 32˚C (Figure 17), with the exception of two periods of extreme warmth (Permo-Triassic (~39˚C) and Cenomanian-Turonian (~34˚C)) and three intervals of extreme cold (Hirnantian(~23˚C), Permo-Carboniferous Ice Age (~23˚C), K/T impact winter (~22˚C))

3.6 Deep Ocean Temperatures

During hothouse times, the temperature gradient in the oceans is reduced and the temperature of deep ocean waters can be as high as 20˚C (Valdes et al., 2020). During icehouse times, cold bottom-water is produced adjacent to the polar ice caps and this cold, salty water sinks to the depths of the ocean basins and refrigerates the oceans. In the modern world, the cool North Atlantic and North Pacific bottom waters, and the colder circum-Antarctic bottom-waters form at latitudes of 60˚ N&S (Emiliani, 1954). We assume that this is the approximate latitude where cold deep ocean waters would have originated in the past. We realize that factors, such as the formation of warm, hyper-saline bottom-water in the wide epeiric seas of the middle and early Paleozoic (Chamberlin, 1906; Brass et al., 1982) may also played an important role. Though this estimate of deep ocean temperatures is simplistic and imprecise, it generally agrees with the deep ocean temperatures obtained through climate modeling (Valdes et al., 2020).

3.7 Polar Temperatures

Polar Temperatures were calculated by averaging the temperatures in the polar region above 67˚ latitude. The results are shown in Figure 17. For example if the Global Average Temperature (GAT) is 14.5˚C (modern value), then the average temperature of the polar region (above 67˚ latitude) is a very cold -20 ˚C. On-the-other-hand, during a hothouse interval like the PETM, the average polar temperature was above 8˚C (Figure 17).

It seems rather remarkable that the mean temperature of the polar regions back to 540 Million years is~ 0˚C. This implies that the polar regions have hovered between ice-free and ice-covered conditions. Average Polar temperatures, for the most part, have fluctuated between 12˚C and -12˚C, with the exception of three periods of extreme warmth (Cambrian hothouse (~14˚C), Permo-Triassic extinction (~17˚C), and the Cenomanian-Turonian Thermal Maximum (~13˚C)) and four intervals of extreme cold (Hirnantian Ice Age (~-32 ˚C), Permo-Carboniferous Icehouse (~-24 ˚C), the KT Impact Winter (~-30˚C) and Late Cenozoic Icehouse (~-20 ˚C). Throughout most of the Phanerozoic the average temperature of the southern polar region (-4˚C) has been considerably colder than the average temperature of the northern hemisphere (4 ˚C). Only for a brief interval in the Late Permian was the northern hemisphere colder than the southern hemisphere.

3.8 Top Priorities for Future Research

There are several important issues and areas of research that need further investigation, these include: variations in the isotopic record due to insufficient sampling in time and space and the fundamental changes in the Earth System that have driven temperature change.

3.8.1 Insufficient Sampling in Time and Space

As is the case for any geological investigation, due to the incompleteness of the geological record, there are bound to be gaps in the record of isotopic temperature. The temporal record of isotopic measurements compiled by Song is ~80% complete. That is to say, average isotopic temperatures have only been calculated for 400 of the 500 one million years intervals of the Phanerozoic. The data density can be directly viewed in Figure 9. The black dots along the x-axis in Figure 9B are the times for which there are no isotopic temperature measurements. The missing data is not randomly distributed. There are large data gaps during the: late Eocene (36 - 40 Ma), early Albian (110 - 115 Ma), Kimmeridgian -Tithonian (157-143 Ma), Norian (213 – 229 Ma), late Cisuralian (278 - 289 Ma), early Visean (336 - 346 Ma), Emsian (396 – 406 Ma), earliest Devonian (417- 420 Ma), and early and middle Ordovician (455 - 495 Ma). We recommend that these gaps in the data record be priority targets for future research.

The sampling of isotopic temperature measurements is also geographically sparse. Most of the sample sites are highly clustered and there are few sample sites from paleolatitudes above 40° N or S. Though the data set can be accurately characterized as “tropical”, the possibility remains that for some time periods the isotopic samples may be biased either towards the Equator, or away from the Equator. As we saw in the case of the late Pennsylvanian data, it is also important to identify environmental variables such as salinity or ocean circulation that may affect the isotopic temperature. One of our future research goals is to carefully analyze the isotopic temperature database for these kinds of geographic and environmental biases (Judd et al., 2020).

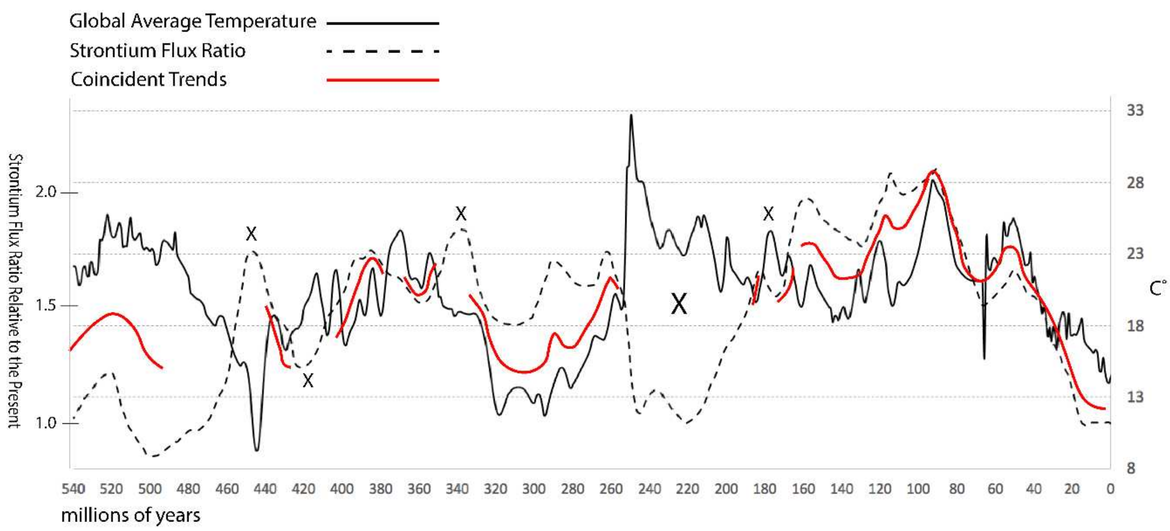

Figure 18. Comparison of Phanerozoic global average temperatures (black line) with strontium flux ratio relative to the present-day flux (dashed line). Red line highlights when the two trends were coincident.

3.8.2 Modeling the Fundamental Causes of Global Temperature Change

Correcting the isotopic artifacts and improving the temporal and geographic sampling of isotopic data are important, but they do not address fundamental questions regarding the ultimate causes of changes in the Earth’s temperature. Long-term changes in temperature (>50 million years) and medium-term changes in temperature (10-20 million years) are primarily driven by the slow and inexorable changes brought on by plate tectonics and continental weathering (van der Meer et al. 2014; Berner, 1994; Brune et al., 2017).

To the first order, the amount of CO_2 released into the atmosphere is proportional to the rates of seafloor spreading and subduction (van der Meer et al., 2014). The isotopic composition of the oceans, in particular the ratio of $^{87}Sr/^{86}Sr$, can be used as a proxy for the rate of sea floor spreading (van der Meer et al. 2017). New ^{86}Sr is introduced into the oceans by the weathering of new basaltic oceanic lithosphere which is rich in non-radiogenic, depleted upper mantle-derived ^{86}Sr. On-the-other-hand, continental sources are richer in ^{87}Sr, which is a decay product of ^{87}Rb.

Faster periods of seafloor spreading introduce more ^{86}Sr into the oceans. This decreases the ratio of ^{87}Sr to ^{86}Sr of seawater. In Figure 18, the non-radiogenic strontium flux ratio (van der Meer et al. 2017) ratio relative to the present (dashed line) is compared to our estimate of Phanerozoic global temperatures (solid line).

There appears to be a remarkably good correlation between the global temperature and non-radiogenic strontium flux. For 65% of the Phanerozoic, when the ratio of $^{87}Sr/^{86}Sr$ in the oceans rose or fell (red line), global temperatures also rose or fell. The correlation is especially good for the last 180 million years (breakup of Pangea) and during the Permo-Carboniferous Ice Age (assembly of Pangea, 320 Ma – 255 Ma). For other time intervals, the isotopic and temperature records are in partial agreement (e.g., Cambrian, 540 – 500 Ma; Devonian – early Carboniferous, 400 – 345 Ma).

However, there are also significant time intervals when the isotopic and temperature record are completely out-of-synch (marked by X's). Most notable are the Hirnantian Ice Age and the Triassic Hothouse. This suggests that there are other factors besides the volcanic degassing of CO_2 that drive global temperature change. E.g. during the Hirnantian Ice Age, a massive bolide impact and subsequent positive ice-albedo feedbacks might have cooled the Earth despite the fact that plate tectonic activity was high at the time. During the Triassic, on-the-other-hand, the increased degree of aridification due to extreme hothouse temperatures (>40˚C) and mega-monsoonal desertification across the interior of Pangea may have slowed down chemical weathering and allowed CO_2 to build up in the atmosphere which increased global temperatures.

We can speculate that other geological processes that occur with rates of change that match the temperature peaks and troughs might also have produced the observed pattern of Phanerozoic temperature change. For example, mountain building and unroofing, periods of ophiolite obduction and subsequent chemical weathering, the opening of oceanic gateways, and some evolutionary events (e.g., the emergence of land plants) all occur on timescales comparable to the rates of change seen in the ΔT°_{trop} curve. A careful and systematic analysis of the evolutionary, paleogeographic, tectonic, paleoceanographic, and environmental changes that may have driven global temperatures will continue to be a fruitful area of research.

Part II. Phanerozoic Paleotemperature Timescale

4. A Phanerozoic Paleotemperature Timescale

The main goal of our research has been to construct a continuous record of temperature change during the last 540 million years (Figures 19-21). In the second half of this paper, we document this record of temperature change with specific paleotemperature events that are analogous to the "golden spikes" (GSSP) of the geological timescale (Gradstein et al., 2012). In some ways, this paleotemperature timescale is similar to the linear magnetic reversal time scale that was assembled at the beginning of the plate tectonic revolution more than 50 years ago. However, instead of normal and reverse magnetic polarity events, the paleotemperature timescale is defined by "warming" and "cooling" temperature intervals called "chronotemps". Our preliminary attempt to identify these warm and cool intervals is illustrated by the cool (black) and warm (white) subdivisions of the global average temperature curve (Figure 19-21).

The Phanerozoic paleotemperature timescale can be subdivided into 24 pairs of warm and cool intervals. It should be noted that the resolution of this version of the timescale is 1 million years; rapid temperature excursions shorter than a million years (e.g. PETM, K/T Impact Winter) are not well-resolved. The cool sections of the temperature timescale are labeled c1 – c24. Some of these cooling events are well-known like the Pleistocene Ice Age (c1) or the Hirnantian Ice Age (c22). Other cool intervals are more speculative (c6, Aptian-Albian Cold Snap) and require further investigation. Similarly, the warm intervals are labeled w1 – w24. Some of these warming events are well-known like the Permo-Triassic Thermal Maximum (w13) and the Toarcian Warm Interval (w9). Other warm intervals are more speculative. Also, there is no strict equivalence between two cool intervals or two warm intervals. Two cool intervals may have very different minimum, maximum, and average temperatures (Tables 3 – 7). The same is true for the warm intervals.

Each warm and cool time interval is illustrated in Figures 19-21 and supporting references are given in Tables 3-7. These tables provide precise information about the name of each interval, the start time and end time, the Tropical Temperature, the Polar Temperature, and the Global Average Temperature (GAT) of each interval, as well as the timing of major LIP eruptions and bolide impacts. Key citations for each chronotemp are also provided. Each interval may contain several discrete short-term temperature events or excursions. For example during the Paleocene-Eocene hothouse (W5, PEH), there were several thermal maxima, the PETM (W5.9, Paleocene-Eocene Thermal Maximum), EETM (W5.6, Early Eocene Thermal Maximum), and METM (W5.1, Middle Eocene Thermal Maximum). Conversely, a few temperature intervals may be grouped into a larger, geologically meaningful temperature interval; for example, the Late Paleozoic Icehouse (C13-C17) consists of the cool intervals: C13 (Late Permian Cooling), C14 Mid-Permian Cool Interval, C15 (Permo-Carboniferous Icehouse), C16 (Early Mississippian Cooling), and C17 (Famennian-Earliest Tournaisian Ice Age), as well as the intervening warm intervals.

We have tried to standardize the names and abbreviations used to describe the various chronotemps depending on the length of a temperature event (icehouse, ice age, cool interval, cool event), its magnitude (e.g. thermal maximum, glacial maximum), or if the chronotemp represents a transition between warm or cool time intervals (e.g. warming or cooling). Often discrete temperature intervals are connected by prolonged periods of warming or cooling (e.g Eocene-Oligocene Transition). We have used a gray scale gradient in Figures 19-21 to schematically represent the rate of cooling or warming.

We do not use the term “climate” as part of the naming convention to avoid confusion with broader climatic considerations (i.e., precipitation, temperature gradients, equability, etc.), and have avoided the use of other somewhat pejorative terms such as “optimum”. Also, whenever possible we have used a specific stage name (e.g., Cenomanian-Turonian Thermal Maximum) rather than a more generic geological description (e.g., Cretaceous Thermal Maximum). We also prefer the term “interval” rather than “period” because of the geological connotation of the latter term. “Events” tend to be temperature phenomena that last only a few million years or less. “Excursions” are events that depart from the norm, i.e, a warm event during a cool interval.

Unfortunately, in our attempt to rationalize and standardize the naming conventions, older more established names that have precedence have been mostly discarded (e.g., the Mid-Miocene Climatic Optimum (MMCO) has become the Middle Miocene Thermal Maximum (MMTM).

What are the advantages to dividing the timescale into discrete temperature events and giving each of them a number and a name? Some may argue that our state of knowledge is still too primitive and that attempting to build a paleotemperature timescale is premature. We would argue that by constructing a paleotemperature timescale, even if this first version is imperfect, we now have a structure that can be built upon, refined, corrected, and expanded. Also having a paleotemperature timescale is essential if we are to understand the tempo and mode of climate change during Earth history. By characterizing, in a quantitative way, the pattern of paleotemperature change through time, we may be able to gain important insights into the history of the Earth System and the fundamental causes of climate change.

5. Climate Modes of the Phanerozoic

5.1 Introduction

In this section we will review the evidence used to construct the Phanerozoic Paleotemperature Timescale (Tables 3-7, Figures 19-21). The 24 pairs of warm and cool temperature intervals listed in Tables 3-7 can be grouped into eight distinct “climate modes” (after Frakes, 1989; Frakes et al., 1992; Vaughan, 2007). Four of these climatic groups represent four warm periods in Earth history (Cambro-Ordovician, Siluro-Devonian, Triassic, and mid Cretaceous-Paleogene), three climatic groups represent cold periods in Earth History (Late Ordovician-Silurian, Late Paleozoic, and Late Cenozoic), and one “cool” period made up of mixture of cool and warm intervals (Jurassic – early Cretaceous). These warm and cool modes are similar to the eight warm and cool modes outlined by Frakes et al., (1992). The only major differences are: the Famennian/Tournaisian Ice Age is included in the Late Paleozoic Icehouse, the early Mesozoic warm mode includes only the Triassic, and the Jurassic – Early Cretaceous Cool Period includes the entire Jurassic. The average global temperature during the cool climate modes is 16 ˚C, the average global temperature during the warm climate modes is ~20˚C, and the average temperature during the mixed or mild mode is 17.5˚C which is close to the average temperature of the Phanerozoic (18˚C). It should be noted that the global temperatures during these climatic modes are not entirely warm or entirely cool, but rather alternate between relatively cooler and relatively warmer times.

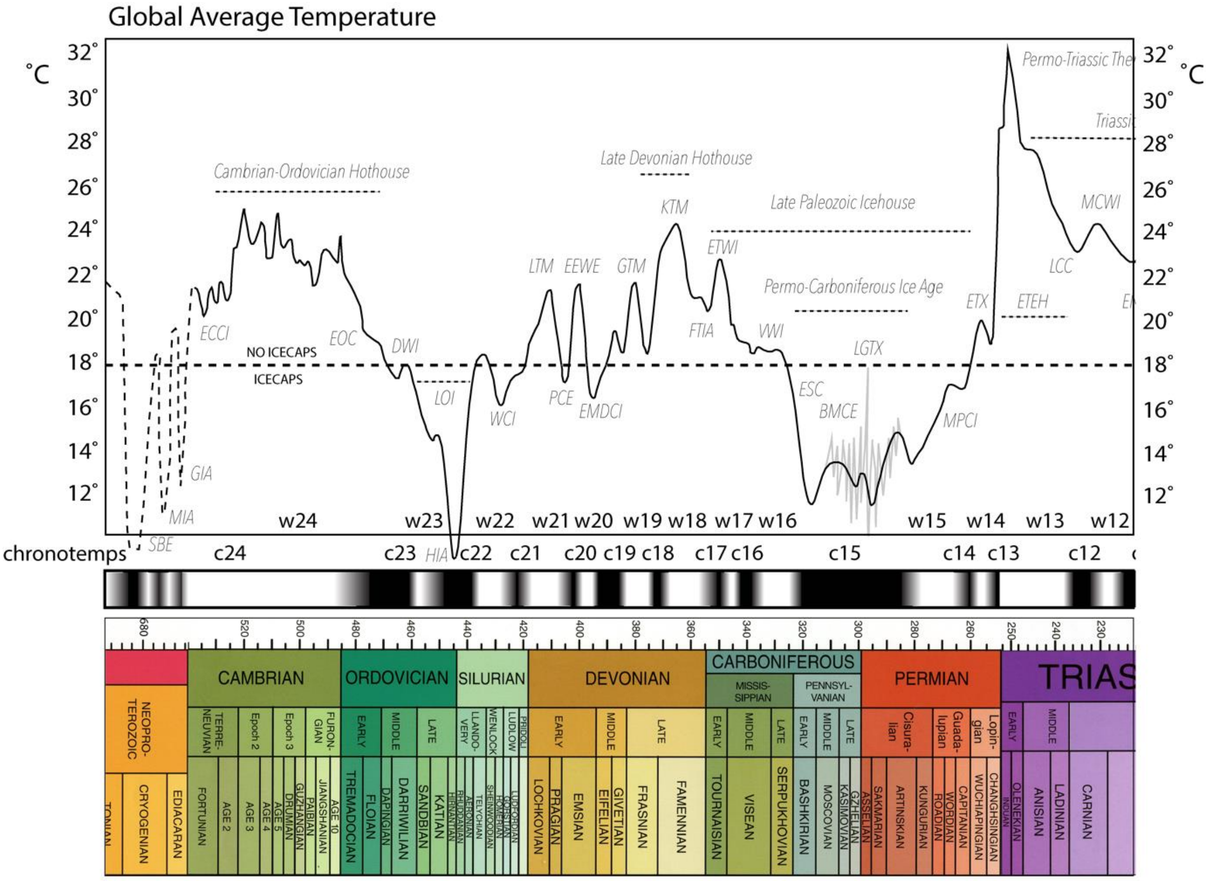

Figure 19. A Paleozoic Paleotemperature Timescale. white = warm time intervals, black = cool time intervals. Solid black line = Global Average Temperatures (GAT), < 18˚C = large permanent, icecaps, > 18˚C = no large, permanent icecaps. Light gray jagged lines = a schematic representation of >50 glacial/interglacial cycles during the Permo-Carboniferous. Timescale = International Chronostratigraphic Chart v2020/01. Refer to Table 3 for more information and sources of data for each chronotemp and abbreviations.

5.2 Cambro-Ordovician Hothouse (W23 – C24, 458–541 Ma), Table 3, Figure 19

The Cambro-Ordovician warm climate mode starts at the base of the Cambrian (541 Ma) and extends through most of the Ordovician (late Darwillian, 458 Ma). Global temperatures were highest during the Cambrian and cooled during the early Ordovician. There is uncertainty regarding the maximum temperatures during the Cambrian because the interpretation of early Paleozoic $\partial^{18}O$ values remains controversial.

Measurements of the isotopic composition of early Paleozoic seawater are enriched in the lighter isotope of oxygen (^{16}O). This apparent enrichment has given rise to two explanations: 1) the composition of seawater has become systematically enriched in the heavier isotope of oxygen (^{18}O)

through time (Kasting et al., 2006; Jaffres et al., 2007) or 2) the composition of seawater has remained constant (Henkes et al., 2018) and therefore the lighter $\partial^{18}O$ values accurately reflect warmer paleo-temperatures during the early Paleozoic and late Precambrian. Recent studies of the $\partial^{18}O$ composition of Precambrian oceans suggest that the composition of seawater has been systematically enriched in the heavier isotope of oxygen (^{18}O) (Galili et al., 2019; Hodel et al., 2018) and therefore, isotopic temperatures for the Early Paleozoic and late Precambrian may be in error.

The proponents of the "hot" early Paleozoic temperature model suggest that prior to the Darwillian, tropical sea surface temperatures were 8˚ - 10˚ warmer than modern tropical sea surface temperatures. This interpretation is supported by clumped isotope estimates of tropical paleotemperatures for the late Precambrian (>50˚C; Bergmann et al., 2018a), late Cambrian (32˚C), early Ordovician (36˚C), and middle Ordovician (~40˚C; Bergman et al., 2018b; Henkes et al., 2018). Measurements of $\partial^{18}O$ from pristine, phosphatic euconodont fossils from England give temperatures of 20˚ - 25˚C for near polar latitudes (>70˚S, Hearing et al., 2018). The equivalent temperature at tropical latitudes would have been > 40˚C. According to "hot" model, temperatures would have exceeded 50˚C during the latest Precambrian (Ediacaran; Bergmann et al., 2018a; see Figure 5).

The "cool" early Paleozoic temperature model proposes that Cambro-Ordovician tropical temperatures were only modestly elevated (28˚ - 32˚C) in comparison to modern average tropical sea surface temperatures (26˚C) and that cool temperate conditions (4˚ -12˚C) prevailed near the poles (Figure 17). This interpretation is consistent with the occurrence of bauxites (Boucot et al., 2013) and "Bahamian-type" carbonates at low latitudes and the restriction of archaeocyathid reefs to tropical and subtropical latitudes (McKerrow et al., 1992). During the early Paleozoic, temperate and polar latitudes were characterized by clastic facies with strata containing unweathered mica flakes indicative of cooler temperatures (Boucot et al., 2013). The late Cambrian and early

Ordovician world was latitudinally subdivided into four distinct trilobite provinces - Bathyurid, Dikelokephalinid, Ptychopygine/Megalaspid, and Calymenacean-Dalmanitacean (Cocks and Fortey, 1990; McKerrow et al., 1992) - indicating a moderate pole-to-equator temperature gradient. Landing et al. (2020) also noted that trilobites first appeared in the warm shelf environments of Siberia and Laurentia and later spread to the cooler, higher latitude waters of Baltica and Gondwana. In the "cool" temperature model, global temperatures increased during the middle and late Cambrian as the continental cratons were flooded and the resulting decrease in the planetary albedo warmed the Earth (Landing and Westrop, 2004; Landing, 2012).

Temperatures continue to fall during the middle Ordovician (Trotter and Barnes, 2008). Trotter and Barnes (2008) proposed that sustained, cooler tropical temperatures (26˚-30˚C) provided a more hospitable environment for evolutionary innovation and may have been the impetus for the Great Ordovician Biodiversification Event (GOBE; Webby et al., 2004).

As noted earlier (section 3.1.2.1), the ~2˚ temperature fluctuations during the Cambrian shown in Figure 19 are speculative. They coincide with 10 proposed Cambrian $\partial^{13}C$ isotopic excursions (Zhu et al., 2006). It should be noted that the global synchroneity of some of these excursions (in particular TOCE and REOCE) has been disputed (Landing, personal communication). The covariance of $\partial^{13}C$ and $\partial^{18}O$ trends has long been noted (Wenzel and Joachimski, 1996; Jenkyns et al., 2002). Approximately 80% of the positive $\partial^{13}C$ excursions are correlated with warmer temperatures (hyperthermals). The correlation is generally attributed to the causal relationship between higher ocean temperatures, the formation of deep water anoxia, and the subsequent preservation of organic carbon.

5.3 Late Ordovician – Silurian Icehouse (C21 – C22, 426-458 Ma), Table 3, Figure 19

The most spectacular, short-term cooling event of the Phanerozoic is the Hirnantian Ice Age (445 – 441 Ma; Brenchley, et al., 1994; Sheehan and Coorough, 1990; Sheehan, 2001; Finnegan et al., 2011). Whether the Hirnantian Ice Age (C22) was preceded by a prolonged, stepwise cool-down is still debated. Biostratigraphic (Brenchley et al., 1994) and geochemical data (Finnegan et al., 2011) indicate that the maximum glacial advance was very short-lived (less than one million years; Ling et al., 2019). The repercussions of the Hirnantian Ice age were felt worldwide and left indelible signatures in the geochemical, paleontological (Sheehan and Coorough, 1990; Finnegan et al., 2012), and sedimentary rock record .

The widespread occurrence of latest Ordovician tillite deposits (Beuf et al., 1971; Boucot et al., 2013) indicates that ice sheets covered ~50% of Gondwana and extended to latitudes of ~35 S. The enormous extent of snow and ice cover increased the Earth's albedo and triggered ice-albedo feedbacks that rapidly cooled the Earth. The asymmetric latitudinal disposition of the Earth's land masses during the late Ordovician, namely the fact that no large continents occupied the northern hemisphere, probably prevented the Earth from slipping into another "Snowball Earth". Only thin sea-ice accumulated on the freely circulating, open northern oceans. This meant that during the late Ordovician, the northern hemisphere remained relatively warm and prevented a runaway Snowball Earth-like global freeze.

Multiple explanations have been proposed for the cause of the Hirnantian Ice Age. Crowley and Baum (1991, 1995) suggested that the growth of the Gondwana ice cap was facilitated by the combination of increased precipitation and cold temperatures along the northern margin of Gondwana. Other authors have invoked increased chemical weathering of young mountains (Taconic ranges) or recently obducted ophiolites that lead to a drawdown in atmospheric CO_2, which promoted globally cooler temperatures (Kump et al., 1995, 1999b,c; Swanson-Hysell and Macdonald, 2017; Landing, 2018). This effect may have been enhanced by the evolution of simple, non-vascular land plants (Lenton et al., 2012).

A more spectacular explanation, as discussed in section 3.3, is that the Hirnantian Ice Age was triggered by a bolide impact as large or larger than the Chicxulub impact. There is no geologic record of this massive impact on the continents. Though the impact site may be buried under younger continental strata, it is more likely that the Khione impact targeted the late Ordovician ocean basin and that the impact crater was subsequently subducted. This hypothesis was first proposed in 1986 by Kent Colbath who noted the rapid extinction of tropical acritarch genera in the southern Appalachian basin and their subsequent replacement with more cosmopolitan taxa in the earliest Silurian. The extinction of warm, shallow water tropical faunas during the latest Ordovician and their replacement by cool-water benthic taxa or cosmopolitan planktonic taxa has been confirmed by numerous other studies (Sheehan, 2001). The Hirnantian extinction event ranks second in terms of taxonomic severity (~46% marine genera extinct). Only the Permo-Triassic Extinction (58% marine genera extinct; Sepkoski, 1996; Bambach et al., 2004) was more cataclysmic.

Though some snow and ice in the polar regions of South America (central Brazil and Bolivia) lingered into the earliest Silurian (Grahn and Caputo, 1992; Grahn and Gutierrez, 2001; Díaz-Martínez and Grahn, 2007), rapid warming during the Llandovery (W22) was followed by a period of slow ecological recovery. The remainder of the early-middle Silurian was characterized by a moderate pole-to-equator temperature gradient which was cool by early Paleozoic standards but warmer than today's world (Moore et al., 1994). Most early and middle Silurian tropical taxa were widely distributed (i.e., cosmopolitan) with the exception of the high latitude, cool-water brachiopods, Clarkeia (southern hemisphere; Boucot, 1990; Benedetto and Sanchez, 1996) and Tuviella (northern hemisphere; Cocks, 1972). Three carbon isotopic excursions occurred during the middle and late Silurian. Two of these excursions (Ireviken and Mulde) bracket the Wenlock and may have been caused by the growth of ephemeral, south polar ice caps (Brand et al., 2006).

5.4 Siluro-Devonian Hothouse (W18 – W21, 365-426 Ma) Table 4, Figure 19

The late Silurian through late Devonian hothouse includes four warm intervals (W21 – W18) separated by three relatively cool episodes (C20 – C18). There is no geological evidence for permanent polar icecaps during any of the cool intervals (Boucot et al., 2013). The following summary of the Siluro-Devonian warm mode is based on the isotopic evidence summarized by Joachimski et al. (2009), the biogeographic information synthesized by Stock (2005), the lithologic indicators of climate assembled by Boucot et al. (2013), and a comprehensive synthesis of the Frasnian-Famennian crisis by Racki (2020).

The Siluro-Devonian Warm Interval spans the early Ludlow to early Lochkovian time interval (Joachimski et al., 2009; Munnecke et al., 2010; Trotter et al., 2016). It is followed by a pair of brief cooling and warming events during the Pragian (C20) and early Emsian (W20), respectively. The Pragian Cool Event coincides with a widespread fall in sea level (~100m) during the earliest Devonian and the resulting unconformity marks the end of the Tippecanoe Supersequence. This fall in sea level is seen on most continents, but is especially prominent on North America (Schuchert, 1910, 1955; Sloss, 1963).

After a brief warming event in the early Emsian, temperatures continued to fall during the remainder of the Emsian and into the middle Devonian (Eifelian – middle Givetian; Joachimski et al., 2004, 2009; van Gelderin et al., 2006). The Early-Middle Devonian Cool Interval (C19, GAT = 18.7˚C) was followed by a brief, rapid rise in temperature during the late Givetian (W19, Givetian Thermal Maximum, GAT = 21.2˚C). Late Givetian warming coincided with the Taghanic onlap (Brett et al., 2009), the start of a global transgressive cycle that would culminate with the highest sea level of the Paleozoic (late Frasnian; Haq et al., 1987; Haq and Schutter, 2009). Global temperatures cooled briefly during the early Frasnian but rose steadily through the remainder of the Frasnian, culminating in the Kellwasser Thermal Maximum (W18.2, 372.5 Ma). A recent synthesis of Frasnian and Famennian isotopic, paleontologic, and tectonic information (Racki, 2020) provides numerous detailed insights into the paleoclimatic events that took place across the Frasnian-Famennian boundary.

According to Racki (2020), the Kellwasser Event, also known as the Frasnian-Famennian Extinction Event, can be subdivided into two pairs of rapid warming/cooling events. The first event, the Early Kellwasser Event (373 Ma), may have been triggered by the eruption of the Vilui and Kola LIPS (see Table 1). Shortly thereafter, continued volcanic eruptions (Pripyat-Dneiper-Donets LIP) triggered a second episode of rapid warming and cooling (Late Kellwasser Event; 372 Ma). An alternate hypothesis invoking a bolide impact has also been proposed (McLaren, 1970, 1983). The combined Kellwasser Extinction Event was the fourth most severe extinction event when measured in terms of ecological severity (McGhee et al., 2013). It is associated with highest sea level of the Paleozoic (Johnson, 1988; Johnson et al., 1985; Sandberg et al., 2000) as well as with a dramatic increase in $^{87}Sr/^{86}Sr$ composition of seawater (Zhang et al., 2020). For a more detailed account of the Frasnian-Famennian Extinction Event see McGhee(1996, 2005), Racki(2005), and Sandberg(2000, 2002).

The isotopically inferred temperature events outlined above are in good agreement with the paleoclimatic conditions inferred from paleobiogeography and lithologic indicators of climate. According to Boucot et al. (2013), the global climatic gradient during the Early Devonian through to the Eifelian was “moderate”, resulting in cool but not freezing temperatures in temperate latitudes. Like much of the earlier Paleozoic, the high southerly latitudes of Gondwana were characterized by an exclusively clastic facies with unweathered mica flakes and a distinctive cool-water fauna (Malvinokaffric province). Conodonts (Girard et al., 2005) and reef-like stromatoporoids (Stock, 2005), which preferred warm waters, were absent from the cooler, temperate shallow seas of central and southern Gondwana. Global temperatures warmed in the Givetian and Frasnian; and the Malvinokaffric province was eliminated, replaced by warmer water faunas. Faunas at low latitudes became less endemic and more cosmopolitan (Stock, 2005). Temperatures continued to warm throughout the Frasnian and Famennian, until the onset of the Late Famennian Ice Age (discussed in the next section).

5.5 Late Paleozoic Icehouse (C13 – C17, 253-365 Ma) Table 4, Figure 19

Spanning more than 100 million years, the Late Paleozoic Icehouse was the longest interval of cold climates during the Phanerozoic. Polar ice existed, more or less continuously, at either the South or North Poles with the exception of brief warming events during the Mississippian (Tournaisian and Visean Warm intervals, W17 and W16, respectively), latest Pennsylvanian (Latest Gzhelian Thermal Excursion, C15.3,) and late Permian (Emeishan Thermal Excursion, W14). Global average temperatures ranged from 13˚C during the depths of the Permo-Carboniferous Ice Age to ~22˚C during the Early Tournaisian Warm Interval, the warmest time period during the Carboniferous or Permian.

The Late Paleozoic Icehouse began in the latest Devonian with the formation of a short-lived, medium-sized south polar icecap (Caputo et al., 2008). This ice cap, centered in Brazil, stretched from the proto-Andean mountains, eastward to Rio de Janeiro and Gabon, and northeastward into equatorial west Africa and Niger. The Famennian Ice Age (C17) lasted less than 5 million years and is correlated with the widespread extinction of marine faunas. This late Devonian extinction event ranks fourth in terms of taxonomic severity (50% genera lost; McGhee et al., 2013).

During the early Mississippian (Tournaisian), global climate first warmed (W17), then cooled dramatically (C16; Grossman et al., 2008). Throughout the remainder of the Mississippian, Gondwana moved steadily northward across the South Pole. Ice sheets contracted, then expanded, moving southward into south-central Argentina. The south polar ice cap nearly vanished during the Visean Warm Interval (W16), retreating to the highlands of the proto-Andes of Bolivia and western Argentina, as well as into the remnants of the Pan-African mountain ranges in southeastern Brazil and southwest Africa (Fielding et al., 2008).

These latest Devonian and Mississippian machinations were just a prelude to the impending Permo-Carboniferous Ice Age (313 – 291 Ma.) Beginning in the early Serpukhovian (latest Mississippian, 330 – 326 Ma), the world began to cool once again. However, this time it would remain cool, with Global

Average Temperatures (GAT) less than 18˚C for nearly 80 million years. Starting in the earliest Pennsylvanian (Bashkirian, 323.2 Ma), a large ice cap began to develop at the South Pole and grew equatorwards reclaiming the southern reaches of the Amazon basin, crossing south-central Africa, and extending across Antarctica and most of Australia (Mory et al., 2008). Though often portrayed as a single, large Ice sheet (Scotese et al., 1999), the South Polar Ice Cap was actually composed of several growing, glacial nuclei (Fielding et al. 2008, 2010; Montañez and Poulsen, 2013) that coalesced and expanded equatorwards reaching latitudes of 35˚ south by the mid-Pennsylvanian (315.2 Ma, Moscovian).

Beginning in the early Moscovian (~313 Ma), the growing South Polar Ice Cap began to rhythmically wax and wane in synchrony with the changes in the shape of Earth's orbit (Milankovitch cycles; Milankovitch, 1920; Kump et al., 1999b; Hay, 2016) that regulated the amount of solar energy received by the Earth. The expansion and contraction of the South Polar Ice Cap caused cyclical changes in sea level. Paired transgressions and regressions, separated by ~400,000 years, pulsed across the broad, flat continental cratons generating more than 55 repeating sedimentary packages called "cyclothems" (Wanless and Weller, 1932). Cyclothems have been mapped across the mid-continent of North America (Illinois and Mid-Continent Basin; Heckel, 2013) and, to a lesser extent, the Appalachian basin. Cyclothems have also been identified in similar aged rocks in Donets Basin of the Ukraine (Montañez et al., 2007; 2016).

The cyclothems are direct evidence of Permo-Carboniferous glacial-interglacial cycles (Wanless and Shepherd, 1936; Heckel, 1994, 2008; Montañez and Poulsen, 2013) and are identical in nature to glacial-interglacial sedimentary sequences deposited during the Pleistocene Ice Age (C1.3). The oldest cyclothems in the mid-continent are middle Pennsylvanian in age (Desmoinesian /early Moscovian, ~313 Ma; Heckel, 2013). During one particularly warm interglacial episode, the Latest Gzhelian Thermal Excursion (C15.3), global temperatures may have warmed sufficiently to have temporarily reduced or eliminated the South Polar Ice Cap (Davydov et al., 2010). However, whatever the cause, the warmth did not last and glacial-interglacial cycles resumed in earnest. The youngest cyclothems are early Permian in age (late Sakmarian, 291 Ma). Cyclothems bracket the coldest phase of the Permo-Carboniferous Ice Age (C15.2, GAT = 13˚C) and disappear shortly after the Permo-Carboniferous Glacial Maximum (C15.1, 299 – 293, early Asselian – early Sakmarian; Montañez and Poulsen, 2013).

The deep oceans were "refrigerated" during much of the Carboniferous and early Permian (Valdes at al., 2020). Cold bottom-waters generated by the seasonal melting of the South Polar Ice Cap filled the oceans with near-freezing waters from the bottom up. Along some continental margins, this cold bottom-water was carried to the surface by upwelling. Glendonites formed in shallow marine sediments where the temperatures were < 4˚C (De Lurio and Frakes, 1999). Glendonites occur in association with the shallow water carbonates of the Rundle Group of western Canada which was located near the equator during the Visean (Brandley and Krause, 1994). At south polar latitudes, numerous glendonites are found in fine-grained clastic sediments deposited along the margins of Gondwana (Boucot et al., 2013). In addition, the thermal continuity of these cool shelf and deep shelf environments allowed early Permian marine faunas to migrate freely between cool temperate southern latitudes, across the tropics, and into cool temperate northern latitudes (Waterhouse and Shi, 2013; Shi, 2001).

By the middle Artinskian (285 Ma), global temperatures had warmed (W15) signalling the end of the Permo-Carboniferous Ice Age (Ziegler et al., 1997). Though the large South Polar Ice Cap was gone for good, intermontane glaciers inhabited the highlands of eastern Australia, the Trans-Antarctic Ranges of Eastern Antarctica (Frank et al., 2015), and the far northern, mountainous reaches of Siberia until the end of the Permian.

Though the coldest portion of the Late Paleozoic Icehouse was over, the Permian remained a "cool" world, with a moderate pole-to-equator temperature gradient (.75˚C per 1 degree of latitude). An exception was the Emeishan Thermal Excursion (W14), which occurred 260 million years ago during the late Capitanian. As the name implies, this brief thermal excursion was the result of the eruption of the Emeishan flood basalts in southwestern China (Ernst, 2014; Rampino and Shen, 2019). The Emeishan eruption was precursor to the much more massive West Siberian eruptions that would end the Late Paleozoic Icehouse, terminate the Paleozoic Era, and cause the greatest extinction event of all time (Erwin, 1993, 1995, 2006).

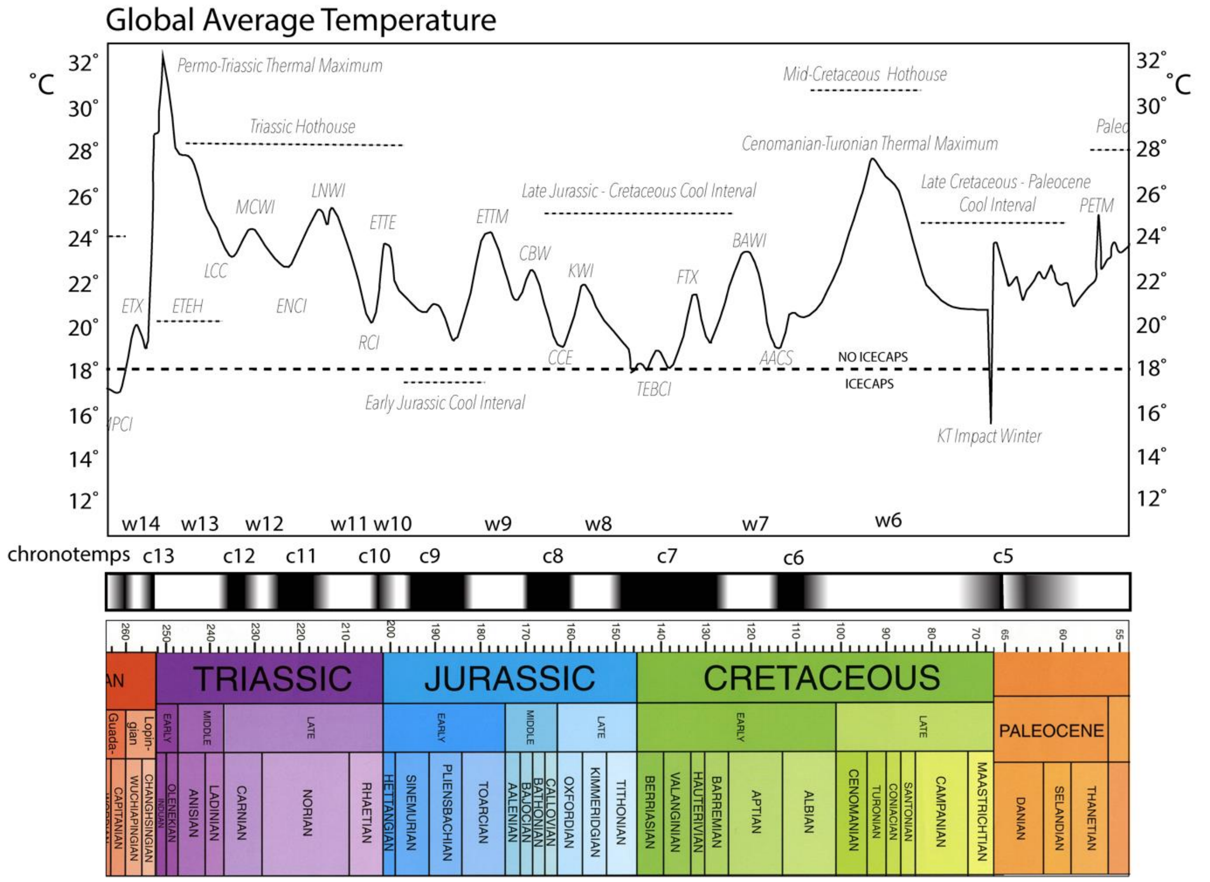

Figure 20. A Mesozoic Paleotemperature Timescale. white = warm time intervals, black = cool time intervals. Solid black line = Global Average Temperatures (GAT), < 18˚C = large, permanent icecaps, > 18˚C = no large, permanent icecaps. Timescale = International Chronostratigraphic Chart v2020/01. Refer to Table 3 for more information and sources of information for each chronotemp and abbreviations.

5.6 Triassic Hothouse (W10 – W13, 253 – 199 Ma), Table 5, Figure 20

At the beginning of the Mesozoic Era, the Earth was an extreme hothouse world with average tropical temperatures approaching 40˚ C. It now widely accepted that the extreme global warming the ended the Late Paleozoic Icehouse was caused by the voluminous eruption of the West Siberian Large Igneous Province (LIP)(Ernst, 2014). During a brief interval (~ 1 million years) at the Permo-

Triassic boundary (252.1 Ma; Kamo et al., 2003), more than 15 million km^3 of basaltic lava flowed from rifts beneath the West Siberian basin (Reichow et al., 2005, 2009; Saunders et al., 2005) and the Putorana and Tunguska plateaus. This outpouring buried more than 50% of Siberia (7 million km^2) under a mantle of basaltic lava 1-4 km deep (maximum 6.5 km). The primoridial, mantle-derived CO_2 released by these eruptions was supplemented by additional CO_2 derived from the combustion of thick, buried coal deposits (late Carboniferous – early Permian) that lay along the subterranean path of the erupting volcanics. The Permo-Triassic Mass Extinction is marked by a $\partial^{13}C$ spike (Gruszczynski, et al., 1989; Grossman, 1994; Scholle, 1995).

The combined primordial and coal-derived CO_2 (~5000 gigatons) more than doubled atmospheric levels of CO_2. As a result, tropical temperatures surged from ~25˚C prior to the eruption to nearly 40˚C. This "Super Hothouse" global warming parched life on land and led to the formation of an anoxic "Strangelove" ocean (Hsu et al., 1985; Kump, 1991; Hotinski et al., 2001; Zhang et al., 2001; Grice et al., 2005; Heydari et al., 2008).

As the atmosphere warmed rapidly, the greatest effect was felt near the poles. The cold polar air masses warmed and the cold surface waters at high latitudes, which were the oceanographic engine that had previously filled the Late Permian oceans with cold oxygenated bottom water, began to warm and the engine stalled. As the oceans warmed, they became stratified and began to stagnate. Organic carbon accumulated in the deep ocean, using up any available oxygen. Anoxia set in (Song et al., 2014). The first ocean to become anoxic from top to bottom was the landlocked PaleoTethys Ocean (Wignall and Hallam, 1992; Şengör and Atayman, 2009). The NeoTethys soon became anoxic; the deeper more isolated portions of Panthalassa (between the Panthalassic mid-ocean ridge and western North America, -were the last to become toxic. The poisonous waters from PaleoTethys, NeoTethys, and Panthalassa spilled onto the shelves and the Late Permian benthic, neritic, and planktonic fauna began to die out. The oceans belched great volumes of CH_4 into the atmosphere and the level of atmospheric oxygen fell. As temperatures rose even higher, the food chain collapsed and many complex marine ecosystems were wiped out forever.

On land the conditions were just as extreme. The equatorial regions baked. Average summer temperatures in the subtropical regions of Pangea exceeded 40 degrees C. Near the poles, temperatures were warm and seasonal changes were nearly eliminated. The movement of warm air masses and ocean currents into the polar regions made any attempt at winter cooling impossible. The interior of Pangea, 1000's of kilometers distant from any source of water, was an intolerably hot, abiotic desert.

A few isolated habitats may have been refugia from the killing heat. Mountains that poked up into the westerly trade winds still received abundant rainfall during the winter months. The young peaks of the Cape Mountains in South Africa, where our burrowing mammal-like reptilian ancestors clung to life, was such a refugia. In the oceans, species that could tolerate the warmer sea surface temperatures or that could retreat to the cooler, deeper environments on shelf-edge and slope, also survived. Most importantly, some species that were able to reproduce rapidly and (e.g. microgastropods) were able to take advantage of the favourable conditions that sporadically appeared.

The Permo-Triassic Mass Extinction dwarfs all other mass extinction events. During the Permo-Triassic Mass Extinction, 57% of all marine families went extinct (Sepkoski, 1989), and an estimated 96% of all marine species were extinguished (Raup, 1979), though time percentage has been revised downwards to 81% by Stanley (2016). At the individual level, this means that 90 - 99% of all living things were wiped out. The Permo-Triassic Mass Extinction killed more species in low latitudes and led to a reduced latitudinal diversity gradient in the Early Triassic (Song et al., 2020). Though the extinction event appears to be geologically "instantaneous" for most taxonomic groups (especially brachiopods, bryozoans, crinoids, tabulate and rugose corals), arguments have been made that other taxa were already in decline (e.g. trilobites, graptolites, conodonts). For these "perched" fauna, the massive warming event was the coup de grace.

Details of the rapid rise and fall of temperatures during the Early Triassic (252-247 Ma) have been described by Sun et al. (2012). The Early Triassic Extreme Hothouse (W13) was not a single spike, but rather a series of ups and downs. The Permo-Triassic Thermal Maximum (W13.4, 253-251 Ma) was followed by a 4˚C fall in temperature (W13.3, Dienerian Cooling, 251-249 Ma), a 6˚C rise in temperature (W13.2, Latest Smithian Thermal Maximum, 249-248 Ma), and finally a 6˚C fall in temperature by the end of the Early Triassic (W13.1, Latest Olenekian Cooling, 248-247 Ma).

The severity of the extinction event is revealed by subsequent "gaps" in the fossil record. Plants and animals were not able to quickly re-establish the complex ecosystems that prevailed before the extinction event. There are no significant coal deposits (i.e. no complex rainforest ecosystems) until 20 million years after the mass extinction event ("coal gap"; Veevers et al., 1994; Looy et al., 1999). The Permo-Triassic Mass Extinction Event wiped out diverse tropical and temperate rainforest flora. It is interesting to note that the forests and scrublands were replenished by a new stock of plants (pteridosperms and conifers) that evolved from xerophytic ancestors (Zechstein flora) that were "pre-adapted" to the hot, dry conditions that prevailed in the Early Triassic (Looy et al., 1999; Hochuli et al., 2010).

In the early Triassic oceans, there were similar reef and chert “gaps”. In the shallow marine seas and on far-flung oceanic atolls, there were no coral reefs (Stanley, 2003). Reef ecosystems did not become re-established until the Middle Triassic (Ladinian), approximately 14 million years after the Permo-Triassic mass extinction wiped out tabulate and rugose corals (Flügel, 2002). These new reefs were built by a new type of coral animal (scleractinians) whose Permian ancestor was a soft-bodied "anemone-like" anthozoan that did not build limestone reefs. The radiolarian plankton were similarly wiped out, resulting in the absence of bedded-chert deposits in the deep oceans.

Global temperatures fell during the Middle Triassic, reaching moderate hothouse temperatures (24˚C) by the end of the Anisian (Trotter et al., 2015). These less extreme temperatures facilitated the re-establishment of tropical and temperate rainforests, coral reefs, and radiolarian plankton. The cooling trend continued through the remainder of the Middle Triassic (Ladinian) and into the early Late Triassic (C12, Ladinian-Carnian Cooling, 242-233 Ma; Trotter et al., 2015). Dense forests of the tree-like lycopod, Pleuromania, grew near the poles (Ziegler et al., 1994). The pattern of growth rings in Pleuromania indicates that these plants grew at rates 10 – 100 times faster than modern trees (Taylor et al., 2000). This suggests that though the climate was highly seasonal, light rather than temperature was the limiting growth factor.

During the middle Carnian, temperatures warmed (Rigo and Joachimski, 2007; Trotter et al., 2015; Sun et al., 2016), rainfall increased and the once extensive carbonate platforms along the margins of southwestern Tethys were flooded by clastic deposits carried onto the continental shelf by hyper-active river systems (Dal Corso et al., 2018a,b). This dramatic change in climate is known as the "Carnian Pluvial Event" (W12.1, 233-230 Ma; Ruffell et al., 2015; Ogg, 2015). It has been proposed that these climatic events were triggered by the formation of the Wrangellian oceanic plateau and associated volcanic islands (Greene et al., 2008; 2009 a, b, 2010). The CO_2 released by the eruption of these basalts warmed the atmosphere which in turn intensified the Pangean monsoonal weather system (Parrish, 1993) and brought more moisture to the interior of the continent. This rainfall fed new river systems that transported vast amounts of sand, silt, and mud to oceans.

The arrival of huge amounts of sediments shut-down carbonate factories, promoted deep water anoxia, and increased environment stress. During the Carnian Pluvial Event (CPE), important ammonite groups became extinct (Balini et al., 2010), conodonts went through a major crisis (Rigo et al., 2007; Martinez-Perez et al., 2014), and other groups such as bryozoans and crinoids show a sharp decline (Simms and Ruffell, 1989). On the continents, new floras evolved that were adapted to wetter conditions (Roghi et al., 2010; Preto et al., 2010; Mueller et al., 2016a,b). After this event, modern conifers and bennetitaleans evolved (Willis and McElwain, 2002; Kustatscher et al., 2018) and dinosaurs emerged as the dominant and most diverse terrestrial fauna (Benton, 1993; Bernardi et al., 2018).

The Mid-Carnian Warm Interval (W12, 234-227 Ma), which included the Carnian Pluvial Interval, was followed by the Early Norian Cool Interval (C11, 227-217 Ma; Trotter et al., 2015). Global temperatures spiked again during the late Norian, (W11, 214-209 Ma; Trotter et al., 2015), before cooling off slightly at the end of the Triassic (C10, Rhaetian Cool Interval, 209-201; Trotter et al., 2015). The dip in temperatures during the late Norian can be attributed to a brief cooling excursion triggered by the Manicouagan impact (W11.1 214 Ma; Spray, 2020).

At the end of the Triassic and into the earliest Jurassic (201.3 Ma), flood basalts erupted across a large portion of North America, South America, Africa, and southern Europe (estimated area ~10 million km^2; Marzoli et al., 1999; McHone and Puffer, 2003; Hames et al., 2003). During a brief episode of ~600,000 years), the Central Atlantic Magmatic Province (CAMP) released approximately 80,000 gigatons of CO_2 into the atmosphere (Whiteside et al., 2010; Torsvik et al., 2020). This exhalation of greenhouse gases increased global temperatures 3˚- 6˚ C (McElwain et al., 1999; Beerling and Berner, 2002; Korte et al., 2009; Dera et al., 2011) giving rise to the brief End Triassic Thermal Event (W10, 201–199Ma). This rapid episode of global warming triggered the now familiar cascade of catastrophic environmental changes: increased terrestrial weathering and erosion Ahlberg et al. (2003), changes in ocean chemistry (i.e., mercury poisoning; Sanei et al., 2012) oceanic acidification (Hautmann, 2004, 2008; Clarkson et al., 2015), photic zone euxinia, falling marine productivity, and possible deep ocean anoxia (Isozaki, 1997).

The End Triassic Extinction (ETE) is ranked third in terms of taxonomic severity, with an estimated 73% extinction of marine genera (McGhee et al., 2013). The once widespread seed fern Dicrodium disappeared from the fossil record (van de Schootbrugge et al., 2009). There was a 90% species turnover in the terrestrial megaflora (McElwain and Punysena, 2007). A "fern-spike" suggests widespread changes in vegetation across Europe and North Atlantic (van de Schootbrugge et al., 2007; Bonis et al., 2010). A number of non-marine clades of vertebrates went extinct, though marine reptiles and fish actually flourished (McCune and Schaeffer, 1986; Benton et al., 2013; Friedman and Sallan, 2012). The End Triassic Extinction was the most severe extinction crisis ever experienced by scleractinian corals (Flügel , 1994; Flügel and Kiessling, 2002; Kiessling et al., 2002) and was catastrophic for reef communities. Bivalves and ammonoids, though they were hit hard by the End Triassic Extinction, had been in decline throughout the latest Triassic (Rhaetian; Hallam, 2002). For excellent summaries of the events surrounding the End Triassic Extinction, see Preto et al. (2010), Whiteside and Grice (2016), Bond and Grasby (2017), and Torsvik et al. (2020).

5.7 Jurassic – Early Cretaceous Cool Interval (C7 – C9, 199-128 Ma), Table 5, Figure 20

Not all climate modes can be neatly pigeon-holed as either a steaming hothouse world or a frigid icehouse world. The 71 million year interval from the beginning of the Jurassic (Hettangian, 199 Ma) through the Early Cretaceous (early Barremian, 128 Ma) is made up of more than 16 distinct warm and cool events (Table 5). Cooler events make up ~67% of this time interval and justify the designation “Jurassic – Early Cretaceous Cool Interval”, though the appellation, “Jurassic – Early Cretaceous Mixed Interval” would work as well.

The Jurassic - Early Cretaceous Cool Interval is made up of three cool, but not cold, intervals separated by two warm intervals. Both of these warmer intervals, the Toarcian Warm Interval (W9) and the Kimmeridgian Warm Interval were hothouse worlds with average global temperatures of 22˚C. The average global temperature during the Jurassic – Early Cretaceous Cool Interval was a relatively mild 17.5˚C, which is close to the average temperature for the entire Phanerozoic (18˚C).

The Early Jurassic Cool Interval (C9, 199-183 Ma) and the Middle Jurassic Cool Interval (C8, 174 – 164 MA) are both characterized by moderate pole-to-equator temperature gradients with annual average polar temperatures several degrees above freezing. Dropstones and glendonites found in northeastern Siberia (Boucot et al., 2013) are evidence of cold winters in the northern hemisphere during much of the early and middle Jurassic (late Pliensbachian – early Bathonian). The winter snow and ice, however, did not persist. The warm summers melted any seasonal snow and ice, preventing the growth of permanent ice caps in either hemisphere (Sellwood and Valdes, 2006).

Distinctive Jurassic plant groups occupied different latitudinal climatic zones. The greatest diversity of plants occurred at mid-latitudes (40˚ N&S) where forest were composed a mixture of ferns, cycads, sphenopsids (like horsetails), pteridosperms (seed ferns), and conifers (Rees et al., 2000). The equatorial regions, which were sparsely populated, were hot and dry and dominated by xeromorphic (arid-adapted) forms, small-leafed conifers, and cycads. Large-leafed conifers and deciduous gingkos grew in the polar regions (Rees et al., 2000). These plant groups suggest that the tempemperatures were seasonally cold, but not frigid. Estimates of tropical seawater temperatures from $\partial^{18}O$ measurements are 4˚ to 6 ˚C cooler than modern tropical temperatures (Dera et al., 2011) indicating a moderate pole-to-equator temperature gradient.

The Early Jurassic Cool Interval (C9) was followed by the Toarcian Warm Interval (W9), during which temperatures spiked 4˚- 8˚C (Dera et al., 2011). This warm pulse has been attributed to increased atmospheric CO_2 arising from the eruption of the Karroo-Ferrar LIP (Pankhurst et al., 1998, 2000; Elliot et al., 1999; Courtillot and Renne, 2003; Jourdan et al., 2005; Ernst, 2014; Ernst and Youbi, 2017). The global nature of this warming event is recorded by widespread oceanic anoxia (Toarcian OAE; Jenkyns et al., 2002; Jenkyns, 2010; van de Schootbrugge et al., 2013).

Much has been made of the extremely arid conditions and unbearable heat of equatorial and subtropical Pangea (30N to 30 S). By modern standards, the climate at low latitudes during the

Toarcian Warm Interval was unbearably hot. Average equatorial sea surface temperatures which were the warmest of the Jurassic exceeded 30˚ C and temperatures in the interior of Pangea often exceeded 40˚ C (Crowley, 1994). The intense summer heating of the large land areas north and south of the Equator strongly deflected the Intertropical Convergence Zone (ITCZ) during the summer months. This modification of the basic Hadley Cell circulation pattern has been called "mega-monsoonal" atmospheric circulation (Parrish 1993). Megamonsoons resulted in drier conditions along the Equator and the formation of a broader Subtropical Arid Belt.

Though the equatorial and subtropical regions of Pangea were arid during the Early Jurassic, most of the world was covered by lush, habitable forest vegetation (Rees et al., 2000). Abundant Early Jurassic coal deposits are found in both the warm and cool temperate belts (up to 60 N& S) (Boucot *et al*., 2013). Bauxite deposits, indicative of warm and wet conditions, are found in Europe and west central Asia (Kazakhstan) (30N - 45N).

The early Jurassic Toarcian hothouse (W9) was followed by a relatively cool period during the middle Jurassic (Jenkyns et al., 2002; Dera et al., 2011). In a rare turnabout, during the early Jurassic, the South Polar region appears to have been warmer than the North Polar region. Dinosaurs and small flying reptiles, which would have had difficulty surviving freezing winters, inhabited the central Antarctica Transantarctic Ranges (Hammer and Hickerson, 1996); whereas dropstones and glendonites, indicative of freezing winter conditions, have been reported from Arctic Siberia (Boucot et al., 2013; 70 N – 80 N).

Global temperatures warmed again during the late Oxfordian and Kimmeridgian (W8, Kimmeridgian Warm Interval, Podlaha et al., 1998; Jenkyns et al., 2002; Dera et al., 2011). The "mega-monsoonal" atmospheric circulation that characterized the earlier Mesozoic (Parrish, 1993) was still in place, but showed signs of weakening. As the newly formed intra-Pangean ocean basins (Central Atlantic Ocean and Western Indian Ocean) widened, they brought new sources of moisture to the interior of Pangea. The influx of moisture from these young ocean basins dampened the severe, seasonal swings in temperature and precipitation that had plagued the dessicated core of Pangea since the Late Permian. For other climate model results for the Late Jurassic see Moore *et al*. (1992), Valdes and Sellwood (1992), Valdes (1994), Sellwood and Valdes (2006).

The Kimmeridgian Warm Interval (164-150 Ma) was followed by a long interval characterized by cool, but not frigid, temperatures (Tithonian-early Barremian Cool Interval, C7, 150 – 128 Ma). The Tithonian-early Barremian Cool Interval was punctuated by isolated warm events (Weissert (136 Ma) and Faraoni (131 Ma) thermal excursions).

Global Climate during the earliest Cretaceous (Berriasian to Barremian) can be characterized as something "in-between" a hothouse and an icehouse (Frakes *et al*., 1992). The average global temperature was about 17˚ C. This was five degrees warmer than the Late Cenozoic Icehouse (C1, 12˚ C), but seven to nine degrees cooler than the Mid-Cretaceous – Paleogene Hothouse (W5-W6). Evidence for more temperate climatic conditions is based on the occurrence of dropstones, glendonites, and a few tillites (pebbly mudstones, Boucot *et al.*, 2013) in polar latitudes that co-occur with evidence of temperate forests (coal, plant fossils) and dinosaurs. Dropstones of Early Cretaceous age (Berriasian/Barremian) are widespread in South Australia, Queensland, New South Wales, and the Northern Territory of Australia (Boucot *et al*., 2013). Glendonites occur in South Australia and New South Wales . In the northern hemisphere there are dropstones in Siberia and Svalbard, and glendonites in northern Siberia, Svalbard and the Arctic Islands (Grasby et al., 2017; Brassell, 2009; Frakes and Francis, 1988; Frakes and Francis, 1990,1993; Frakes et al., 1995; De Lurio and Frakes, 1999; Vickers et al., 2019).

The best interpretation for this mixture of cool and warm climatic indicators is that it was cold enough in the winters for lakes and rivers to freeze over. Snow covered the ground and there were glaciers at higher elevations. In the summer months it was warm enough to support the growth of lush vegetation and an influx of dinosaurs migrating in from warmer regions.

It is interesting to note that the Kimmeridgian Anoxic Event is the only potential oceanic anoxic event for the time interval spanning the middle Jurassic (Aalenian, 174 Ma) to the early Barremian (128 Ma). It does not appear to be as widespread as the Cretaceous OAE events. The lack of anoxic basins during the earliest Cretaceous seems quite unusual in light of the fact that there were many "restricted" marine basins that would have been ideal habitats for anoxia to develop. The lack of OAEs may have been due to the fact that the bottom waters during the middle and late Jurassic through to the earliest Cretaceous were relatively well-oxygenated. The occurrence of glendonites at high latitudes during much of the Early Cretaceous indicates that cool, oxygen-rich bottom waters were being generated at polar latitudes preventing the bottom waters in lower latitudes from becoming anoxic.

5.8 Mid Cretaceous – Paleogene Hothouse (W5 – W7, 39.4-128 Ma), Table 6, Figure 20

If one imagines where the current phase of anthropogenic global warming is heading, one immediately thinks of the hothouse worlds of the Late Cretaceous and Eocene (Huber, 1998; Huber et al., 2000). During the Mid Cretaceous – Paleogene Hothouse global temperatures were indeed much warmer than the present-day (GAT = 28˚C during the Late Cretaceous versus GAT = 15˚C for the Modern). It remains to be seen whether we will succeed in warming the Earth to that degree, but at least we now know what a warmer world would look like.

The Mid Cretaceous – Paleogene Hothouse is one of the best documented paleotemperature intervals. Table 6 lists some of the key references for this time interval and summarizes their primary conclusions regarding regional and global temperatures. The best single source for information about the Cretaceous portion of this hothouse interval is the O'Brien et al. (2017) summary of sea surface temperatures (SSTs) based on oxygen isotope and TEX_{86} temperature estimates. The TEX_{86} technique uses the lipid chemistry of the cell membrane of a common group of pelagic protokaryotes (Thaumarchaeota) to estimate temperatures (Schouten et al., 2002). The paleotemperatures are derived by measuring the ratio of key lipids (crenarchaeols). It has been noted that TEX$_{86}$ temperature estimates tend to be ~50% higher than ∂^{18}O temperature estimates (O'Brien et al., 2017; Figure 8). Approximately 90% of the available TEX$_{86}$ paleotemperature estimates for the Cretaceous have been obtained from samples that are Aptian or younger in age. Moreover, there are very few ∂^{18}O temperature estimates for times older than the mid-Albian (O'Brien et al., 2017). Fortunately, as noted earlier, geological evidence (glendonites, dropstones, and rare tillites) from the Early Cretaceous helps to fill in these data gaps.

Both oxygen isotope and TEX$_{86}$ measurements identify an early Barremian – middle Aptian warm interval (W7, 128 – 118 Ma, GAT = 22˚C), which was followed by a cooler period during the late Aptian-early Albian (C6, 118 – 111 Ma, GAT = 19˚C), which preceded the rapid ramping up to a thermal maximum during the latest Cenomanian- earliest Turonian (W6.2, 94 – 93 Ma, GAT = 28˚C). According to O'Brien et al. (2017), temperatures cooled gradually during the remainder of the Late Cretaceous reaching a minimum of ~21˚C in the late Maastrichtian, just prior to the KT impact event.

The Mid Cretaceous – Paleogene Hothouse (W6) began in the latest Barremian – earliest Aptian (~128 Ma) with two thermal events, the Haupblatterton Thermal Event (W7.5; Mutterlose et al., 2009) and the oldest Cretaceous oceanic anoxic event, OAE1a, the Selli/Goguel Thermal Maximum (W7.4; Erba et al., 2015; Herrle et al., 2015; O'Brien et al., 2017). Average global temperatures during the Mid Cretaceous – Paleogene Hothouse was a ~23˚ C. Surface waters in the Cool Temperate regions (SST = 21-23˚C) were only slightly cooler than the superheated tropical seas (29˚ C; O'Brien et al., 2017). Oceanic bottom waters were also much warmer than the present-day (9˚ - 17˚ C; Valdes et al., 2020).

The Selli/Goguel Thermal Maximum (OAE1a) is the first of nearly a dozen potential thermal spikes that characterize this time interval (see Table 3). The nature and origin of these OAEs has been much debated (Schlanger and Jenkins, 1976; Arthur and Sageman, 1994; Meyer and Kump, 2008).

Previous notions that OAEs were simply the result of rapid rises in sea level (Arthur and Sageman, 1994) or due to the stagnation of the ocean basins caused by thermohaline density stratification, have fallen out of favour. There are two current schools of thought. The first argues that the OAE's were "unusual", synchronous, global events. According to this argument, "catastrophic" tectonic events triggered "unusual" atmospheric, biologic, geochemical, and oceanographic conditions that promoted extensive deepwater anoxia that resulted in the formation of carbon-rich black shales (Total Organic Carbon often > 30%). Proponents of this school of thought argue that the following scenario may explain the widespread occurrence of the carbon-rich black shales associated with the early Aptian Selli/Goguel Thermal Maximum (OAE1a):

- The eruption of the mid Cretaceous superplume (Larson, 1991; Larson and Erba, 1999) radically changed atmospheric and oceanic chemistry.
- Greenhouse gases from the erupting lavas, (i.e. CO_2), warmed the Earth.
- Increased warmth accelerated chemical weathering on land; consequently, a greater flux of nutrients was carried to the oceans.
- Land-derived nutrients, together with a higher concentrations of biolimiting metals made available by increased hydrothermal activity associated with the extensive submarine eruptions (Duncan and Huard, 1997; Jones and Jenkyns, 2001) promoted greater marine productivity resulting in more carbon deposition.
- The increased productivity depleted the available supply of oxygen in the water column, which led to basin-wide anoxic or dysoxic conditions.
- Water-column anoxia, in turn, favoured the preservation of the carbon by inhibiting bacterial decay and carbon recycling.
- The results were widespread carbon-rich black shales (Demaison and Moore, 1980)

A second school of thought argues that the OAEs do not represent unusual or catastrophic, global events, but rather represent "business as usual". In other words, a certain constellation of biologic, geochemical, tectonic, atmospheric, and oceanographic conditions favour the development of local, basin-wide anoxia. The Cretaceous were unusual only in the sense that this constellation of favorable conditions was more likely to occur than one might have been expected. In essence the paleogeography of the Aptian/Albian (and Cenomanian/Turonian) was especially favourable for the formation of highly productive, anoxic basins that promoted “nutrient trapping” (Meyer and Kump, 2008).

These two schools of thought epitomize the classical conflict between “catastrophic” versus “uniformitarian” explanations of Earth processes. As in the case of most false dichotomies, each hypothesis may hold part of the answer. Each hypothesis may explain different aspects of the Earth System processes that produce oceanic anoxic events. The “catastrophic” hypothesis may be the best explanation for the rare, but truly global, “mega” OAE events (i.e. Selli/Goguel Thermal Maximum (OAE1a) and Cenomanian-Turonian Thermal Maximum (OAE2), whereas the “uniformitarian” hypothesis may be a better explanation for the more frequent, regional, and less intense OAE events (OAE1b, OAE1c, OAE1d, OAE3).

The Aptian-Albian Cold Snap (C6, 118-111 Ma) separates the Selli/Goguel Thermal Maximum (OAE1a) from the remaining Late Cretaceous OAE’s. For a brief interval in the late Aptian and Early Albian, the global climate cooled off sufficiently for winter snow and ice to return to the northern and southern polar regions (Pucéat et al., 2003; Jenkyns et al., 2012; Erba et al., 2015; Herrle et al., 2015; O’Brien et al., 2017). Glendonites are reported from Ellesmere Island, Axel Heiberg Island, Svalbard, northern Greenland, and east-central Australia (Eromanga Sea) indicating that cool bottom waters once again had chilled the deep ocean basins (Frakes and Francis, 1988; Grasby et al., 2017; VIckers et al., 2019).

The warmest Cretaceous temperatures occurred during the Cenomanian-Turonian Thermal Maximum (W6.2, 94 – 93 Ma). Second only to the Permo-Triassic Thermal Maximum (W13), the global average temperature reached 28˚C and the pole-to equator temperature gradient was flattened with a temperature differential of only ~20˚C degrees between the polar region (13˚C) and the tropics (34˚C). Not even a hint of ice existed at the poles during the Cenomanian-Turonian Thermal Maximum (Ziegler et al., 1985). The presence of tropical plants and dinosaurs on Antarctica (Dettmann, 1989; Cantrill and Poole, 2012) and above the Arctic Circle indicates that temperatures rarely fell below freezing even during the winter months (Wolfe and Upchurch, 1987; Parrish and Spicer, 1988). Recent descriptions of angiosperm leaf floras from Antarctica indicate that similar warm and wet conditions existed near the South Pole during the Late Cretaceous (Hayes *et al*., 2006). In general, during times of hothouse conditions, the equatorial and subtropical belts expand slightly poleward; the Polar and Cool Temperate belt are replaced by an expanded Warm Temperate belt that brings tropical conditions to latitudes above 50° north and south (Paratropical Belt of Boucot et al., 2013; the megathermal rainforests of Morley, 2011).

Despite the overwhelming geological and paleontological evidence for warm polar regions during the Mid-Cretaceous Hothouse, early climate simulations tended to "run cold" and had a difficult time modeling these warmer polar temperatures (Barron and Washington, 1982). Various attempts have been made to modify the input parameters to the climate models to produce simulations more consistent with the geological data. Initial attempts to fix this problem used extremely elevated levels of greenhouse gases to warm the poles (15x modern CO_2; Bice and Norris, 2002). However, there is no geological support for CO_2 concentrations in the Cenomanian/Turonian much above 5x the modern value (van der Meer et al., 2014). The extreme high levels of CO_2 needed to keep the polar regions ice-free would necessarily make terrestrial and shallow marine habitats at low latitudes uninhabitable (Jacobs et al., 2005).

Another way to make the polar regions warmer is to modestly increase the concentration of greenhouse gases and also modify the land cover in polar regions to a darker, denser vegetation (Upchurch *et al*., 1999). The darker vegetation has a lower albedo and consequently more solar energy is absorbed at the surface. In this model, positive feedbacks between high-latitude forests, the atmosphere, and the ocean all contribute to significantly warmer temperatures at high latitudes during the Late Cretaceous (Upchurch *et al.*, 1999).

A third explanation invokes a Late Cretaceous “Super-Gulf Stream” that vigorously carried warmth from the Equator to the Poles (Brady *et al*., 1998). Though intuitively appealing, an analysis of the dynamics indicates that it is not possible to carry enough heat poleward using ocean currents alone. The atmosphere must also play an important role. In addition, much like today, the paleogeography of the Late Cretaceous presents a nearly landlocked polar region that would have been isolated from Gulf Stream-like ocean currents.

One of the more promising approaches has been to change the high-altitude cloud parameterization that is used in climate models like the Community Climate System Model version 3 (CCSM3, Kiehl and Shields, 2013). The high albedo of low-altitude cumulus clouds reflects incoming sunlight back to space, which cools the Earth. Wispy, high-altitude clouds, on the other hand, reflect thermal energy back to the surface of the Earth resulting in net global warming (Kump and Pollard, 2008). Fewer “warm clouds” form in the modern world because anthropogenic atmospheric pollution reduces the amount of warm cloud condensation nuclei. When cloud parameters characteristic of pristine regions are introduced into the climate model, significant additional warming occurs, especially in polar regions (Upchurch et al., 2015). Combined with a modest elevation in the concentration of atmospheric CO_2 (2x – 6x modern levels), the modelled temperature of polar regions remains above freezing throughout most of the year.

The most radical hypothesis that has been proposed to explain the warm polar climates of the Late Cretaceous involves a fundamental rethinking of the way the atmosphere circulates. One of the basic features of the modern atmosphere is Hadley Cell circulation. In the Hadley Cell, warm air rises at the Equator, moves poleward, cools and descends over the subtropical desert belt (~35° N&S). In Hay’s model (Hay,2008; Hay *et al*., 2016), this simple, well-organized convective flow is replaced by a chaotic system of super-cyclonic eddies, which are like mega-hurricanes. Hundreds of these mega-hurricanes would have annually transferred vast amounts of heat from the Equator to the Poles during the Late Cretaceous. Though an intriguing and out-of-the-box proposition, no climate model can currently simulate this complex alternative to Hadley Cell circulation.

After reaching peak Cretaceous temperatures during the Cenomanian-Turonian Thermal Maximum, temperatures gradually fell during the remainder of the Cretaceous. Maximum sea surface temperatures did not drop below 30˚C until late in the Santonian (84 Ma) or early in the Campanian (O'Brien et al., 2017). This gradual cooling may have been punctuated by several, ephemeral cooling events at ~85Ma, ~76 Ma, and ~71 Ma (Miller et al., 1999, 2004, 2005a,b) as evidenced by $\partial^{18}O$ temperature estimates from planktonic foraminifera. Also, an enigmatic dropstone deposit of Campanian – Maastrichtian age (75 – 70 Ma) has been reported from the region of the Anadyr River in Chukotka (Ahlberg et al., 2002).

The modest, but steady, fall in temperatures during the Late Cretaceous was catastrophically interrupted by the arrival of the bolide that produced the 150 km diameter impact crater near the town of Chicxulub (Devil's Tail) in northern Yucatan (Alvarez and Alvarez, 1980; Schulte et al., 2010; Hildebrand et al., 1991). The Chicxulub impact is the largest known bolide impact of the Phanerozoic (Spray, 2020).

The most likely scenario is that the impact event vaporized 3000 megatons of crustal material and injected this fine particulate matter high into the atmosphere. This material fell back to Earth forming a global "clay layer". The K/T boundary clay layer contains several unusual stratigraphic markers: 1) an iridium anomaly (Alvarez and Alvarez, 1980; Smit, 1999; Miller et al., 2010), 2) microtektites (Yancey and Guillemette,2008), 3) shocked quartz (Bohor et al., 1987; Smit, 1999), and 4) soot (from forest fires) that connect it directly to the Chicxulub impact event. (It should noted that the authors prefer to use the term "K/T" rather than the more precise "K-Pg" to describe events occurring at the Cretaceous -Paleogene boundary. The term "K/T" has precedence, is still widely used, is more familiar to most readers, and is therefore a clearer descriptor than the technically correct, but more obscure and less euphonius, “K-Pg”.)

While suspended in the atmosphere, this delicate shroud of material blocked the sun and turned day into night - a night that lasted several months to a year. Without sunlight, plants on land and plankton in the oceans died. Small and large herbivores gradually starved. Without herbivores to prey on, predators then starved - all the while, snow continued to fall (probably for several decades). As a consequence of the collapse of the food chain, ~75% of all species were wiped out (Sepkoski, 1996). The effect of this extinction event on global ecosystems was second only to the great Permo-Triassic Extinction (McGhee et al., 2013).

The ensuing “Impact Winter” scenario plunged the Earth into a frigid deep-freeze comparable to the coldest glacial stages of any Phanerozoic ice age. The drastic cooling, however, was short-lived (Vellekoop et al., 2014, 2016) and was followed by an equally short-lived period of global warming triggered by the final, massive eruption of the Deccan LIP (Ernst, 2014; Keller et al.,2017). The first eruptions of the Deccan LIP predate the Chicxulub impact by 1-2 million years (Chenet et al., 2008; Keller et al., 2011, 2014). It has been proposed that an earlier impact event (Shiva impact) triggered the Deccan eruptions (Chatterjee et al., 2006), however this hypothesis has not received much support. It seems likely, however, that the Chicxulub impact did influence or enhance Deccan volcanism. It has been noted by several authors (E. Shoemaker, pers. comm.) that the impact site in Yucatan is nearly antipodal to the eruption site of the Deccan LIP in India. Though the antipodal paleolatitudes are identical (26˚ N vs 26˚ S), the antipodal paleolongitudes are offset by several thousand kilometers. Nevertheless, it seems plausible that shockwaves from the impact passed through the earth and were reconcentrated beneath the Deccan hotspot stimulating more voluminous eruptions (Richards et al., 2015; Renne et al., 2015). In any event, the excess atmospheric CO_2 from the Deccan eruptions caused a 4-8˚ spike in global temperatures (Petersen et al., 2016; Bond and Grasby, 2017) that ushered in the Paleogene Warm interval.

Following the KT impact Winter, global temperatures warmed during the Paleocene, reaching a maximum during the early-middle Eocene (Paleocene - Eocene Hothouse, W5, 62 - 39.4 Ma). This period of global warmth was probably triggered by CO_2 injected into the atmosphere by massive volcanic eruptions in the North Atlantic Igneous Province (NAIP; Ernst, 2014). It was in this global, tropical "Garden of Eden" that our mammalian ancestors diversified, crossed newly-erupted volcanic land bridges between northern Europe and Greenland, and expanded across the globe (Wallace, 2004).

The classic record of deep ocean temperatures based on benthic foraminifera assembled by James Zachos (Zachos et al., 2001, 2008; also Westerhold et al., 2020) provides a framework for describing the temperature fluctuations during the Paleocene-Eocene Hothouse and the Late Cenozoic Icehouse (Koeberl and Montanari, 2009). These deep ocean temperatures have been converted to global average temperatures using the technique described in section 3.3.

The three most prominent features of this detailed temperature record are: 1) the Paleocene-Eocene Thermal Maximum (W5.8, 55.6 Ma; Rea et al., 1990; Kennett and Stott, 1991; Wing et al., 2003; McInerney and Wing, 2011), 2) the Early Eocene Thermal Maximum (W5.5, ~50 Ma), and the Middle Eocene Thermal Maximum (W5.1, ~41 Ma). These are certainly "event" driven changes in climate. The one explanation for these spikes in temperature is the rapid release of massive amounts of methane hydrates (clathrates) from the deep sea (Zeebe et al., 2009). Methane is a powerful greenhouse gas and the release of gigatons of methane into the atmosphere would have produced the observed rapid rise in global temperature. Other hypotheses, summarized by Wing and McInerney (2011, p 494), suggest that the excess amount of greenhouse gases may have come from wildfires, volcanic intrusions into organic-rich sediments, drying of epicontinental seas, or the thawing of Antarctic permafrost. Most recently, Gutjhar et al. (2017) and Jones et al. (2019) have proposed that massive eruptive episodes associated with the North Atlantic Igneous Province (NAIP) provided the excess CO_2 responsible for these thermal maxima.

A prominent feature of the early Eocene Hothouse is the broad, dome-shaped rise and fall in temperature that defines the Middle Eocene Warm Interval (W5.4, 56-46 Ma). The shape of this curve indicates that systematic changes were taking place over millions of years (Huber and Caballero, 2011). These changes in global temperature were probably driven by gradually changing paleogeographic, plate tectonic, or paleoceanographic conditions. The final notable feature of the Zachos Curve is the rapid fall in temperature at the end of the Eocene (C4.3, Eocene Oligocene Rapid Cooling, 33-34 Ma). It has been proposed by many authors that this cooling event was driven by the development of a through-going Circum-Antarctic Current and the subsequent isolation and refrigeration of Antarctica.

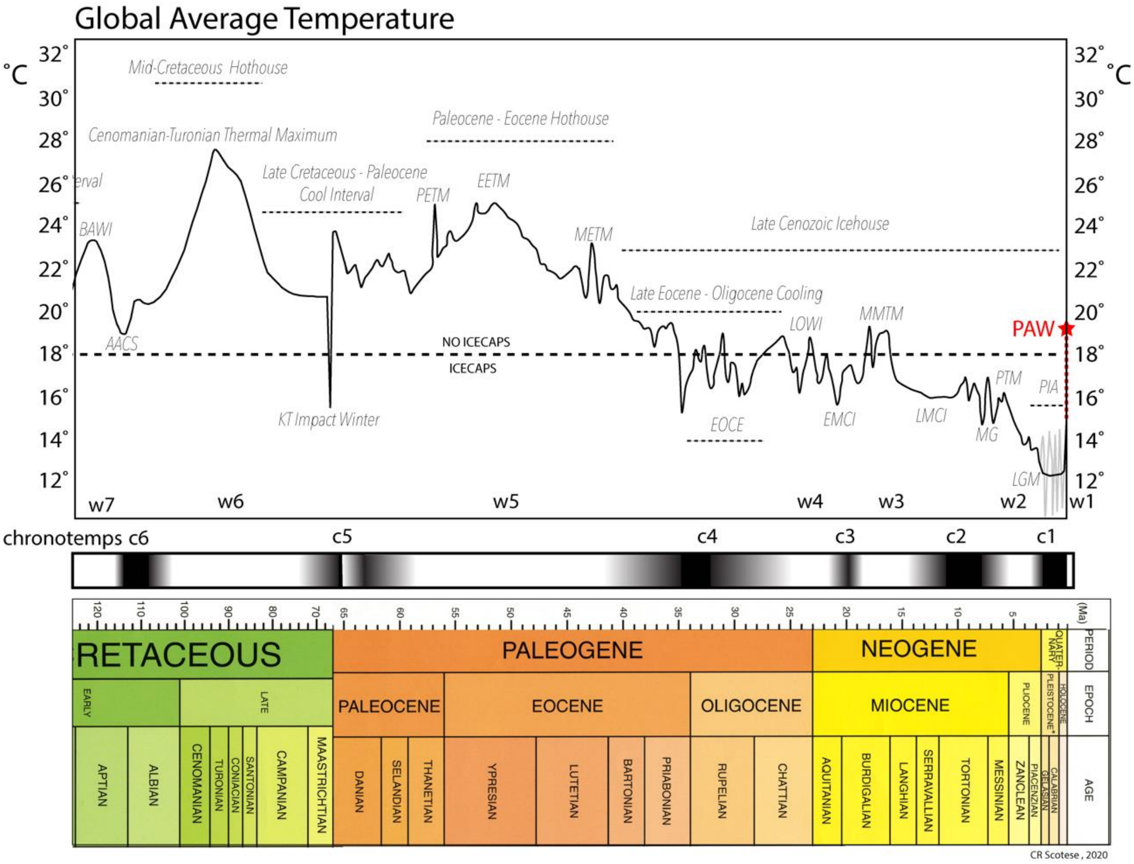

Figure 21. A Cenozoic Paleotemperature Timescale. white = warm time intervals, black = cool time intervals; Light gray jagged lines = a schematic representation of >50 glacial/interglacial cycles during the Plio-Pleistocene. Solid black line = Global Average Temperatures (GAT),), < 18˚C = large, permanent icecaps, > 18˚C = no large, permanent icecaps. Timescale = International Chronostratigraphic Chart v2020/01. Refer to Table 3 for more information and sources for each chronotemp and abbreviations.

5.9 Late Cenozoic Icehouse (C1 – C4, 1880 CE – 39.4 Ma), Table 7, Figure 21

"And now there came both mist and snow

And it grew wondrous cold
And ice, mast-high, came floating by
As green as emerald."
Samuel Taylor Coleridge, Rime of the Ancient Mariner (1798)

As illustrated in Figure 21, the cooling trend that began after the Early Eocene Thermal Maximum (W5.5, 52-50 Ma) continued during the middle and late Eocene, though it was interrupted briefly by the Middle Eocene Thermal Maximum (W5.1, 41 Ma). What Earth System event initiated the Late Cenozoic Icehouse? The generally accepted explanation is that the collision of India, which took place at the height of the Early Eocene Thermal Maximum (~50 Ma; Molnar and Tapponier, 1975; Rowley, 1996, 1998), triggered a cascade of events that lead to global cooling (Raymo and Ruddiman, 1992). The collision of India with south-central Asia resulted in the rapid uplift of the Himalaya Mountains. By ~35 Ma (late Eocene – early Oligocene), the Himalayas and Tibetan plateau had achieved 90% of their modern height (Rowley and Currie, 2006), though the Tibetan plateau was less than half its present area. These young mountains were in the path of the Asian monsoon, which brought warm temperatures and abundant moisture. This lead to rapid mechanical and chemical weathering. The flux of calcium to the world's oceans increased and these calcium cations combined with carbonate ions to form limestone which drew-down the amount of CO_2 in the atmosphere. The gradual decrease in atmospheric CO_2 cooled the Earth.

As global temperatures began to cool, the high altitude glaciers on the Gamburtsev mountains and Trans-Antarctic Ranges (> 1000 m) coalesced into ice sheets. At the Eocene-Oligocene boundary (C4.3, 34-33 Ma), temperatures plunged precipitously signalling the first major accumulation of ice on Antarctica. Permanent sea ice also formed around the periphery of Antarctica generating increasing amounts of cold bottom water. Icebergs coursed through the southern oceans and the first record of ice-rafted debris appeared in the deep-sea record. The global cooling also forced plants to adapt to the harsher winter conditions (Wolfe, 1971, 1978, 1992, 1994). Paleoceanographic events in the Southern Hemisphere, in particular the formation of the Circum-Antarctic Current, played a key role in the chronology of these events (Kennett, 1995).

The Drake Passage is the seaway that flows between the southern tip of South America (Patagonia) and the northern tip of the West Antarctic Peninsula (Palmer Peninsula). In the early Mesozoic, these two regions were part of a continuous Andean mountain range. The ligation between Patagonia and the Palmer Peninsula was tested when Gondwana began to rift apart in the late Jurassic. Despite being stretched and extended as the Weddell Sea opened during the Cretaceous, Patagonia and the Palmer Peninsula were not completely separate until the late Eocene (~40 Ma). The best estimate for the age of the opening of the Drake Passage is 45 Ma (shallow water connection, <1000m) to 35 Ma (deep water connection, >1000 m) (Livermore *et al*., 2005). An age of 41 Ma for the opening of the Drake Passage is based on the change in neodymium isotope ratios from sediments on the Agulhas Ridge that suggests an influx of shallow Pacific water (Scher and Martin, 2006).

When the Southeast Indian Ocean between southern Australia and Antarctica (Wilkes Land) began to open in the Late Cretaceous, the eastern end of the rifted margin made a right-angle bend, hooking southward around Tasmania. This strike-slip boundary, the Tasman Fracture Zone, effectively closed off the eastern end of the Southeast Indian Ocean during the earliest phases of opening. When Australia began to move rapidly northward during the Late Eocene (40 Ma – 35 Ma), the overlapping bits of the Australian and Antarctic plates (South Tasman Rise and North Victoria Land, respectively) separated, allowing deep waters from the Indian Ocean and South Pacific Ocean to mix. The first deep water connection between the Indian Ocean and the South Pacific was through the Tasman Straits.

Both the Drake Passage and the Tasman Gateway (Kennett et al., 1974; Exon et al., 2004; Kennett and Exon, 2004) were fully opened by the early Oligocene (34-30 Ma; Lawver and Gahagan, 2003).

As a consequence, the Circum-Antarctic Current was able to isolate Antarctica from the world's oceans resulting in the "refrigeration" of Antarctica (C4.2, 34-28 Ma). The rapid growth of the Antarctic icecap during the Early Oligocene produced a major regression at the Rupelian/Chattian boundary (28.1 Ma). During the Oligocene, the massive Antarctic ice cap grew and shrank in fits and starts. These chaotic transitions are recorded in a dozen cooling and warming events (C4.1 and C4.2).

Global temperatures remained cool until the end of the Oligocene when there was a slight warming (W4, 27-23 Ma). Though parts of West Antarctica were still forested during the Oligocene, mountain glaciers grew in the highlands of the Palmer Peninsula, reaching the ocean by the latest Oligocene. In the Northern Hemisphere there were local glaciers in Svalbard and central Greenland, but no permanent icecap.

It is also worth noting that by the Early Oligocene, the collision between the Arabian peninsula and Iran was nearly complete. Though all the ocean floor had been subducted, a shallow seaway, the proto-Persian Gulf, filled the foredeep of the Zagros mountains of Iran and Iraq. During brief highstands of sea level during the late Oligocene and early Miocene, this shallow seaway connected with the deeper waters of the eastern Mediterranean. The closure of this westernmost extension of Tethys in the earliest Oligocene eliminated the westward flowing "Subtropical Eocene NeoTethys" (STENT) current. Some authors have speculated that this may have contributed to global cooling during the early Oligocene (Toggweiler et al. (2000), Hotinski and Toggweiler, 2003; Jovane et al., 2009).

At the start of the Miocene, only Antarctica, straddling the South Pole, was covered by a permanent icecap. Cool conditions prevailed in the northern hemisphere as well, but there was no permanent ice. Global temperatures warmed in the middle Miocene (W3, 18 – 11 Ma), the Antarctic ice cap shrank and snow and ice disappeared from the northern hemisphere. By the end of the Miocene (~ 5 Ma), conditions had once again cooled (C2, 11 - 5.3Ma) and a permanent icecap had begun to form in the Arctic. The initiation of the Greenland ice sheet in the middle-late Miocene corresponds with the minimum sea level for the Miocene (~50 m; Miller et al., 2020).

The growth of the Arctic icecap may have been triggered by two paleogeographic-paleoceanographic changes: 1) In the late Neogene (4-5 Ma), the Panama volcanic archipelago rose above sea level, creating the Panama land bridge. This land bridge connected North and South America, permitting the interchange of fauna and flora (Marshall *et al*., 1982). More importantly, this land bridge served as a blockade, isolating the equatorial Atlantic and Pacific Oceans. Warm, equatorial Atlantic waters were diverted northward (the Gulf Stream). The warm waters of the Gulf Stream warmed the Arctic regions, but more importantly, provided a new source of moisture which fed winter snows. Increased snowfall lead to the growth of glaciers and the Arctic ice sheets grew large. 2) In the eastern hemisphere, the northward movement of Australia during the early Miocene and the collision of Australia with Southeast Asia during the middle-late Miocene (~10-15 Ma) blocked equatorial circulation between the western Pacific Ocean and the Indian Ocean. As a consequence, the distance that ocean waters circulated along the Equator was shortened resulting in a net cooling of tropical surfaces waters. This reduction in the Earth's thermal budget, in turn, may have led to increased cooling at the poles.

Global temperatures continued to plummet during the Pliocene. During the late Pliocene (~3.3 Ma), global temperatures warmed sufficiently to melt enough of the North and South polar icecaps so that sea level rose (~60 m), flooding the continental margins (W2.1, Pliocene Thermal Maximum).

The Pleistocene Ice Age (C1) began in the latest Pliocene (2.7 Ma) and ended 11,700 years ago (Younger C1.1 Dryas). Driven by the tilt of the Earth (obliquity) and the shape of the Earth's orbit (eccentricity), the polar ice sheets waxed and waned causing global sea level to rise and fall (Miller et al., 2020). When ice sheets were at their maximum, sea level was ~100 meters lower than today. During the interglacial part of the cycle, when much of the polar ice caps had melted away, sea level was ~70 meters higher than today.

Sea level has risen and fallen more than 50 times during the last 2 million years. This cycle of sea level change has been recorded in the changing ratio of the $^{18}O/^{16}O$ preserved in benthic/planktonic foraminifera (Lisiecki and Raymo, 2005). This fluctuating record begins nearly 2.7 million years ago; for the first ~2 million years, the cycle of icecap growth and retreat was modulated by the changing tilt of the Earth's axis (40,000 year obliquity cycle). Starting nearly one million years ago, the frequency of ice cap formation slowed from every 40,000 years to every 100,000 years, as the changing, eccentric shape of the Earth's orbit became the major forcing function. It should be noted that most of these marine isotopic sequences (MIS) match a similar cycle of changing CO_2 concentration recorded in mile-long ice cores from Greenland and Antarctica (Barnola et al., 1987; Petit et al, 1999; Alley, 2000; EPICA Community Members, 2004; Jouzel et al, 2007).

We are currently about halfway through a typical glacial/interglacial cycle. If humans did not inhabit the Earth, about 20,000 years from now, global temperatures would have once again begun to fall and ice sheets would have expanded into the oceans surrounding Antarctica and would have descended from the Arctic to begin a slow and steady march across the northern continents. However, this will not happen. The Earth has entered a "super-interglacial". The injection of CO_2 into the atmosphere as a consequence of the burning of fossil fuels has warmed the Earth more than 1˚C and will continue to warm the Earth for another 300 years (~2300 CE). In the next section, we discuss how long anthropogenic global warming will continue and how warm the Earth will become.

5.10 Post-Anthropogenic Warming (W1) (2300 CE – 10,000 years in the future), Table 7, Figure 21

It is well-established fact that burning fossil fuels releases CO_2, a greenhouse gas, into the atmosphere, causing the Earth to warm faster than it would naturally (Archer, 2005; Archer et al., 2009a,b; Kidder and Worsley, 2012; Steffen et al., 2019). How warm will it get? How quickly will it warm to those new levels? In order to answer these questions, we need to know future trends in 1) global population (United Nations, 2019), 2) the average "energy footprint" per global resident

(British Petroleum, 2019), 3) the future mix of energy sources (oil, gas, coal, hydroelectric, nuclear, and renewables; British Petroleum, 2019; Rogner, 2012; Shell,2018), 4) the rate at which the natural environment will absorb excess CO_2 emissions (Tans, 2009), and 5) the warming effect of greenhouse gases (climate sensitivity; Royer, 2016; Farnsworth et al., 2019). Though these parameters are not known with any certainty, we can nevertheless make an informed estimate of future trends and produce a reasoned prediction of the potential amount of global warming during the next 300 years (Scotese, 2020).

We have estimated the amount of future global warming using a straightforward carbon budget model that predicts the changing amount of atmospheric CO_2. This CO_2 budget model is described in Table 8. Using these carbon budget equations, a dynamic model was constructed that predicts the amount of global warming during the next 300 years.

Assuming that the Global Average Temperature (GAT) in 2000 was roughly 14.5˚C (58˚ F), and the concentration of atmospheric CO_2 was 369 ppm. This model predicts that in 2200 the concentration of atmospheric CO_2 will be ~777 ppm, which is a little more than double the concentration of CO_2 in the year 2000 and the global temperature will rise about 5˚ C from 14.5˚C (58˚F) to 19.5˚C (67˚ F). This change in temperature is indicated by the red star in Figure 21.

As has been widely reported (Collins et al., 2013), most future warming takes place during the mid-to-late twenty-first century. Rapid global warming is nearly unavoidable because two key parameters - global population and energy use per capita - will rapidly rise during the next several decades.

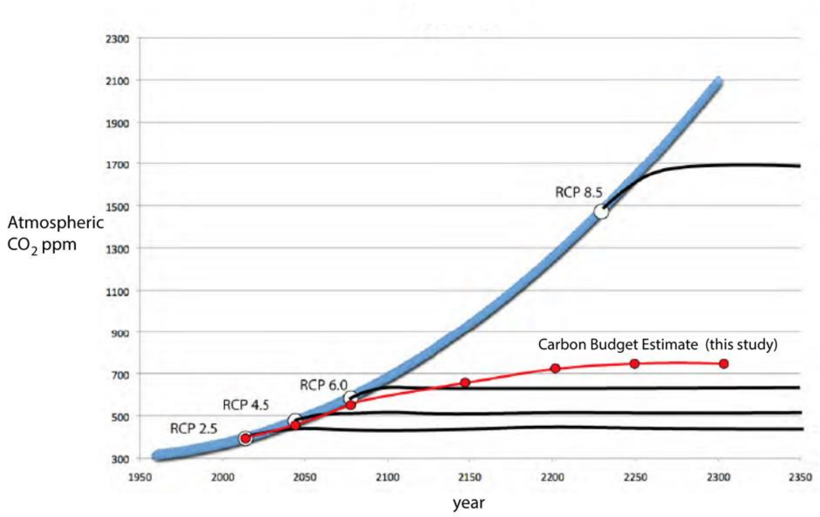

Figure 22. IPCC Estimates of Global Warming compared to the Results Predicted by the Carbon Budget Model (this study). The blue curve represents the projected increase in atmospheric CO2 based on the continued burning of fossil fuels at the "modern rate" (1970 – 2020). The black curves are the CO2 levels used in the IPCC models RCP 2.5, RCP 4.5, RCP 6.0, and RCP 8.5. The red curve is the projected CO2 levels obtained in our model (between 750 ppm and 800 ppm at 2200 CE). Estimates from RCP 2.5 and RCP 4.5 are too low. The estimate of CO2 used in RCP 8.5 is much too high. Estimates of CO2 used in RCP 6.0 are about right.

According to the model, in the year 2100, global climate will have warmed beyond the 2˚C limit recommended by the Paris Accords (Figure 22). In 2200, after reaching a maximum temperature of 19.5˚C, the global climate will begin to cool. This is due in part to natural processes, but most of the modelled decrease in global temperature is the result of proposed human intervention (i.e. carbon sequestration; Shell, 2018). If 10,000 carbon sequestration plants are built in the next 300 years, then by 2300 the combined action of these carbon sequestration plants will have removed 1.8 trillion gigatons of CO_2 from the atmosphere and the temperature will stabilize at 19.5˚C (Shell, 2018). If no carbon sequestration plants are built, then the projected future temperature will be closer to 20.5 C˚. Both of these predictions are in line with IPCC estimates.

What will the world be like after the Warming? This is the question that is probably the most on people's minds. One can answer this question two ways. The first approach, taken by the Intergovernmental Council on Climate Change (IPCC) and Burke et al. (2018), has been to run hundreds of climate simulations that predict global climatic conditions using various global warming scenarios (Figure 22). These results are very detailed and make explicit predictions (IPCC, 2007, 2018, 2019; Collins et al., 2013).

Another way to understand our warmer future world is to compare the various possible warming outcomes to the climates of the past. The area shaded in red on Figure 23 represents the temperatures that lie within the range of the global warming predicted by the model presented here (16.5˚C – 19.5˚C). You can see that this shaded region is much cooler than some of the hothouse climates of the past. It is very good news that future global warming will likely not reach these extreme hot house temperatures. Along the time-axis in Figure 23, several boxes highlight time intervals in the deep past that had similar global climates. Of these, the Late Eocene – Miocene Icehouse is probably the best analog to the climate we might experience after this period of Post-Anthropogenic Warming (PAW).

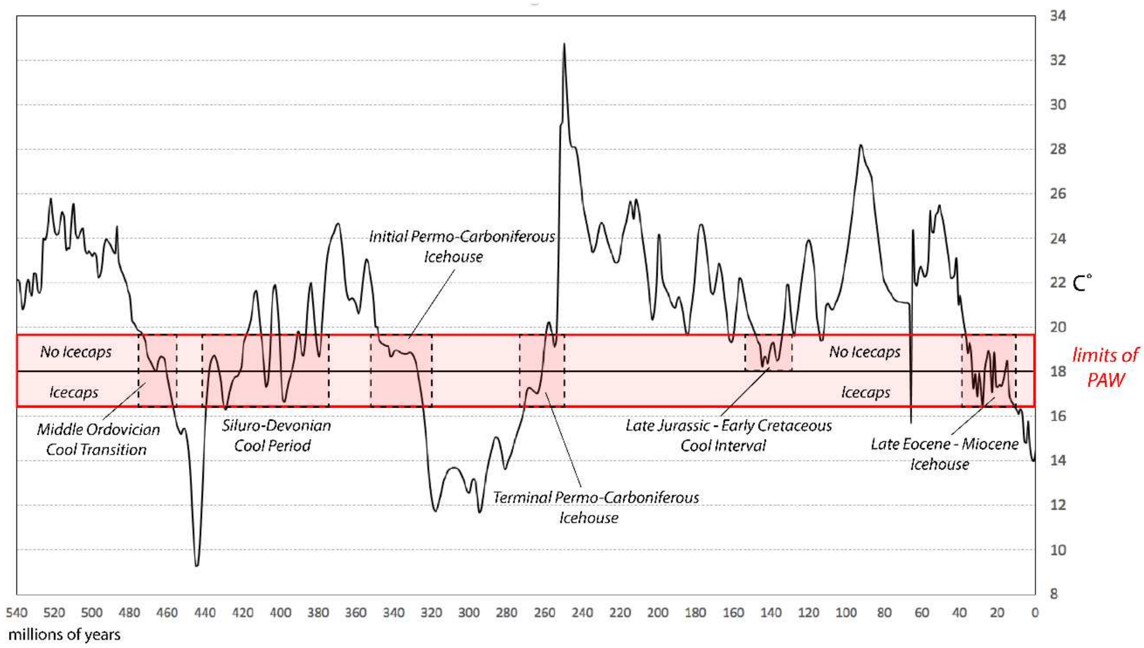

Figure 23. Projection of Future Global Warming onto Phanerozoic Temperature Time Scale. The likely amount of Post-Anthropogenic Warming (PAW) (red line). The boxes indicate times in the geological past when global temperatures were within the range of predicted PAW. When the Global Average Temperature is below 18˚C large polar icecaps can form. When the Global Average Temperature is above 18˚C large polar icecaps are unlikely to form.

The geography of the early Oligocene world (30 million years ago) and the early Miocene world (15 Ma) resembled the modern world (Figure 24). The continents were essentially in the same places and the oceans were about as wide as they are today. A large ice cap covered Antarctica, which was isolated from the other continents by the Circum-Antarctic Ocean. The northern hemisphere lacked any permanent ice cover, though snow covered the northernmost reaches of the continents during the winter.

Unlike today's climate, the climate during the Oligocene and early Miocene was a little warmer near the Equator, and a diverse fauna thrived in tropical rain forests and in the oceans. Modern-sized desert belts separated the tropics from an expanded warm temperate belt that stretched across the northern hemisphere. The northern sub-polar regions, as well as Australia, were both wetter and warmer.

These were worlds where land mammals thrived, diversified, and spread across the continents. Whales and enormous sharks ruled the seas. Plants also diversified. Grasslands covered the steppes and savannas and tropical and temperate forests provided a diverse set of habitats. All in all, the world was a reasonably nice place to live. Given enough time (5,000 -10,000 years; Archer, 2005; 2009a,b), we might expect the same equable conditions to prevail after the Warming.

The other five climatic "matches", though they had similar ranges of global temperature, had very different geographies. The climatic zones on a global Pangea would have been very different than the modern climatic belts.

In conclusion, we are leaving our Ice Age heritage behind. A new, warmer world awaits us. The problem we face is not so much where we are headed, but rather how we will get there. The time for decisive action is quickly slipping away. Our stern challenge is to adapt to the rapid period of global warming that will take place during the next 100 years. To do this we must immediately take action to reduce our CO_2 emissions and take the steps needed to mitigate the undeniable damage that will be done to our environment, civilization, and society in the near future.

6. Summary and Conclusions

It has been long recognized that the Earth’s climate, in particular the average global temperature, has alternated between ”icehouse” and “hothouse” states. More than 70 years ago, Umbgrove (1947), and later Fischer (1981, 1982, 1984) recognized that these climatic “modes” varied on short-term, medium-term, and long-term timescales. During the past 20 years, beginning with the comprehensive pioneering work of Veizer et al. (1999) and followed by the insightful syntheses of Royer et al, (2004), Zachos et al. (2001, 2008), Grossman (2012 a,b), Boucot et al. (2013), Veizer and Prokoph (2015), O’Brien et al. (2017), Henkes et al. (2018), Valdes et al. (2018), and most recently Song et al. (2019), we now stand at the threshold to a deeper, more complete understanding of both the tempo and mode of global temperature change during the Phanerozoic.

The goal of this essay has been to synthesize all of the available evidence for temperature change during the last 540 million years into a single, coherent, well-constrained global temperature curve (Figure 19-21, Table 3-7). Though the details may vary, there is good agreement between the temperature curve we present and earlier work (see Figure 1).

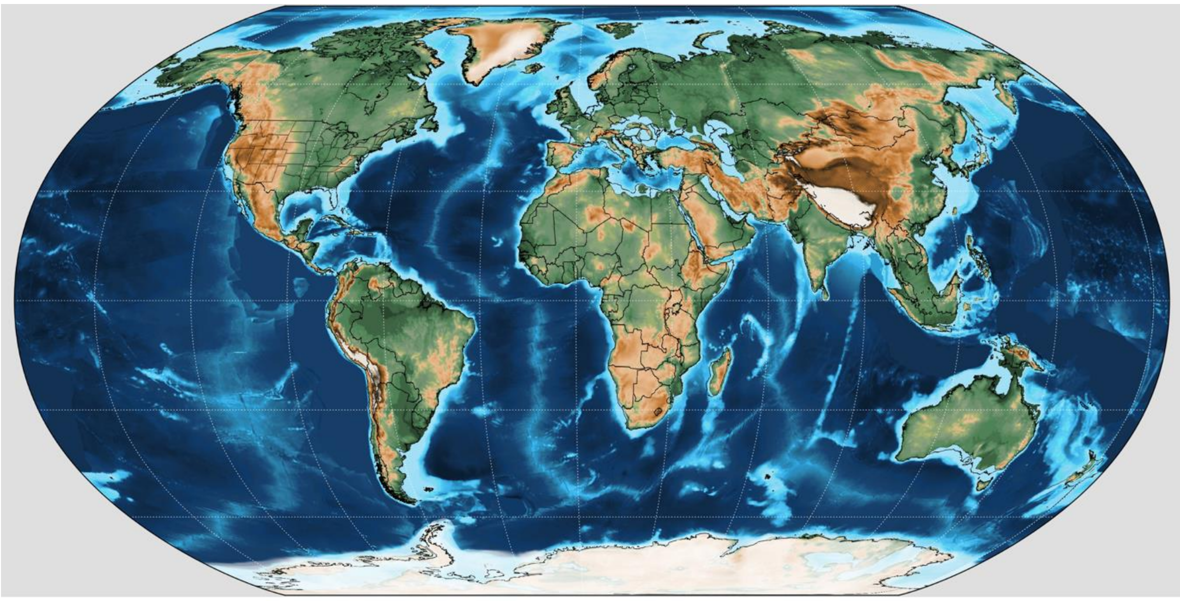

Middle Miocene Thermal Maximum (Langhian, 14.9 Ma)

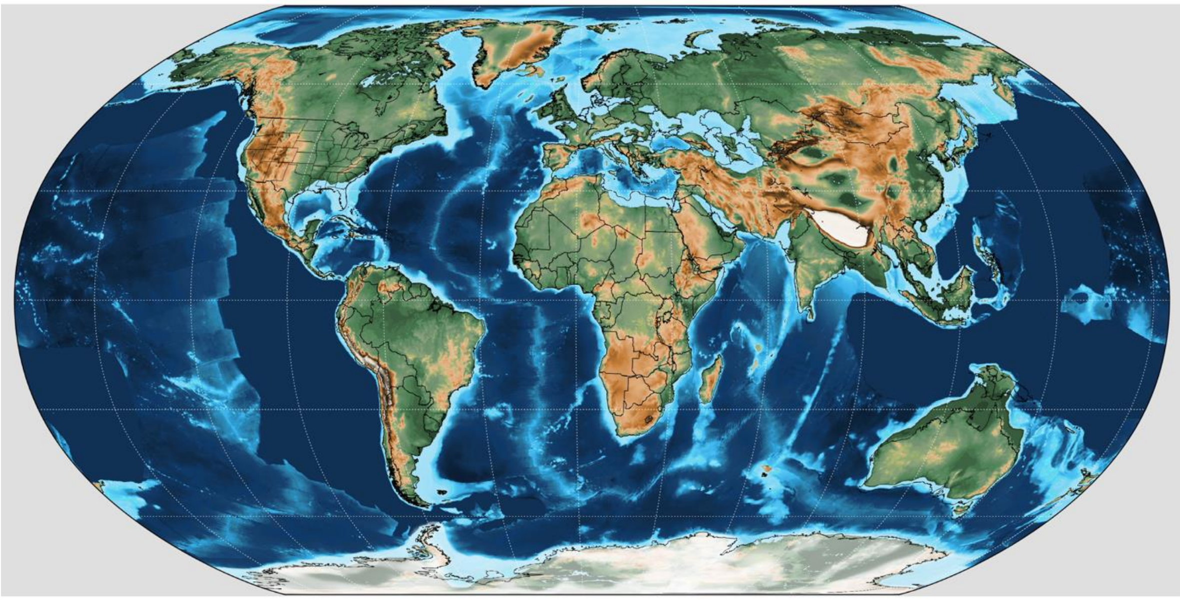

Early Oligocene Cool Interval (Rupelian, 31 Ma)

Figure 24. Paleogeographic maps for the early Oligocene (30 Ma) and early Miocene (15 Ma). These past time periods are a good climatic match for world after Anthropogenic Warming.

We have produced this model of Phanerozoic temperatures by deconstructing temperature change into three components: 1) long-term (>50 million years) temperature changes, 2) medium-term (10 – 20 million years), and 3) short-term temperature changes (a few million years or less).

The Earth’s long-term temperature change is controlled by multiple tectonic and environmental processes that drive the Earth’s climate from icehouse to hothouse conditions, and vice versa. These changes can be described by mapping the changing Pole-to-Equator gradient revealed by paleogeographic distribution of lithologic indicators of climate such as: tillites, dropstones, glendonites, high latitude mangroves, palms, and crocodiles; temperate coal, evaporites, calcretes, tropical coals, bauxites, and laterites, (see Figures 4 and 5; Boucot et al., 2013). Long-term temperature changes occur due to changes in the Earth's "climatic equilibrium" which is controlled by the level of greenhouse gases in the atmosphere (principally CO_2), the geographic configuration of the continents and ocean basins (paleogeography and paleoceanography), the effectiveness of erosion and chemical weathering, and the reflectivity of the Earth's surface (albedo). Many of these factors are interconnected by a complex network of positive and negative feedback loops that can accelerate or decelerate changes in long-term global temperature (Hay, 2016; Ruddiman, 2001). Figure 13 illustrates our best estimate of the long-term temperature of the Earth during the past 540 million years.

Medium-term (10 – 20 million years) changes in the Earth's temperature are revealed by the record of isotopic temperatures measured in carbonate and phosphatic fossils. Recent global compilations of isotopic measurements of temperature (Grossman, 2012a&b, Veizer and Prokoph, 2015; Song et al., 2019; Grossman and Joachimski, 2020) have allowed us to generate a first-order model that describes the variation in tropical and polar temperatures for the last 540 million years (Figure 17). There are still numerous uncertainties regarding the interpretation of isotopic temperatures. For example, the isotopic composition of seawater can vary due to excess evaporation or the local influx of freshwater, as well as the removal of ^{16}O from the oceans due to the growth of vast continental ice sheets. Also, the role that geographic and oceanographic variations play in $\delta^{18}O$ variability has yet to be rigorously examined. Despite these caveats, we believe that the temperature record obtained from oxygen isotope data is robust and that a testable, first-order signal is generally recognizable (Figure 9).

The causes of medium-term fluctuations in temperature are many and complex. We have not yet unravelled these forcing functions, but they are likely to include tectonic and geologic events such as: continental collisions and subsequent mountain building and unroofing, periods of ophiolite obduction and subsequent chemical weathering, the opening of oceanic gateways, and some mega-evolutionary events such as the evolution of land plants. One of the predictions made by our analysis of medium-term temperature changes is that there may have been several “mini-ice ages”, interspersed between the major glacial episodes (e.g. Hirnantian Ice Age, Late Paleozoic Icehouse, and Late Cenozoic Icehouse; Figure 16).

Short-term changes in the Earth’s temperature are probably the most demonstrable because they are related to well-documented geologic events, namely the eruption of enormous volcanic provinces (LIPs) and the impact of large bolides. In this essay, we have documented that the eruption of ~20 large LIPs are strongly correlated with times of warmer global temperatures (Figure 15 Tables 3-7). Conversely, it appears that large bolide impacts are well-correlated with cooler periods in Earth history (Figure 15, Tables 3-7), though a cause and effect relationship is less certain. It remains possible that a few of the most dramatic cooling events in Earth history may have been caused by as yet unrecognized large impact events (e.g. “Khione” event, Hirnantian Ice Age).

In this essay, we combined the long-term, medium-term, and short-term changes in global temperature to produce the Phanerozoic Temperature Timescale (Figure 19-21, Tables 3-7). The Phanerozoic Temperature Timescale is divided into 24 “chronotemps”, or distinct warm and cool intervals. The youngest chronotemp (W1) is the current period of anthropogenic warming. The oldest postdates the Cryogenian “Snowball Earth”. Tables 3-7 list the names, timing, and temperatures associated with each chronotemp.

It can certainly be argued that constructing a Phanerozoic Temperature Timescale is premature and an effort filled with error and unproven assumptions. Though this is probably true, we believe that the effort is worthwhile because we now have a structure that can be built upon, refined, corrected, expanded, and compared to other temperature models that use data sets that we did not use (i.e., clumped isotopes, TEX_{86}). Moreover, having a paleotemperature timescale is essential if we are to understand the tempo and mode of climate change during the past 720+ million years. By characterizing, in a quantitative way, the pattern of paleotemperature change through time, we may be able to gain important insights into the history of the Earth System and the fundamental causes of climate change. These insights may be helpful guide as we traverse an uncertain path into the future.

7. Acknowledgements

CRS would like to thank the past industrial sponsors of the PALEOMAP Project. H.S. is supported by the National Natural Science Foundation of China (41821001). B.J.W.M. is supported by the UK Natural Environment Research Council (NE/S009663/1). This work is part of the PhanTASTIC project led by Scott Wing and Brian Huber at the Smithsonian Institution National Museum of Natural History. The workshop was supported by a gift from Roland and Debra Sauermann. CRS especially benefitted from discussions of past climate with Dana Royer, Linda Ivany, Paul Valdes, Dan Lunt, Colin Summerhayes, Jan Veizer, and Ethan Grossman. CRS would like to thank Joseph Westrich, Colin Summerhayes, David Archer, Daniel Horton, and Peter Lange for their valuable scientific and critical input on the future global warming essay. Seth Stein and his class at Northwestern University (EPS 362) provided valuable feedback on my essay describing future global warming and convinced me to rewrite my initial essay as a do-it-yourself global warming calculator. Class members Peter Puleo, Tim Coston, and Chutian Chen provided especially helpful reviews. Special thanks to Phyllis Richmond for correcting grammar, clarifying prose, and corralling verbiage. This essay is dedicated to the life-long work and research of Larry Frakes.

References Cited

Ahlberg, A., Herman, A.B., Raikevich, M., Rees, A., and Spicer, R., 2002. Enigmatic Late Cretacoeous high paleo-latitude lonestones in Chukotka, northeasternmost Asia, GFF, v. 124, p. 197-199.

Ahlberg, A., Olsson, I., Simkevicius, P., 2003. Triassic–Jurassic weathering and clay mineral dispersal in basement areas and sedimentary basins of southern Sweden. Sedimentary Geology, v. 161, p. 15–29.

Alley, R.B., 2000. The Two-Mile Time Machine, Princeton University Press, Princeton, 229 pp.

Alley, N.F., and Frakes, L.A., 2003. First known Cretaceous glaciation: Livingstone Tillite Member of the Cadna-owie formation, Australian Journal of Earth Sciences, v. 50, p. 139-144.

Alsenz, H., Regnery, J., Ashckenazi-Polivoda, S., Meilijson, A., Ron-Yankovich, L., Abramovich, S., Illner, P., Almogi-Labin, A., Feinstein, S., Berner, Z., Püttmann, W., 2013. Sea surface temperature record of a Late Cretaceous tropical southern Tethys upwelling system. Palaeogeogr. Palaeoclimatol. Palaeoecol. 392, 350–358.

Alvarez, L.W., and Alvarez, W., Asaro, F., and Michel, H.V., 1980. Extraterrestrial cause for the Cretaceous-Tertiary extinction, Science, 208:1095-1107, doi: 10.1126/science.208.4448.1095

Archer, D., 2005. Fate of fossil-fuel CO_2 in geologic time, Journal of Geophysical Research, Oceans, doi: 10.1029/2004JC002625.

Archer, D., 2009. The Long Thaw, How Humans Are Changing the Next 100,000 years of Earth's Climate, Princeton University Press, Princeton, 180 pp.

Archer, D., Eby, M., Brovkin, V., Ridgwell, A., Cao, I., Mikolajewicz, U., Caldiera, K., Matsumoto, K., Munhoven, G., Montenegro, A., and Tokos, K., 2009. Atmospheric lifetime of fossil fuel carbon dioxide, Annual Review of Earth and Planetary Sciences, v. 37, pp. 117-134.

Arthur, M.A., and Sageman, B.B., 1994. Marine black shales: Depositional mechanisms and environments of Ancient Deposits, Annual Review of Earth and Planetary Sciences, 22: 499-552.

Azmy, K., Veizer, J., Bassett, M.G., Copper, P., 1998. Oxygen and carbon isotopic composition of Silurian brachiopods: Implications for coeval seawater and glaciations, Geological Society of America, v. 110, no. 11, p. 1499–1512.

Balini, M., Lucas, S.G., Jenks, J.F, and Spielmann, J.A., 2010. Triassic ammonoid biostratigraphy: an overview, Geological Society of London, Special Publications, v.334:221–262.

Bambach, R.K., Knoll, A.H., Wang, S.C., 2004. Origination, extinction, and mass depletions of marine diversity. Paleobiology, v. 30, p. 522–542.

Barnola, J.M., Raynaud, D., Korotkevich, Y.S., and Lorius, C., 1987. Vostok ice core provides 160,000-year record of atmospheric CO2, Nature, v. 329, p. 408-414

Barral, A, Gomez, B., Legendre, S., Lécuyer, C., 2017. Evolution of the carbon isotope composition of atmospheric CO_2 throughout the Cretaceous. Palaeogeography, Palaeoclimatology, Palaeoecology, http://dx.doi.org/10.1016/j.palaeo.2017.01.034

Barron, E.J. and Washington,W.M., 1982. Cretaceous climate: A comparison of atmospheric simulations with the geologic record, Palaeogeography, Palaeoclimatology, and Palaeoecology, v. 40, p. 103-133, doi: 10.1016/0031-0182(82)90086-4.

Beerling, D.J., Berner, R.A., 2002. Biogeochemical constraints on the Triassic-Jurassic boundary carbon cycle event, Global Biogeochemical Cycles, v. 16, no. 3, p.1036, doi:10. 1029/2001GB001637

Benedetto, J.L., and Sanchez, T.M., 1996. The "Afro-South American Realm" and Silurian "Clarkeia Fauna", in P. Copper and J. Jin (editors), Brachiopods, Balkema, p. 29-33.

Benton M.J., 1993. Late Triassic extinctions and the origin of the dinosaurs, Science, v. 260, p. 769–770.

Benton M.J., Zhang, Q., Hu, S., Chen, Z.Q., Wen. W,, et al., 2013. Exceptional vertebrate biotas from the Triassic of China, and the expansion of marine ecosystems after the Permo-Triassic mass extinction. Earth-Science Reviews, v. 125, p. 199–243.

Bergmann, K.D., Al Balushi, S.A.K., Macley, T., Grotzinger, J.P., and Eiler, J.M., 2018a. A 600-million year carbonate clumped-isotope record from the Sultanate of Oman, Journal of Sedimentary Research, v. 88, p. 960–979, doi:org/10.2110/jsr.2018.51.

Bergmann, K.D., Finnegan, S., Creel, R., Eiler, J.M., Hughes, N.C., Popov, L.E., and Fischer, W.W., , 2018b. A paired apatite and calcite clumped isotope thermometry approach to estimating Cambro-Ordovician seawater temperatures and isotopic composition, Geochimica et Cosmochimica Acta, v. 224, p.18-41, doi: 10.1016/j.gca.201 7.11.015.

Bernardi, M., Gianolla, P., Petti, F.M., Mietto, P., and Benton, M.J., 2018. Dinosaur diversification linked with the Carnian Pluvial Episode, Nature Communications, v. 9 :1499, doi: 10.1038/s41467-018-03996-1.

Berner R. A., 1994. GEOCARB II: A revised model of atmospheric CO_2 over Phanerozoic time. American Journal Science 294(1):56–91.

Berner, R.A., 2004. The Phanerozoic Carbon Cycle: CO2 and O2. Oxford University Press, New York.

Berner, R.A., Lasaga, A.C., & Garrels, R.M. (1983). The carbonate silicate geochemical cycle and its effect on atmospheric carbon dioxide over the past 100 million years. *American Journal Science,* 283, 641-683.

Beuf, S., Biju-Duval, B., deCharpal, O., Rognon, P., Gariel, O., and Bennacef, A., 1971. Les Gres du Paleozoique inferieur au Sahara, Editions Technip, Paris, 464 pp

Bice, K.L., and Norris, 2002, Possible atmospheric CO_2 extremes of the middle Cretaceous (late Albian to Turonian), Paleoceanography, 17:1-17.

Black, B.A., and Gibson, S.A., 2019. Deep Carbon and the life cycle of Large Igneous Provinces, Elements, v. 15, p. 319-324.

Bluth, G.J.D., & Kump, L.R., 1991. Phanerozoic paleogeology. American Journal Science, 291, 284-308

Bohor, B.F., Triplehorn, D.M., Nichols, D.J., and Millard, H.T.,Jr., 1987. Dinosaurs, spherules, and the "majic" layer: A new K-T boundary clay site in Wyoming, Geology,15:896-899.

Bond, D.P.G., and Grasby, S.E., 2017. On the causes of mass extinctions, Palaeogeography, Palaeoclimatology, Palaeoecology, v. 478, p. 3–29, doi.org/10.1016/j.palaeo.2016.11.005

Bonis, N.R., Ruhl, M., Kurschner, W.M., 2010. Climate change driven black shale deposition during the end-Triassic in the western Tethys. Palaeogeography, Palaeoclimatology, Palaeoecology, v. 290, p. 151–159.

Boucot, A.J., Chen Xu, and Scotese, C.R, 2013. Phanerozoic Paleoclimate: An Atlas of Lithologic Indicators of Climate, SEPM Concepts in Sedimentology and Paleontology, (Print-on-Demand Version), No. 11, 478 pp., ISBN 978-1-56576-289-3, October 2013, Society for Sedimentary Geology, Tulsa, OK.

Boucot, A.J., 1990. Silurian biogeography, in W.S. McKerrow and C.R. Scotese (editors), Palaeozoic Palaeogeography and Biogeography, Geological Society of London Memoir No. 12, p. 191-196.

Brady, E.C., DeConto, R., Thompson, S.L., 1998, Deepwater formation and poleward ocean heat transport in the warm climate extreme of the Cretaceous (80 Ma), Geophysical Research Letters, 25: 4205-4208.

Brand, U., Azmy, K., and Veizer, J., 2006. Evaluation of the Salinic I tectonic, Cancañiri glacial and Ireviken biotic events: Biochemostratigraphy of the Lower Silurian succession in the Niagara Gorge area, Canada and U.S.A., Palaeogeography, Palaeoclimatology, Palaeoecology, v. 241, p. 192–213, doi:10.1016/j.palaeo.2006.03.004

Brass, G.W., Southam, J.R., Peterson, W.H., 1982. Warm Saline Bottom Water in the Ancient Ocean. Nature 296, 620-623.

Brassell, S.C., 2009. Steryl ethers in a Valanginian claystone: molecular evidence for cooler waters in the central Pacific during the Early Cretaceous? Palaeogeogr. Palaeoclimatol. Palaeoecol. 282, 45–57.

Brandley, R.T., and Krause, F.F., 1994. Thinolite-type pseudomorphs after ikait: indicators of cold water on the subequatorial western margin of Lower Carboniferous North America, Canadian Society of Petroleum Geologists Memoir 17, p. 333-334.

Brenchley, P.J., Marshall., J.D., Carden, G.A.F., Robertson, D.B.R., Long, D.G., Meidla, T., Hints, L., and Anderson, T.F., 1994. Bathymetric and isotopic evidence for a short-lived Late Ordovician glaciation in a greenhouse period, Geology, v. 22, p. 295-298.

Brett, C.E., Ivany, L.C., Bartholomew, A.J., Desantis, M.K., and Baird, G.C., 2009. Devonian ecological-evolutionary subunits in the Appalachian Basin: a revision and test of persistence and discreteness, in Devonian Change: Case Studies in Palaeogeography and Palaeoecology, P. Konigshof (editor), Geological Society of London, Special Publication v. 314, p. 7-36.

British Petroelum (BP), 2019, "BP Energy Outlook, 2019". https://www.bp.com/content/dam/bp/business-sites/en/global/corporate/pdfs/energy-economics/energy-outlook/bp-energy-outlook-2019.pdf

Bruckschen, P., Oesmann, S., and Veizer, J., 1999. Isotope stratigraphy of the European Carboniferous: proxy signals for ocean chemistry, climate and tectonics, Chemical Geology, v. 161, p. 127–163.

Brune, S., Williams, S.E., Müller, R.D., 2017. Potential links between continental rifting, CO_2 degassing and climate change through time,

Buggisch, W., Joachimski, W.M., Sevastopulo, G., and Morrow, J.R., 2008. Mississippian $\delta^{13}C_{carb}$ and conodont apatite $\delta^{18}O$ records - Their relation to the Late Palaeozoic Glaciation, Palaeogeography, Palaeoclimatology, Palaeoecology, v. 268, p. 273–292, doi:10.1016/j.palaeo.2008.03.043

Burke, K.D., Williams, J.W. Chandler, M.A., Haywood, A.M., Lunt, D.J., and Otto-Bliesner, B.L., 2018. Pliocene and Eocene provide best analogs for near-future climates, Proceedings of the National Academy of Sciences, v. 115, no. 52, 13288-13293.

Cantrill, D.J., and Poole, I., 2012. The Vegetation of Antarctica Through Geological Time, Cambridge University Press, Cambridge, England, 480 pp.

Cao, W., Williams, S., Flament, N., Zahirovic, S., Scotese, C.R., and Müller, R.D., 2019. Paleolatitudinal distribution of lithologic indicators of climate in a paleogeographic framework, Geological Magazine, v. 156, no. 2, p. 331-354.

Caputo, M.V., de Melo, J.H.G., Streel, M., and Isbell, J.L., 2008. Late Devonian and Early Carboniferous glacial records of South America, in C.R. Fielding, T.D. Frank. and J.L. Isbell (editors), Resolving the Late Paleozoic Ice Age in Time and Space, Geological Society of America Special Paper v. 441, p. 161-174.

Chamberlin, T.C., 1906. On a possible reversal of deep sea circulation and its influence on geologic climates, Proceedings of the American Philosophical Society, v. 45, n. 182, p. 33-43.

Chatterjee, S., Guven, N., Yoshinobu, A., and Donofrio, R., 2006. Shiva structure: A possible KT boundary impact cater on the western shelf of India, Museum of Texas Tech University, Special Publication, 40 pp.

Chen, B., Joachimski, M. M., Shen, S.-Z., Lambert, L. L., Lai, X.-L., Wang, X.-D., Chen, J., and Yuan, D.-X., 2013, Permian ice volume and palaeoclimate history: Oxygen isotope proxies revisited, Gondwana Research, v. 24, no. 1, p. 77-89.

Chen, B., Joachimski, M. M., Wang, X.-D., Shen, S.-Z., Qi, Y.-P., and Qie, W.-K., 2016, Ice volume and paleoclimate history of the Late Paleozoic Ice Age from conodont apatite oxygen isotopes from Naqing (Guizhou, China), Palaeogeography, Palaeoclimatology, Palaeoecology, v. 448, p. 151-161.

Chenet, A. L., Fluteau, F., Courtillot, V., Gerard, M., & Subbarao, K. V., 2008. Determination of rapid Deccan eruptions across the Cretaceous- Tertiary boundary using paleomagnetic secular variation: Results from a 1200-m-thick section in the Mahabaleshwar escarpment. Journal of Geophysical Research, 113, B04101. https://doi.org/10.1029/2006JB004635

Clapham, M.E., and Renne, P.R., 2019. Flood Basalts and Mass Extinctions. Annual Review of Earth Planetary Sciences, v. 47, p. 275–303, doi: 10.1146/annurev-earth-053018-060136

Clarkson, M.O., Kasemann, S.A., Wood, R.A., Lenton, T.M., Daines, S.J., et al., 2015. Ocean acidification and the Permo-Triassic mass extinction, Science, v. 348, p. 229–232, Cocks, L.R.M., 1972. The origin of the Silurian Clarkeia shelly fauna of South America, and its extension to West Africa, Palaeontology, v. 15, p.623-630.

Cocks, L.R.M., and Fortey, R.A., 1990. Biogeography of Ordovician and Silurian faunas, in Palaeozoic Palaeogeography and Biogeography, W.S. McKerrow and C.R. Scotese (editors), Geological Society of London Memoir No. 12, p. 97-104.

Colbath, G.K., 1986. Abrupt terminal Ordovician extinction in phytoplankton associations, southern Appalachians, Geology, v. 14, p. 943-946.

Collins, M.R., R. Knutti, J. Arblaster, J.-L. Dufresne, T. Fichefet, P. Friedlingstein, X. Gao, W.J. Gutowski, T. Johns, G. Krinner, M. Shongwe, C. Tebaldi, A.J. Weaver, and M. Wehner, 2013: Long-term Climate Change: Projections, Commitments and Irreversibility. In Climate Change 2013: The Physical Science Basis. Contribution of Working Group I to the Fifth Assessment Report of the Intergovernmental Panel on Climate Change [Stocker, T.F., D. Qin, G.-K. Plattner, M. Tignor, S.K. Allen, J. Boschung, A. Nauels, Y. Xia, V. Bex, and P.M. Midgley (eds.)]. Cambridge University Press, Cambridge, United Kingdom and New York NY, USA.

Courtillot, V., and Renne, X., 2003. On the ages of flood basalt events, Comptes Rendus Geosciences, v. 335, p. 113-140.

Cramer,B.S., Toggweiler, J.R., Wright, J.D., Katz, M.E., and Miller, K.G., 2009. Ocean overturning since the Late Cretaceous: Inferences from a new benthic isotope compilation, Paleoceanography 6, v. 24, PA4216, p. 1-14, doi: 10.1029/2008PA001683.

Crowley, T.J., 1994. Pangean Climates, in Pangea: Paleoclimate, Tectonics, and Sedimentation during Accretion, Zenith, and Breakup of a Supercontinent, (editor), G. D. Klein, Geological Society of America Special Paper 288, p. 25-39.

Crowley,T.J., and Baum, S.K., 1991. Toward reconciliation of Late Ordovician (~440 Ma) glaciation with very high CO_2 Levels, Journal of Geophysical Research, v. 96, no. D12, p. 22,597-22,610.

Crowley,T.J., and Baum, S.K., 1995. Reconciling Late Ordovician (440 Ma) glaciation with very high (14X) CO_2 Levels, Journal of Geophysical Research, v. 100, no. D1, p. 1093-1101.

Dal Corso, J., Benton, M. J., Bernardi, M., Franz, M., Gianolla, P., Hohn, S., and Zhang, Y., 2018a. First Workshop on the Carnian Pluvial Episode (Late Triassic): a report, Albertiana, v. 44, p. 49-57.

Dal Corso, J., Gianolla, P., Rigo, M., Franceschi, M., Roghi, G., Mietto, P., Manfrin, S., Raucsik, B., Budai, T., Jenkyns, H.C., Reymond, C.E., Caggiati, M., Gattolini, G., Breda, A., Merico, A., Preto, N., 2018b. Multiple negative carbon-isotope excursions during the Carnian Pluvial Episode (Late Triassic), Earth-Science Reviews, v. 185, p. 732–750, doi:org/10.1016/j.earscirev.2018.07.004

Davydov, V.I., and Cozar, P., 2017. The formation of the Alleghenian Isthmus triggered the Bashkirian glaciation: Constraints from warm-water benthic foraminifera, Palaeogeography, Palaeoclimatology, Palaeoecology, http://dx.doi.org/10.1016/j.palaeo.2017.08.012

Davydov, V.I., 2014. Warm water benthic foraminifera document the Pennsylvanian–Permian warming and cooling events — The record from the Western Pangea tropical shelves, Palaeogeography, Palaeoclimatology, Palaeoecology, v. 414, p. 284-295, doi.org/10.1016/j.palaeo.2014.09.013

Davydov, V.I., Korn, D., Schmitz, M.D., 2010. The Carboniferous Period, Chapter 23, in The Geologic Time Scale 2012, volume 2, F.M. Gradstein, J.G. Ogg, M.D. Schmitz, and G.M. Ogg (editors), Elsevier, Amsterdam, p. 603-651.

De Lurio, J.L. and Frakes, L.A., 1999. Glendonites as a paleoenvironmental tool: Implications for early Cretaceous high latitude climates in Australia, Geochimica et Cosmochimica Acta, Vol. 63, No. 7/8, pp.

Demaison, G.J., and Moore, G.T., 1980. Anoxic environments and oil source bed genesis, American Association of Petroleum Geologists Bulletin, 64:1179-1209.

Dera, G., Brigaud, B., Monna, F., Laffont, R., Pucéat, E., Deconinck, J.-F., Pellenard, P., Joachimski, M.M., and Durlet, C., 2011. Climatic ups and downs in a disturbed Jurassic world, Geology, v. 39, no. 3., p. 215-218, doi: 10.1130/G31579.1

Dettmann, M.E., 1989. Antarctica: Cretaceous cradle of austral temperate rainforests?, in Origins and Evolution of the Antarctic Biota, Geological Society of London Special Publication, J.A. Crame (editor), v. 47, p. 89-105.

Díaz-Martínez, E., and Grahn, I., 2007. Early Silurian glaciation along the western margin of Gondwana (Peru, Bolivia and northern Argentina): Palaeogeographic and geodynamic setting. Palaeogeography, Palaeoclimatology, Palaeoecology, v. 245, p. 62–81, doi:10.1016/j.palaeo.2006.02.018

Duncan, R.A., and Huard, J., 1997. Trace metal anomalies and global anoxia: the OJP-Selli hydrothermal plume connection, EOS Transactions American Geophysical Union, 78, F774.

Elliot, D.H., Fleming, T.H., Kyle, P.R., and Foland, K.A., 1999. Long-distance transport of magmas in the Jurassic Ferrar large igneous province, Antarctica, Earth and Planetary Science Letters, v. 167, p. 89-104.

Elrick, M., and Scott, L. A., 2010, Carbon and oxygen isotope evidence for high-frequency (10^4–10^5yr) and My-scale glacio-eustasy in Middle Pennsylvanian cyclic carbonates (Gray Mesa Formation), central New Mexico, Palaeogeography, Palaeoclimatology, Palaeoecology, v. 285, no. 3, p. 307-320.

Emiliani, C. 1954. Temperatures of Pacific bottom waters and polar superficial waters during the Tertiary, Science, v. 119, issue 3103, p. 853-855, doi: 10.1126/science.119.3103.853

Emiliani, C., 1955. Pleistocene temperatures, Journal of Geology, v. 63, no. 6, p. 538-578.

EPICA Community Members, 2004. Eight glacial cycles from an Antarctic ice core, Nature 429: 623-628.

Epstein, S. and Mayeda, T., 1953. Variation of O18 content of waters from natural sources, Geochemica et Cosmochemica Acta. 4 (5), 213-224.

Erba, E., Bartolini, A., and Larson, R.L., 2004. Valanginian Weissert oceanic anoxic event, Geology 32(2):149-152, doi 10.1130/G20008.1

Erba, E., Duncan, R.A., Bottini, C., Tiraboschi, D., Weissert, H., Jenkyns, H.C., and Malinverno, A., 2015, Environmental consequences of Ontong Java Plateau and Kerguelen Plateau volcanism, in Neal, C.R., Sager, W.W, Sano, T., and Erba, E., eds., The Origin, Evolution, and Environmental Impact of Oceanic Large Igne- ous Provinces: Geological Society of America Special Paper 511, p. 271–303, doi:10.1130/2015.2511(15).

Ernst, R.E., 2014. Large Igneous Provinces, Cambridge University Press, Cambridge, UK, 653 pp.

Ernst, R.E., and Youbi, N., 2017. How Large Igneous Provinces affect global climate, sometimes cause mass extinctions, and represent natural markers in the geological record, Palaeogeography, Palaeoclimatology, Palaeoecology, v. 478, p. 30–52., doi:10.1016/j.palaeo.2017.03.014

Erwin, D.H., 1993. The Great Paleozoic Crisis: Life and Death in the Permian, Columbia University Press, New York, 327 pp.

Erwin, D.H., 1995. The End-Permian Mass Extinction, in *The Permian of the Northern Hemisphere*, volume 1: Paleogeography, Paleoclimates, Stratigraphy, P.A. Scholle, T.M. Peryt, D.S Ulmer-Scholle (editors), Springer-Verlag, Berlin, p. 3-19.

Erwin, D.H., 2006. Extinction: How Life on Earth Nearly Ended 250 Million Years Ago, Princeton University Press, Princeton, 296 pp.

Exon, N.F., Kennett, J.P., and Malone, M., 2004.The Cenozoic Southern Ocean: Tectonics, Sedimentation, and Climate Change between Australia and Antarctica, American Geophysical Union, Geophys. Monograph 151.

Farnsworth, A., Lunt, D.J., O'Brien, C., Foster, G.L., Inglis, G.N., Markwick, P., Pancost, R.D., and Robinson, S.A., 2019. Climate sensitivity on geological timescales controlled by non-linear feedbacks and ocean circulation, Geophysical Research Letters.

Fielding, C.R., Frank, T.D., Isbell, J.L., Henry, L.C., and Domack, E.W., 2010. Stratigraphic signature of the late Palaeozoic Ice Age in the Parmeener Supergroup of Tasmania, SE Australia, and inter-regional comparisons , Palaeogeography, Palaeoclimatology, Palaeoecology, v. 298, p. 70–90, doi:10.1016/j.palaeo.2010.05.023

Fielding, C.R., Frank, T.D., Birgenheier, L.P., Rygel, M.C., Jones, A.T., and Roberts, J., 2008. Stratigraphic imprint of the Late Palaeozoic Ice Age in eastern Australia: a record of alternating glacial and nonglacial climate regime, Journal of the Geological Society, London, v. 165, p. 129–140.

Fielding, C.R., Frank, T.D., Birgenheier, L.P., Rygel, M.C., Jones, A.T., and Roberts, J., 2008. Stratigraphic record and facies associations of the Late Paleozoic ice age in eastern Australia (New South Wales and Queensland), in C.R. Fielding, T.D. Frank. and J.L. Isbell (editors), Resolving the Late Paleozoic Ice Age in Time and Space, Geological Society of America Special Paper v. 441, p. 41-58.

Finnegan, S., Bergmann, K., Eiler, J.M., Jones, D. S., Fike, D. A., Eisenman, I., Hughes, N. C., Tripati, A. K., and Fischer, W. W., 2011. The magnitude and duration of Late Ordovician – Early Silurian Glaciation, Science, v. 331, no. 6019, p. 903-906, doi: 10.1126/science.12000803.

Finnegan, S., Heim, N.A., Peters, S.E., Fischer, and Fischer, W.W., 2012. Climate change and selective signature of the Late Ordovician mass extinction, Proceedings of the National Academy of Sciences, v.109, no. 18, p. 6829-6834.

Fischer, A. G., 1981. Climatic oscillations in the biosphere, in M.H. Nitecki (editor), Biotic Crises in Ecological and Evolutionary Time, Academic Press, pp. 103-131.

Fischer, A. G., 1982. Long-term Climatic Oscillations Recorded in Stratigraphy, in Studies in Geophysics: Climate in Earth History, W.H. Berger and J.C. Crowell (editors), Chapter 9., National Academy Press, Washington, D.C., pp. 97-104.

Fischer, A. G., 1984. The Two Phanerozoic Supercycles, in Catastrophes and Earth History: The New Uniformitarianism, W.A. Berggren and J.A. Van Couvering, (editors), Chapter 7, Princeton University Press, Princeton, N.J., pp. 129 – 150.

Flügel, E., 1994. Pangean shelf carbonates: Controls and paleoclimatic significance of Permian and Triassic reefs, in Pangea: Paleoclimate, Tectonics, and Sedimentation during the Accretion, Zenith, and Breakup of a Supercontinent, George D. Klein (ed.), Geol. Soc. America Special Paper, 288: 247-266.

Flügel, E., 2002. Triassic reef patterns, In Kiessling, W., Flügel,, E. & Golonka, J. (eds): Phanerozoic Reef Patterns. SEPM (Society for Sedimentary Geology) Special Publications 72, 391-464.

Flügel,, E. & Kiessling, W., 2002. Patterns of Phanerozoic reef crises. In Kiessling, W., Flügel,, E. & Golonka, J. (eds): Phanerozoic Reef Patterns. SEPM (Society for Sedimentary Geology) Special Publications 72, 691-733.

Foster, G.L., Royer, D.L., and Lunt, D.J., 2017. Future Climate Forcing Potentially without precedent in the last 420 million years, Nature Communications, v. 8, 14845, doi:10.1038/ncomms14845.

Fraenkel, G., 1960. Lethal High Temperatures for Three Marine Invertebrates: Limulus Polyphemus, Littorina littorea and Pagurus longicarpus, Oikos, v. 11 fasc. 2, p. 171-182.

Frakes, L.A., 1989. Climates Through Geologic Time, Elsevier, Amsterdam, 310 pp.

Frakes, L., and Francis, J.E., 1988. A guide to Phanerozoic cold polar climates from high latitude ice-rafting in the Cretaceous. Nature 333, 547–549.

Frakes L. A. and Francis J. E., 1990. Cretaceous palaeoclimates. In Cretaceous Resources, Events, and Rhythms (ed. R. N. Ginsburg and B. Beaudoin), pp. 373–287. Kluwer Academic Publishers.

Frakes, L.A., Francis, J.E., and Syktus, J.I., 1992. Climate Modes of the Phanerozoic, Cambridge University Press, Cambridge, 274 pp. Freeman and Hayes

Francis J. E. and Frakes L. A., 1993. Cretaceous climates. Sediment. Rev. **1,** 17–30.

Frakes, L.A., Alley, N.F., and Deynoux, M., 1995. Early Cretaceous ice rafting and climate zonation in Australia, International Geology Review, v. 37, p. 567-583.

Frank, T.D., Schultis, A.I., Fielding, C.R., 2015. Acme and demise of the late Palaeozoic ice age: A view from the southeastern margin of Gondwana, Palaeogeography, Palaeoclimatology, Palaeoecology, v. 418, p. 176–192, doi.org/10.1016/j.palaeo.2014.11.016

Friedman, M., Sallan, L.C., 2012. Five hundred million years of extinction and recovery: a Phanerozoic survey of large-scale diversity patterns in fishes, Palaeontology, v. 55, p. 707–742.

Galili, N., Shemesh, A., Yam, R., Brailovsky, I., Sela-Adler, M., Schuster, E.M., Collom, C., Bekker, A., Planavsky, N., Macdonald, F.A., Préat, A., Rudmin, M., Trela, W., Sturesson, U., Heikoop, J.M., Aurell, M., Ramajo, J., and Halevy, I., 2019. The geologic history of seawater oxygen isotopes from marine iron oxides, Science, v. 365, p. 469–473.

Gasson, E.G.W., and Kiessling, B.A., 2020. The Antarctic Ice Sheet, A Paleoclimate Modeling Perspective, Oceanography, June 2020 Online Release, pp. 11, doi.org/10.5670/oceanog.2020.208

Gersonde, R. Kyte, F.T., Bleil, U., Diekmann, J.A., Flores, J.A., Gohl, K, Grahl, G., Hagen, R., Kuhn, G., Sierro, F.J., Volker, D., and Bostwick, J.A., 1997. Geological record and reconstruction of the late Pliocene impact of the Eltanin asteroid in the Southern Ocean, Nature, 390: 357-363.

Gibbs, M.T., Bluth, G.J.S., Fawcett, P.J., & Kump, L.R., 1999. Global chemical erosion over the last 250 My: variations due to changes in paleogeography, paleoclimate, and paleogeology. American Journal Science, 299, 611–651.

Girard, C., Klapper, G., and Feist, R., 2005. Subdivision of the terminal Frasnian linguiformis conodont Zone, revision of the correlative interval of Montagne Noire Zone 13, and discussion of stratigraphically significant Associated trilobites, in Understanding Late Devonian and Permian-Triassic Biotic and Climatic Events; Towards an Integrated Approach, D.J. Over, J.R. Morrow, and P.B. Wignall (editors), Developments in Palaeontology & Stratigraphy, v. 20, p. 181-198, Elsevier, Amsterdam.

Goddéris, Y., Donnadieu, Y., Lefebvre, V., Le Hir, G., & Nardin, E., 2012. Tectonic control of continental weathering, atmospheric CO_2, and climate over Phanerozoic times: Comptes Rendus Geoscience, 344, 652–662.

Goddéris, Y., Donnadieu, Y., Le Hir, G., Lefebvre, V., & Nardin, E., 2014. The role of palaeogeography in the Phanerozoic history of atmospheric CO_2 and climate. Earth-Science Reviews, 128, 122–138.

Gough, D.O., 1981. Solar interior structure and luminosity variation, Solar Physics, v. 74, p. 21-34.

Gradstein, F.M., Ogg, J.G., Schmitz, M.D., and Ogg., G.M., 2012. The Geologic Time Scale 2012, v. 1, Elsevier, 435 pp.

Grahn, Y., Caputo, M.V., 1992. Early Silurian glaciations in Brazil Palaeogeography, Palaeoclimatology, Palaeoecology, v. 99, p. 9–15.

Grahn, Y., Gutiérrez, P., 2001. Silurian and Middle Devonian chitinozoa from the Zapla and Santa Bárbara Ranges, Tarija Basin, northwestern Argentina. Ameghiniana, v. 38, p. 35–50.

Grasby, S.E., McCune, G.E., Beauchamp, B., Galloway, J.M., 2017. Lower Cretaceous cold snaps led to widespread glendonite occurrences in the Sverdrup Basin, Canadian High Arctic. Geol. Soc. Am. Bull. 129, 771–787. http://dx.doi.org/10.1130/B31600.1.

Grice, K., Cao, C., Love, G.D., Böttcher, M.E., Twitchett, R.J., et al., 2005. Photic zone euxinia during the Permian- Triassic superanoxic event, Science v. 307, p. 706–709.

Greene, A.R., Scoates, J.S., and Weis, D., 2008. Wrangellia flood basalts in Alaska: A record of plume-lithosphere interaction in a Late Triassic accreted oceanic plateau. Geochemistry Geophysics Geosystems, v. 9, Q12004, doi: 10.1029/2008GC002092.

Greene, A.R., Scoates, J.S., Weis, D., and Israel, S., 2009a. Geochemistry of flood basalts from the Yukon (Canada) segment of the accreted Wrangellia oce- anic plateau. Lithos, v. 110, p. 1–19, doi: 10.1016/j .lithos.2008.11.010.

Greene, A.R., Scoates, J.S., Weis, D., Nixon, G.T., and Kieffer, B., 2009b. Melting history and magmatic evolution of basalts and picrites from the accreted Wrangellia oceanic plateau, Vancouver Island, Canada: Journal of Petrology, v. 50, p. 467–505, doi: 10.1093/petrology/ egp008.

Greene, A.R., Scoates, J.S., Weis, D., Katvala, E.C., Israel, S., and Nixon, G.T. 2010. The architecture of oceanic plateaus revealed by the volcanic stratigraphy of the accreted Wrangellia oceanic plateau, Geosphere, v. 6, p. 47–73.

Grossman, E. L., I994. The carbon and oxygen isotope record during the evolution of Pangea Carboniferous to Triassic, in Klein. G. D., ed., Pangea: Paleoclimate, Tectonics, and Sedimentation During Accretion, Zenith, and Breakup of a Supercontinent: Boulder, Colorado, Geological Society of America Special Paper 288, p. 207-228.

Grossman, E.L., 2012a. Oxygen Isotope Stratigraphy, in The Geologic Time Scale 2012, F. M. Gradstein, J.G. Ogg, M.D. Schmitz, and G.M. Ogg (editors), Elsevier, Amsterdam, volume 1, p. 181-206.

Grossman, E.L., 2012b. Applying Oxygen Isotope Paleothermometry in Deep Time, in Reconstructing Earth's Deep-Time Climate: State of the Art in 2012, L. Ivany and B. Huber (editors), Paleontological Society Short Course, November 3, 2012, The Paleontological Society Papers, v. 18, pp. 39-67.

Grossman, E.L., and Joachimski, M.M., 2020. Oxygen Isotope Stratigraphy, Chapter 10, in The Geologic Time Scale 2020, F. M. Gradstein, J.G. Ogg, M.D. Schmitz, and G.M. Ogg (editors), Elsevier, Amsterdam, volume 1, (in press).

Grossman, E.L., Joachimski, M.M., Barney, B., Henkes, G.A., Ivany, L.C., Lunt, D.L., MacLeod,K.G., Montañez, I.P., Scotese, C., and Wing, S.L., 2018. Toward a Phanerozoic History of Earth's Surface Temperature: The Oxygen Isotope Record of the Paleozoic to Early Cretaceous Time Slice (PalECTS), (abstract), American Geophysical Union, Monday, December 10, 2018, Convention Center, Hall A-C (Poster Hall), Fall Meeting 2018, #PP11F-11319, Washington, D.C.

Grossman, E.L., Yancey, T.E., Jones, T.E., Bruckschen, P., Chuvashov, B., Mazullo, S.J., and Mii, Horng-sheng, 2008. Glaciation, aridification, and carbon sequestration in the Permo-Carboniferous: The isotopic record from low latitudes, Palaeogeography, Palaeoclimatology, Palaeoecology, v. 268, p. 222–233, doi:10.1016/j.palaeo.2008.03.053

Gruszczynski, M., Halas S., Hoffman, A., and Malkowski, K., 1989. A brachiopod calcite record of the oceanic carbon and oxygen isotope shifts at the Permian/Triassic transition. Nature, v. 337, p. 64-68.

Gutjahr, M., Ridgwell, A., Sexton, P.F., anagnoustou, E., Pearson, P.N., Pälike, H., Norris, R.D., Thomas, E., and Foster, G.L., 2017. Very large release of mostly volcanic carbon during the Paleocene-Eocene Thermal Maximum, Nature, v. 548, p. 573-577.

Haig, D.W., McCartain, E., Mory, A.J., Borges, G., Davydov,V.I., Dixon, M., Ernst, A., Groflin, S., Håkansson, E., Keep, M., Dos Santos, Z., Shi, G.R., and Soares, J., 2014. Postglacial Early Permian (late Sakmarian–early Artinskian) shallow-marine carbonate deposition along a 2000 km transect from Timor to west Australia, Palaeogeography, Palaeoclimatology, Palaeoecology, v. 409, p. 180–204, doi.org/10.1016/j.palaeo.2014.05.009

Hallam, A., 2002. How catastrophic was the end-Triassic mass extinction? Lethaia, v.35, p.147-157, doi: org/10.1111/j.1502-3931.2002.tb00075.x

Hames, W., McHone, J.G., Renne, P., and Ruppel, C., 2003. The Central Atlantic Magmatic Province: Insights from Fragments of Pangea, American Geophysical Union, Geophys. Monogr. Ser., vol. 136, 267 pp.

Hammer, W.R., and Hickerson, W.J., 1996. Implications of an early Jurassic vertebrate fauna from Antarctica, in M. Morales (editor), The Continental Jurassic, Transactions of the Continental Jurassic Symposium, October 21-23, 1996, Museum of Northern Arizona, Flagstaff, Arizona, Museum of Northern Arizona Bulletin, v. 60, p. 215-218.

Haq, B. U., & Schutter, S. R., 2009. A chronology of Paleozoic sea-level changes. Science, 322, 64-68.

Haq, B. U., Hardenbol, J., & Vail, P. R., 1987. Chronology of fluctuating sea levels since the Triassic. Science, 235, 1156-1167.

Hautmann, M., 2004. Effect of end-Triassic CO_2 maximum on carbonate sedimentation and marine mass extinction. Facies 50: 257–261.

Hautmann, M., Benton, M.J., and Tomašových, A., 2008. Catastrophic ocean acidification at the Triassic-Jurassic boundary. Neues Jahrb. Geologie Paläontologie, v. 249, p.119–127.

Hay, W.W., 2008. Evolving ideas about the Cretaceous climate and ocean circulation, Cretaceous Research, 29: 725-753.

Hay, W.W., 2016. Experimenting on a Small Planet: A History of Scientific Discoveries, a Future of Climate Change and Global Warming, Springer, Switzerland, 819 pp.

Hayes, P.A., Francis, J.E., Cantrill, D.J., and Crame, J.A., 2006. Palaeoclimate analysis of Late Cretaceous angiosperm leaf floras, James Ross Island, Antarctica, in *Cretaceous-Tertiary High-Latitude Palaeoenvironments, James Ross Basin, Antarctica*, J.E., Francis, D. Pirrie, and J.A. Crame, (editors), Geol. Soc. London Special Publications 258:49-62.

Hays, P. D., and Grossman, E. L., 1991, Oxygen isotopes in meteoric calcite cements as indicators of continental paleoclimate, Geology, v. 19, no. 5, p. 441-444.

Hearing, T.W., Harvey, T,H.P., Williams, M., Leng, M.J., Lamb, A.L., Wilby, P.R., Gabbott, S.E., Pohl, A., and Donnadieu, Y., 2018. An early Cambrian greenhouse climate, Science Advances, 4:eaar5690 9.

Heckel, P.H., 1994. Evaluation of evidence for glacio-eustatic control over marine Pennsylvanian cyclothems in North America and consideration of possible tectonic effects in J.M. Dennisonand F.R. Ettensohn (editors), Tectonic and Eustatic Controls on Sedimentary Cycles, SEPM Concepts in Sedimentology and Paleontology, v4, p. 65-87.

Heckel, P.H., 2008. Pennsylvanian cyclothems, in Midcontinent North Ameri- ca as far-field effects of waxing and waning of Gondwana ice sheets, in C.R. Fielding, T.D. Frank, and J.L. Isbell (editors), Resolving the Late Paleozoic Ice Age in Time and Space, Geological Society of America, Special Paper 441, p. 275-289.

Heckel, P.H., 2013. Pennsylvanian stratigraphy of Northern Midcontinent Shelf and biostratigraphic correlation of cyclothems, Stratigraphy, v. 10, no. 1–2, pp. 3–39.

Henderson, C.M., Davydov, V.I., Wardlaw, B.R., 2012. The Permian Period, Chapter 24, in The Geologic Time Scale 2012, volume 2, F.M. Gradstein, J.G. Ogg, M.D. Schmitz, and G.M. Ogg (editors), Elsevier, Amsterdam, p.653-679.

Henkes, G.A., Passey, B.H., Grossman, E.L., Shenton, B. J., Yancey, T. E., and Pérez-Huerta, A., 2018. Temperature evolution and oxygen isotope composition of Phanerozoic oceans from carbonate clumped isotope thermometry, Earth and Planetary Science Letters, v. 490, pp. 40-50, doi:10.1016/j.epsl.2018.02.001.

Herrle, J.O., Schröder-Adams, C.J., Davis, W., Pugh, A.T., Galloway, J.M., and Fath, J., 2015. Mid-Cretaceous High Arctic stratigraphy, climate, and Oceanic Anoxic Events. Geology, 43(5): 403-406.

Heydari, E., Arzani, N., and Hassanzadeh, J., 2008. Mantle plume: The invisible serial killer - Application to Permian-Triassic boundary mass extinction, Palaeogeography, Palaeoclimatology, Palaeoecology, v. 264, p. 147-162.

Hildebrand, A.R., Penfield, G.T., Kring, D.A., Pilkington, M., Camargo, Z.A., Jacobsen, S.B., and Boynton, W.V., 1991. Chicxulub crater: A possible Cretaceous-Tertiary boundary impact crater on the Yucutan Peninsula, Mexico, Geology, 19:867-871.

Hilgen, F.J., Lourens, L.J., and Van Dam, J.A., 2012. The Neogene Period, Chapter 29, in The Geologic Time Scale 2012, volume 2, F.M. Gradstein, J.G. Ogg, M.D. Schmitiz, and G.M. Ogg, (editors), p. 923-978, Elsevier, Amsterdam.

Hochuli, P.A., Hermann, E., Vigran, J.O., Bucher, H., and Weissert, H., 2010. Rapid demise and recovery of plant ecosystems across the end-Permian extinction event, Global and Planetary Change, v. 74, p. 144-155.

Hodel, F., Macouin, M., Trindade, R.I.F., Triantafyllou, A., Ganne, J., Chavagnac, V., Berger, J., Rospabé, M., Destrigneville, C., Carlut, J., Ennih, N., and Agrinier, P., 2018. Fossil black smoker yields oxygen isotopic composition of Neoproterozoic seawater, Nature Communications, 9:1453, doi: 10.1038/s41467-018-03890

Hoffman, P.F., Kaufman, A.J., Halverson, G.P., and Schrag, D.P., 1998. A Neoproterozoic snowball Earth, Science, 281: 1342-1346.

Hoffman,P.F., and Schrag, D.P., 2000. Snowball Earth, Scientific American, v. 282, p. 68-75.

Hoffman, P.F., and Schrag, D.P., 2002. The snowball Earth hypothesis: testing the limits of global change, Terra Nova, v. 14, p. 129-155.

Hoffman, P.F., and Li, Z.-X., 2009. A palaeogeographic context for Neoproterozoic glaciation, Palaeogeogrphy, Palaeoclimatology, Palaeoecology, v. 277 (3-4), p 158-172.

Hotinski, R., Bice, K.L., Kump, L.R., Najiar, R.G., and Arthur, M.A., 2001. Ocean stagnation and end-Permian anoxia. Geology, v. 29, p. 7-10.

Hotinski, R.M., and Toggweiler, J.R., 2003. Impact of a Tethyan circumglobal passage on ocean heat transport and "equable" climates, Paleoceanography, 18:1007-1015.

Hsu, K.J., Oberhansli, H., Gao, J.Y., Shu, S., Haihong, C., and Krahenbuhl, U., 1985. 'Strangelove ocean' before the Cambrian. Nature, v. 316, p. 809-811.

Huber, B.T., 1998. Tropical paradise at the Cretaceous poles?, Science, v. 282, p. 2199-2200.

Huber, B.T., MacLeod, K.G., and Wing, S.L., 2000. Warm Climates in Earth History, Cambridge University Press, 462 pp.

Huber, M., and Caballero, R., 2011. The early Eocene equable climate problem revisited: Climate of the Past Discussions, v.7., p. 241-304, doi: 10.5194/cpd-7-241-2011.

Hughes, D.W., 2003. The approximate ratios between the diameters of terrestrial impact craters and the causative incident bolides, Mon. Not. R. Astron, Soc., v. 338, p. 999-1003.

IPCC 2007: Summary for Policymakers. IN: Climate Change 2007: The Physical Science Basis. Contribution of Working Group I to the Fourth Assessment Report of the Intergovernmental Panel on Climate Change [Solomon, S., D. Qin, M. Manning, Z. Chen, M. Marquis, K.B. Averyt, M. Tignor, and H.L. Miller (eds.)]. Cambridge University Press, Cambridge, United Kingdom and New York, USA.

IPCC 2018: Summary for Policymakers. In: Global Warming of 1.5˚C. An IPCC Special Report on the impacts of global warming of 1.5˚C above pre-industrial levels and related greenhouse gas emission pathways, in the context of strengthening the global response to the threat of climate change, sustainable development, and efforts to eradicate poverty [Masson-Delmotte, V., P. Zhai, H.-O. Portner, D. Roberts, J. Skea, P.R. Sukla, A. Pirani, W. Moufouma-Okia, C. Pean, R. Pidcock, S. Connors, J.B.R. Matthews, Y. Chen, X. Zhou, M.I. Gomis, E. Lonnoy, T. Maycock, M. Tignor, and T. Waterfield (eds.)] Cambridge University Press, Cambridge, United Kingdom and New York, USA.

IPCC 2019: Summary for Policymakers. In: IPCC Special Report on the Ocean and Cryosphere in a Changing Climate [H.-O. Portner, D.C. Roberts, V. Masson-Delmotte, P. Zhai, M. Tignor, E. Poloczanska, K. Mintenbeck, M. Nicolai, A. Okem, J. Petzold, B. Rama, N. Weyer(eds.)] Cambridge University Press, Cambridge, United Kingdom and New York, USA.

Isozaki, Y., 1997. Permo-Triassic boundary superanoxia and startified superocean: Records from Lost Deep Sea. Science, v. 276, p. 235-238.

Jacobs, L.L., Polcyn, M.J., Taylor, L.H., and Ferguson, K., 2005, Sea-surface temperatures and paleoenvironments of dolichosaurs and early mosasaurs, Netherlands Journal of Geosciences, Geologie en Mijnbouw, 84-3:269-281.

Jaffres, J.B.P., Shields, G.A., and Wallman, K., 2007. The oxygen isotope evolution of seawater: a critical review of a long-standing controversy and an improved geological water cycle model for the past 3.4 billion years, Earth-Science Reviews, 83:83-122.

Jenkyns, H.C., Jones, C.J., Groeke, D.R., Hesselbo, S.P., and Parkinson, D.N., 2002. Chemostratigraphy of the Jurassic System: applications, limitations and implications for palaeoceanography, Journal of the Geological Society, London, v. 159, p. 351–378.

Jenkyns, H.C., 2010. Geochemistry of oceanic anoxic events. Geochemical Geophysical Geosystems, 11:Q03004.

Jenkyns, H.C., Schouten-Huibers, L., Schouten, S., and Sinninghe Damste, J.S., 2012. Warm Middle Jurassic–Early Cretaceous high-latitude sea-surface temperatures from the Southern Ocean, Climate of the Past, 8:215-226, doi:10.5194/cp-8-215-2012

Joachimski, M. M., von Bitter, P. H., and Buggisch, W., 2006, Constraints on Pennsylvanian glacioeustatic sea-level changes using oxygen isotopes of conodont apatite, Geology, v. 34, no. 4, p. 277-280.

Joachimski, W.W., van Gelderin, R., Breisig, S., Buggisch, W., and Day, J., 2004. Oxygen isotope evolution of biogenic calcite and apatite during the Middle and Late Devonian, International Journal of Earth Sciences (Geol Rundsch), v. 93, p. 542–553, doi: 10.1007/s00531-004-0405-8

Joachimski, M.M., Breisig, S., Buggisch, W., Talent, J.A., Mawson, R., Gereke, M., Morrow, J.R., Day, J., and Weddige, K., 2009. Devonian climate and reef evolution: Insights from oxygen isotopes in apatite, Earth and Planetary Science Letters, v. 284, p. 599–609, doi:10.1016/j.epsl.2009.05.028

Johnson, J.G., Klapper, G., Sandberg, C.A., 1985. Devonian eustatic fluctuations in Euramerica. Geological Society of America Bulletin, v. 96, p. 567–587.

Johnson, J.G., 1988. Volcanism, eustacy, and extinctions. Geology, v. 16, p. 573–574.

Jones, C.E., and Jenkyns, H.C., 2001. Seawater strontium isotopes, oceanic anoxic events, and seafloor hydrothermal activity in the Jurassic and Cretaceous, American Journal of Science, 301:112-149.

Jones, S.M., Hoggett, M., Greene, S.E., and Jones, T.D., 2019. Lareg Igneous Province thermogenic greenhouse gas flux could have intiated Paleocene-Eocene Thermal Maximum climate change, Nature Communications, v.10, article number 5547.

Jourdan, F., Féraud, G., Bertrand, H., Kampunzu, A.B., Tshoso, G., Watkeys, M.K., and Le Gall, B. 2005. Karoo large igneous province: brevity, origin, and relation to mass extinction questioned by new $^{40}Ar/^{39}Ar$ age data. Geology, v. 33, p.745–748.

Jouzel, J., Masson-Delmotte, V., Cattani, O., Dreyfus, G., Falourd, S., Hoffmann, G., Minster, B., Nouet, J., Barnola, J.M., Chappellaz, J., Fischer, H., Gallet, J.C., Johnsen, S., Leuenberger, M., Loulergue, L., Luethi, D., Oerter, H., Parrenin, F., Raisbeck, G., Raynaud, D., Schilt, A., Schwander, J., Selmo, E., Souchez, R., Spahni, R., Stauffer, B., Steffensen, J.P., Stenni, B., Stocker, T.F., Tison, J.L., Werner, M., and Wolff. E.W., 2007. Orbital and Millennial Antarctic Climate Variability over the Past 800,000 Years, Science, v. 317, p.793-796.

Jovane, L., Coccioni, R., Marsili, A., Acton, G., 2009. The late Eocene greenhouse-icehouse transition: Observations from the Massignano global stratotype and point (GSSP), in C. Koeberl and A. Montanari, (eds.), The Late Eocene Earth: Hot House, Ice House, and Impacts, Geol. Soc. America, Special Paper 452149-168.

Judd, E., Bhattacharya, T., Ivany, L.C., 2020. A dynamical framework for interpreting ancient sea surface temperatures, Geophysical Research Letters, 47 (15):1-10, doi.org/10.1029/2020GL089044

Kamber, B.S., and Petrus, J.A., 2019. The influence of large bolide impacts on the Earth's Carbon Cycle, Elements, v.15, p.313-318.

Kamo, S.L., Czamanske, G.K., Amelin, Y., Fedorenko, V.A., Davis, D.W., and Trofimov, V.R., 2003. Rapid eruption of Siberian flood-volcanic rocks and evidence for coincidence with the Permian-Triassic boundary and mass extinction at 251 Ma. Earth and Planetary Science Letters, v. 214, p. 75-91.

Kasting, J.F., Howard, M.T., Wellman, K.T., Veizer, J., Shields, G., and Jaffres, J., 2006. Paleoclimates, ocean depth, and the oxygen isotopic composition of seawater, Earth and Planetary Science Letters, v. 252, p. 82-93.

Keller, G., 2011. Defining the Cretaceous-Tertiary boundary: a practical guide and return to first principles. In: Keller, G., Adatte, T. (Eds.), The KT Mass Extinction and the Chicxulub impact in Texas. SEPM Special Publication, 100, 23-42.

Keller, G., 2014. Deccan volcanism, the Chicxulub impact, and the end-Cretaceous mass extinction: Coincidence? Cause and effect? In: Keller, G., Kerr, A. (Eds.), Volcanism, Impacts and Mass Extinctions: Causes and Effects. Geological Society of America Special Papers, 505, 57-89, doi:10.1130/2014.2505(03).

Keller, G., Mateo, P., Punekar, J., Khozyem, H., Gertsch, B., Spangenberg, J., Bitchong, A., and Adatte, T., 2017. Environmental Changes during the Cretaceous-Paleogene Mass Extinction and Paleocene-Eocene Thermal Maximum: Implications for the Anthropocene, Gondwana Research, v. 56, p. 69-89, doi.org/10.1016/j.gr.2017.12.002

Kennett,J.P., and Stott, L.D., 1991. Abrupt deep-water warming, palaeoceanographic changes and benthic extinctions at the end of the Paleocene, Nature, v. 353, p.225-229.

Kennett, J.P., Houtz, R.E., Andrews, P.B., Edwards. A. R., Gostin, V.A., Hajos, M., Hempton, M.A., Jenkins, D.G., Margolis, S.V., Ovenshine, A.T., and Perch-Nielsen, K., 1974. Development of the Circum-Antarctic current, Science, 186:144-147.

Kennett, J.P., 1995. A review of polar climate evolution during the Neogene based on the marine sediment record, in Paleoclimate and Evolution with Emphasis on Human Origins, E.S. Vrba, G.H. Denton, T.C. Patridge, and L.H. Burckle (eds.), Yale University Press, New Haven, p.49-64.

Kennett, J.P., and Exon, N.F., 2004. Paleoceanographic evolution of the Tasmanian Seaway and its climatic implications, in N.F. Exon, J.P. Kennett and M. Malone, (eds.), The Cenozoic Southern Ocean: Tectonics, Sedimentation, and Climate Change between Australia and Antarctica, American Geophysical Union, Geophys. Monograph 151:345-367.

Kidder, D.L. and Worsley, T.R., 2010. Phanerozoic Large Igneous Provinces (LIPs), HEATT (Haline Euxinic Acidic Thermal Transgression) episodes, and mass extinctions, Palaeogeography, Palaoeclimatology, Palaeoecology, v. 295, pp. 162-191.

Kidder, D.L. and Worsley, T.R., 2012. A human-induced hothouse climate?, GSA Today, v. 22, no. 2, pp. 4 – 11, doi: 10.1130/G131A.1.

Kiehl, J.T., and Shields, C., 2013. Sensitivity of the Palaeocene-Eocene Thermal Maximum climate to cloud properties: Royal Society of London Philosophical Transactions, ser. A, v. 371, 20130093, doi:10.1098/rsta.2013.0093.

Kiessling, W., Flügel, and Golonka, J., 2002. Phanerozoic Reef Patterns, SEPM (Society for Sedimentary Geology) Special Publication Number 72, 775 pp.

King, C., A., 2016. A Revised Correlation of Tertiary Rocks in the British Isles and adjacent areas of NW Europe, A.S. Gale & T.L. Barry (editors), Geological Society Special Report no. 27, 719 pp.

Koeberl, C., and Montanari, A., 2009. The Late Eocene Earth: Hot House, Ice House, and Impacts, Geol. Soc. America, Special Paper 452, Boulder, Colorado, 322 pp.

Köppen, W., 1918. Klassification der Klimate nach Temperatur, Niederschlag and Jahreslauf, Petermanns Geographische Mitteilungen, v. 64, pp.193-248.

Korte, C., Hesselbo, S.P., Jenkyns, H.C., Rickaby, R.E.M., Spotl, C., 2009. Palaeoenvironmental significance of carbon- and oxygen-isotope stratigraphy of marine Triassic–Jurassic boundary sections in SW Britain, Journal of the Geological Society of London, v. 166, p. 431–445.

Korte, C., Jones, P.J., Brand, U., Mertmann, D., and Veizer, J., 2008. Oxygen isotope values from high-latitudes: Clues for Permian sea-surface temperature gradients and Late Palaeozoic deglaciation, Palaeogeography, Palaeoclimatology, Palaeoecology, v. 269, p. 1–16, doi:10.1016/j.palaeo.2008.06.012

Korte, C., Jasper, T., Kozur, H.W., and Veizer, J., 2005. $d^{18}O$ and $d^{13}C$ of Permian brachiopods: A record of seawater evolution and continental glaciation, Palaeogeography, Palaeoclimatology, Palaeoecology, v. 224, p. 333–351, doi:10.1016/j.palaeo.2005.03.01

Kustatscher, E., Ash, S.R., Karasev, E., Pott, C., Vajda, V., Yu, J. & McLoughlin, S. 2018. Flora of the Late Triassic. In: Tanner, L. (ed.) The Late Triassic World: Earth in a Time of Transition, Topics in Geobiology, v. 46, p. 545-622, Springer, ISBN 978-3-319-68008-8.

Kump, L.R., Arthur, M.A., Patkowsky, M.E., Gibbs, M.T., Pinkus, D.S., and Sheehan, P.M., 1999a. A weathering hypothesis for glaciation at high atmospheric CO_2 during the Late Ordovician, Palaeogeography, Palaeoclimatology, and Palaeoecology, v. 152, p. 173-187.

Kump, L.R., Kasting, J.F., and Crane, R.G., 1999b. The Earth System, Prentice Hall, Upper Saddle River, N.J., 351 p.

Kump, L.R., Arthur, M.A., 1999c. Interpreting carbon-isotope excursions: carbonates and organic matter. Chemical Geology, v. 161, p. 181–198.

Kump. L.R., Gibbs, M.T., Arthur, M.A., Patzkowsky, M.E., and Sheehan, P.M., 1995.Hirnantian Glaciation and the Carbon Cycle, Ordovician Odyssey: Short Papers for the Seventh International Symposium on the Ordovician System, Las Vegas, Nevada, USA, June, 1995, (editors) J.D. Cooper, M.L. Droser, and S.C. Finney, p. 299-302, Society for Sedimentary Geology (SEPM), Pacific Section, Fullerton, CA.

Kump, L.R., Pollard, D., 2008. Amplification of Cretaceous warmth by biological cloud feedbacks. Science 320, 195.

Kump, L.R., 1991. Interpreting carbon-isotope excursions: Strangelove oceans. Geology, v. 19, p. 299-302.

Ladant, J.-B., Donnadieu, Y., 2016. Palaeogeographic regulation of glacial events during the Cretaceous supergreenhouse. Nat. Commun. 7.

Landing, E., 2012. Time-specific black mudstones and global hyperwarming on the Cambro-Ordovician slope and shelf od the Laurentia palaeocontinent, Palaeogeog., Paleaoclim., Palaeoecol., v. 367-368, p.256-272. Doi.org/10.1016/j.palaeo.2011.09.05

Landing, E. 2018. Tropical weathering of the Taconic orogeny (i.e. “orogen”) as a driver for Ordovician cooling, Geology Forum, doi.org/10.1130/G3998.7c1

Landing, E., Schmitz, M.D., Geyer, G., Trayler, R.B., and Bowring, S.A., 2020. Precise early Cambrian U–Pb zircon dates bracket the oldest trilobites and archaeocyathids in Moroccan West Gondwana, Geological Magazine https://doi.org/10.1017/ S0016756820000369

Landing E and Westrop SR, 2004. Environmental patterns in the origin and evolution loci of Early Cambrian skeletalized Metazoa: evidence from the Avalon microcontinent. In Neoproterozoic–Cambrian Biological Revolutions (eds JH Lipps and B Waggoner), pp. 93–105. Paleontological Society, Special Paper no. 10.

Larson, R.L., 1991. Geological consequences of superplumes, Geology, 19:963-966.

Larson, R.L., and Erba, E., 1999. Onset of the mid-Cretaceous greenhouse in the Barremian-Aptian: Igneous events and biological sedimentary, and geochemical responses, Paleoceanography, 14:663-678.

Lawver, L.A., and Gahagan, L.M., 2003. Evolution of Cenozoic seaways in the circum-Antarctic region, Palaeogeog., Paleaoclim., Palaeoecol., 198:11-37.

Lécuyer, C., Amiot, R., Touzeau, A., 2013. Calibration of the phosphate $\delta^{18}O$ thermometer with carbinate-water oxygen isotope fractionation equations, Chemical Geology, v. 347, pp. 217-226, doi:10.13039/501100004794.

Legates, D.R., and Wilmott, C.J., 1990. Mean seasonal and spatial variability in global surface air temperature, Theoretical and Applied Climatology, v. 41, pp. 11-21.

Lenton, T.M., Crouch, M., Johnson, M., Pires, N., and Dolan, L., 2012. First plants cooled the Ordovician, Nature Geoscience, v.5, p. 86-89.

Ling, M.-X., Zhan, R.-B., Wang, G.-X., Wang, Y., Amelin, Y., Tang, P., Liu, J.-B., Jin, J., Huang, B., Wu, R.-C., Xue, S., Fu, B., Bennett, V.C., Wei, X., Luan, X.-C., Finnegan, S., Harper, D.A.T., Rong, J.-Y., 2019. An extremely brief end Ordovician mass extinction linked to abrupt onset of glaciation. Solid Earth Sciences, 4(4): 190-198.

Lisiecki, L.E., and Raymo, M.E., 2005. A Pliocene-Pleistocene stack of 57 globally distributed benthic $\delta^{18}O$ records. Paleoceanography 20 (1), PA1003. http://dx.doi.org/10.1029/ 2004PA001071.

Livermore, R., Nankivell, A., Eagles, G., And Morris, P., 2005. Paleogene opening of the Drake Passage, Earth and Planetary Science Letters, 236:459-470.

Looy, C.V., Brugman, W.A., Dilcher, D.L., and Visscher, H., 1999. The delayed resurgence of equatorial forests after the Permian-Triassic ecologic crisis, Proc. National Acad. Sci., 96:13857-13862.

Luz, B., Kolodny, Y., and Kovach, J., 1984, Oxygen isotope variations in phosphate of biogenic apatites, III. Conodonts, Earth and Planetary Science Letters, v. 69, no. 2, p. 255-262.

Malchus, N., and Steuber, T., 2002. Stable isotope records (O, C) of Jurassic aragonitic shells from England and NW Poland: palaeoecologic and environmental implications, Geobios, v. 35, p. 29–39.

Marshall, H.G., Walker, J.C.G., & Kuhn, W.R., 1988. Long-term climate change and the geochemical cycle of carbon. Journal of Geophysical Research, 93, 791–801.

Marshall, L.G., Webb, D.S., Sepkoski, J.J., Raup, D.M., 1982. Mammalian evolution and the Great American Interchange, Science, 215:1351-1357.

Martinez-Peréz, C., Cascales-Minana, B., Plasencia, P., and Botella, H., 2014. Exploring the major depletions of conodont diversity during the Triassic, Historical Biology, v. 27, p. 503–507.

Marzoli, A., Renne, P.R., Piccirillo, E.M., Ernesto, M., Bellieni, G., and DeMin, A., 1999. Extensive 200-million-year-old continental flood basalts of the Central Atlantic Magmatic Province (CAMP), Science, v 284, p. 616-618.

McArthur, J.M., Janssen,N.M.M, Reboulet, S., Leng, M.J., Thirwall, M.F., van de Schootbrugge, B.,

2007. Palaeotemperatures, polar ice-volume, and isotope stratigraphy (Mc/Ca, ∂18O, ∂13C, 87Sr/86Sr): The Early Cretaceous (Berriasian, Valanginian, Hauterivian), Palaeogeography, Palaeoclimatology, Palaeoecology, v. 248, p. 391-430, doi:10.1016/j.palaeo.2006.12.015

McCune A.R., and Schaeffer, B., 1986. Triassic and Jurassic fishes: patterns of diversity in The Beginning of the Age of Dinosaurs, (editor), Kevin Pandian, p. 171–181, Cambridge University Press, Cambridge, UK.

McElwain J.C., Beerling D.J., and Woodward F.I., 1999. Fossil plants and global warming at the Triassic-Jurassic boundary, Science, v. 285, p. 1386–1390.

McElwain J.C., Punyasena S.W., 2007. Mass extinction events and the plant fossil record. Trends in Ecology and Evolution, v. 22, p. 548–557.

McGhee, G.R., Clapham, M.E., Sheehan, P.M., Bottjer, D.J., and Droser, M.L., 2013. A new ecological-severity ranking of major Phanerozoic biodiversity crises, Palaeogeography, Palaeoclimatology, Palaeoecology 370: 260–270

McGhee, G.R., Jr., 1996. The Late Devonian Mass Extinction: The Frasnian/Famennian Crisis, Critical Moments in Paleobiology and Earth History Series,D. J. Bottjer and R.K. Bambach (editors), Columbia University Press, New York, 303 pp.

McGhee, G.R., Jr., 2005. Modelling Late Devonian extinction hypotheses, in Understanding Late Devonian and Permian-Triassic Biotic and Climatic Events; Towards an Integrated Approach, D.J. Over, J.R. Morrow, and P.B. Wignall (editors), Developments in Palaeontology & Stratigraphy, v. 20, p. 37 – 50. Elsevier, Amsterdam.

McHone, J.G., and Puffer, J.H., 2003. Flood Basalt Provinces of the Pangean Atlantic Rift: Regional Extent and Environmental Significance, in P.M. LeTourneau & P.E. Olsen (eds.), The Great Rift Valleys of Pangea in Eastern North America: Tectonics, Structure, and Volcanism, Volume 1, Columbia University Press, New York, p.141-154.

McInerney, F.A., Wing, S.L., 2011. The Paleocene-Eocene Thermal Maximum: a perturbation of carbon cycle, climate, and biosphere with implications for the future. Annual Review of Earth Planetary Sciences,v. 39, p. 489–516.

McKenzie, N.R., and Jiang,H., 2019. Earth’s outgassing and climatic transitions: The slow burn towards environmental “catastrophes”?, Elements, v.15, p.325-330.

McKerrow, W.S., Scotese, C.R., and Brasier, M., 1992. Early Cambrian continental reconstructions, Journal of the Geological Society of London, v. 149, p. 599-606.

McLaren, D.J., 1970. Presidential address: Time, Life and Boundaries, Journal of Paleontology, v. 48, p. 801-815.

McLaren, D., 1983. Bolides and biostratigraphy. Geol. Soc. Am. Bull. 94, 313–324.

Melosh, H.J., 1989. Impact Cratering, A Geologic Process, Oxford University Press, New York, 253 p.

Meyer, K.M., and Kump, L.R., 2008. Oceanic Euxinia in Earth History: Causes and Consequences, Annual Review of Earth and Planetary Sciences, 36:251-288.

Mii, H.-S., Shi, G.R., Wang, C.-A., 2013. Late Paleozoic middle-latitude Gondwana environment-stable isotope records from Western Australia, Gondwana Research, v. 24, p. 125–138, doi.org/10.1016/j.gr.2012.10.013

Mii, H.-S., Grossman, E.L., and Yancey, T.E., 1999. Carboniferous isotope stratigraphies of North America: Implications for Carboniferous paleoceanography and Mississippian glaciation, Geological Society of America Bulletin, v. 111, no. 7, p. 960–973.

Mii, H.-S., Shi, G.R., Cheng, C.-J., and Chen, Y.-Y., 2012. Permian Gondwanaland paleoenvironment inferred from carbon and oxygen isotope records of brachiopod fossils from Sydney Basin, southeast Australia, Chemical Geology, v. 291, p. 87–103, doi:10.1016/j.chemgeo.2011.10.002

Milankovitch, M., 1920. Theorie Mathematique des Phenomenes Thermiques produits par la Radiation Solaire, Gauthier-Villars, Paris, 340 p.

Miller, C.S., Petersen, F., da Silva, A.-C., Baranyi, V., Reichart, G.J., and Kürschner, W.M., 2017. Astronomical age constraints and extinction mechanisms of the Late Triassic Carnian crisis. Nature, Scientific Reports 7: doi:10.1038/s41598-017-02817-7.

Miller, K.G., Fairbanks, R.G., and Mountain, G.S., 1987. Tertiary oxygen isotope synthesis, sea level history, and continental margin erosion, Paleoceanography, v. 2, p. 1-19.

Miller, K.G., Barrera, E., Olsson, R.K., Sugarman, P.J., Savin, S.M., 1999. Does ice drive early Maastrichtian eustasy? Geology 27, 783–786.

Miller, K.G., Sugarman, P.J., Browning, J.V., Kominz, M.A., Olsson, R.K., Feigenson, M.D., Hernández, J.C., 2004. Upper Cretaceous sequences and sea-level history, New Jersey coastal plain. Geol. Soc. Am. Bull. 116, 368–393.

Miller, K.G., Kominz, M.A., Browning, J.V., Wright, J.D., Mountain, G.S., Katz, M.E., Sugarman, P.J., Cramer, B.S., Christie-Blick, N., Pekar, S.F., 2005a. The Phanerozoic record of global sea-level change. Science 310, 1293–1298.

Miller, K.G., Wright, J.D., J. V. Browning, J.V., 2005b. Visions of ice sheets in a greenhouse world. *Mar. Geol.* **217**, 215–231.

Miller, K.G., Sherrell, R.M., Browning, J.V., Field, M.P., Gallagher, W., Olsson, R.K., Sugarman, P.J., Tuorto, S., and Wahyudi, H., 2010. Relationship between mass extinction and iridium across the Cretaceous-Paleogene boundary in New Jersey, Geology, 38:867-870.

Miller, K.G., Browning, J.V., Scmetz, W.J., Kopp, R.E., Mountain, G.S., and Wright, J.D., 2020. Cenozoic sea-level and cryosphere evolution from deep-sea geochemical and continental margin records, Science Advances, 6, eaaz1346.

Mills, B.J.W., Krause, A.J., Scotese, C.R., Hill, D.J., Shields, G.A., and Lenton, T.M., 2019. Modelling the long-term carbon cycle, atmospheric CO_2, and Earth surface temperature from late Neoproterozoic to present-day, Gondwana Research, v. 67, p. 172-186, doi: 10.1016/j.gr.2018.12.001 1342-937.

Molnar, P., and Tapponnier, P., 1975. Cenozoic tectonics of Asia: Effects of a continental collision, Science, 189:419-426.

Montañez, I.P., Tabor, N.J., Niemeier, D., DiMichele, W.A., Frank, T.D., Fielding, C.R. Isbell, J.L., Birgenheier, L.P., and Rygel, M.C., 2007. CO_2 -Forced Climate and Vegetation Instability During Late Paleozoic Deglaciation, Science, v. 315, n. 5808, p. 87-91, doi: 10.1126/science.1134207

Montañez I.P., McElwain, J.C., Poulsen, C.J., White, J.D., DiMichele, W.A., Wilson, J.P., Griggs, G., and Hren, M.T., 2016. Climate, p CO_2, and terrestrial carbon cycle linkages during late Palaeozoic glacial-interglacial cycles, Nature Geoscience, v.9, p. 824-828, doi :10.1038/NGEO2822

Montañez, I.P., and J.C., Poulsen, 2013. The Late Paleozoic Ice Age: An Evolving Paradigm, Annual Reviews of Earth and Planetary Sciences, v41, p.629-656.

Moore, G.T., Hayashida, D.N., Ross, C.A., and Jacoboson, S.R., 1992, Paleoclimate of the Kimmeridgian/Tithonian (Late Jurassic) world: I. Results using a general circulation model, Palaeogeography, Palaeoclimatology, and Palaeoecology, 93:113-150.

Moore, G.T., Jacobson, S.R., Ross, C.A., and Hayashida, D.N., 1994. A paleoclimate simulation of the Wenlockian (late Early Silurian) world using a general circulation model with implications for early land plant paleoecology, Palaeogeog., Paleaoclim., Palaeoecol., 110:115-144.

Morley, R.J., 2011. Cretaceous and Tertiary climate change and the past distribution of megathermal rainforests,in Tropical Rainforest Responses to Climatic Change, M.B. Bush, J.R. Flenley, W.D. Gosling, (editors), p. 1-34, Springer-Verlag, Berlin.

Mory, A.J., Redfern, J., and Martin, J.R., 2008. A review of Permian-Carboniferous glacial deposits in Western Australia, in C.R. Fielding, T.D. Frank. and J.L. Isbell (editors), Resolving the Late Paleozoic Ice Age in Time and Space, Geological Society of America Special Paper v. 441, p. 29-40.

Mueller, S., Krystyn, L., and Kürschner, W.M. 2016a. Climate variability during the Carnian Pluvial Phase – a quantitative palynological study of the Carnian sedimentary succession at Lunz am See, Northern Calcareous Alps, Austria, Palaeogeography, Palaeoclimatology, Palaeoecology, v. 441, p. 198–211.

Mueller, S., Hounslow, M.W., and Kürschner, W.M. 2016b. Integrated stratigraphy and palaeoclimate history of the Carnian Pluvial Event in the Boreal realm; new data from the Upper Triassic Kapp Toscana Group in central Spitsbergen (Norway), Journal of the Geological Society, v. 173, p. 186–202.

Munnecke, A., Calner, M., Harper, D.A.T., and Servais, T., 2010. Ordovician and Silurian sea–water chemistry, sea level, and climate: A synopsis, Palaeogeography, Palaeoclimatology, Palaeoecology, v. 296, p. 389–413, doi:10.1016/j.palaeo.2010.08.001

Mutterlose, J., Pauly, S., and Steuber, T., 2009. Temperature controlled deposition of early Cretaceous (Barremian–early Aptian) black shales in an epicontinental sea, Palaeogeography, Palaeoclimatology, Palaeoecology, 273:330-345, doi:10.1016/j.palaeo.2008.04.026

Nance, R.D., Murphy, J.B., Santosh, M., 2014. The supercontinent cycle: A retrospective essay, Gondwana Research, v. 25, p. 4-29, doi: 10.1016/j.gr.2012.12.026.

Nance, R.D., and Murphy, J.B., 2018. Supercontinents and the case for Pannotia, in Fifty Years of the Wilson Cycle Concept in Plate Tectonics, R.W. Wilson, G.A. Houseman, K.J.W. McCaffrey, A.G. Dore, and S.J.H. Butler, Geological Society, London, Special Publications, 470, p. 1-17, doi:/10.1144/SP470.5.

Nardin, E., Goddéris, Y., Donnadieu, Y., Le Hir, G., & Blakey, R.C., 2011. Modeling the early Paleozoic long-term climatic trend. *Geological Society of America Bulletin.* doi: 10.1130/B30364.1

Navarro-Ramirez, J.P., Bodin, S., Consorti, L., and Immenhauser, A., 2017. Response of western South American epeiric-neritic ecosystem to middle Cretaceous Oceanic Anoxic Events, Cretaceous Research, v. 75, p. 61–80

O'Brien, C.L., Robinson, S.A., Pancost, R.D., Sinninghe Damsté, J. S., Schouten, S., Lunt, D. J., Alsenz, H., Bornemann, A., Bottini, C., Brassell, S. C., Farnsworth, A., Forster, A., Huber, B. T., Inglis, G. N., Jenkyns, H. C., Linnert, C., Littler, K., Markwick, P., McAnena, A., Mutterlose, J., Naafs, B. D. A., Püttmann, W., Sluijs, A., van Helmond, N. A. G. M., Vellekoop, J., Wagner, T., and Wrobel, N. E., 2017. Cretaceous sea-surface temperature evolution: Constraints for TEX 86 and planktonic foraminiferal Oxygen isotopes, Earth-Science Reviews, v. 172, p. 224-247, doi: 10.1016/j.earscirev.2017.07.012. 2018

Ogg, J.G. 2015. The mysterious Mid-Carnian "Wet Intermezzo" global event, Journal of Earth Science, v. 26, p. 181–191.

Ogg, J.G., Ogg, G.M., and Gradstein, F.M., 2016. A Concise Geological Time Scale 2016, Elsevier, Amsterdam, 234 pp.

Otto-Bliesner, B.L., 1995. Continental drift, runoff, and weathering feedbacks: Implications from climate model experiments. *Journal of Geophysical Research*, 100, 11,537-11,548

Pankhurst, R.J., Leat, P.Y., Sruoga, P., et al., 1998. The Chon Aike province of Patagonia and related rocks in West Antarctica: a silicic large igneous province, Journal of Volcanology and Geothermal Research, 81: 113-136.

Pankhurst, R.J., Riley, T.R., Fanning, C.M.,and Kelley, S.P., 2000. Episodic silicic volcanism in Patagonia and the Antarctic peninsula: chronology of magmatism associated with the break-up of Gondwana, Journal of Petrology, 41:605-625.

Park, J., and Royer, D.L., 2011. Geological constraints on the glacial amplification of Phanerozoic climate sensitivity, American Journal of Science, v. 311, p. 1-26, doi: 10.2475/01.2011.01.

Parrish, J.T., 1993, Climate of the supercontinent Pangea, J. Geology, v. 101, p. 217-235.

Parrish, J.T., 1998. Interpreting Pre-Quaternary Climate from the Geologic Record, Columbia University Press, New York, 338 pp.

Parrish, J.T., and Spicer, R.A., 1988, Late Cretaceous terrestrial vegetation: A near polar temperature curve, Geology, 16:22-25.

Peng, S., Babcock, L.E., and Cooper, R.A., 2012. The Cambrian Period, Chapter 19, in The Geologic Time Scale 2012, volume 2, F.M. Gradstein, J.G. Ogg, M.D. Schmitz, and G.M. Ogg (editors), Elsevier, Amsterdam, p. 437-488.

Petersen, S.V., Dutton, A., Lohmann, K.C., 2016. End-Cretaceous extinction in Antarctica linked to both Deccan volcanism and meteorite impact via climate change, Nature Communications, 7:12079 doi: 10.1038/ncomms12079

Petit J.R., Jouzel,J., Raynaud, D., Barkov, N.I., Barnola, J.-M., Basile, I., Bender, M., Chappellaz, J., Davis, M., Delaygue, G., Delmotte, M., Kotlyakov, V.M., Legrand, M., Lipenkov, V.Y., Lorius, C., Pe´pin, L., Saltzman, E., and Stievenard,M., 1999. Climate and atmospheric history of the past 420,000 years from the Vostok ice core, Antarctica, Nature, V. 299, p. 429-436.

Pillans, B., and Gibbard, P., 2012. The Quaternary Period, Chapter 30, in The Geologic Time Scale 2012, volume 2, F.M. Gradstein, J.G. Ogg, M.D. Schmitiz, and G.M. Ogg, (editors), p. 855-922, Elsevier, Amsterdam.

Pirrie, D., Doyle, P., Marshall, J., Ellis, G., 1995. Cool Cretaceous climates: new data from the Albian of Western Australia. J. Geol. Soc. 152: 739–742.

Pirrie, D., Marshall, J., Doyle, P., Riccardi, A., 2004. Cool early Albian climates; new data from Argentina. Cretaceous Research 25:, 27–33.

Podlaha, O.G., Mutterlose, J., and Veizer, J., 1998. Preservation of d18O and d13C in belemnite rostra from Jurassic/early Cretaceous successions, American Journal of Science, v. 298, p. 324-347.

Powell, C. McA., Li, Z.X., McElhinny,M.W., Meert, J.G., and Park, J.K., 1993. Paleomagnetic constraints on the timing of the Neoproterozoic breakup of Rodinia and the Cambrian formation of Gondwana, Geology, v. 21, pp. 889-892.

Powell, C. McA., 1995. Are Neoproterozoic glacial deposits preserved on the margins of North America related to the fragmentation of two supercontinents (Comment), Geology, v. 23, pp. 1053-1054.

Preto, N., Kustatscher, E., and Wignall, P.B. 2010. Triassic climates—state of the art and perspectives. Palaeogeography, Palaeoclimatology, Palaeoecology, 290:1–10.

Price, G.D., 1999. The evidence and implications of polar ice during the Mesozoic. Earth Sci. Rev. 48, 183–210.

Price, G., Mutterlose, J., 2004. Isotopic signals from late Jurassic–early Cretaceous (Volgian–Valanginian) sub-Arctic belemnites, Yatria River, Western Siberia. J. Geol. Soc. 161, 959–968.

Price, G.D., Nunn, E.V., 2010. Valanginian isotope variation in glendonites and belemnites from Arctic Svalbard: transient glacial temperatures during the Cretaceous greenhouse. Geology 38, 251–254.

Price, G.D., Passey, B.H., 2013. Dynamic polar climates in a greenhouse world: evidence from clumped isotope thermometry of Early Cretaceous belemnites. Geology 41, 923–926.

Prokoph, A., Shields, G. A., and Veizer, J., 2008, Compilation and time-series analysis of a marine carbonate $\delta^{18}O$, $\delta^{13}C$, $^{87}Sr/^{86}Sr$ and $\delta^{34}S$ database through Earth history, Earth-Science Reviews, v. 87, no. 3, p. 113-133.

Pucéat, E., Lécuyer, C., Sheppard, S.M., Dromart, G., Reboulet, S., Grandjean, P., 2003. Thermal evolution of Cretaceous Tethyan marine waters inferred from oxygen isotope composition of fish tooth enamels. Paleoceanography 18, 1029. http://dx.doi. org/10.1029/2002PA000823.

Punekar, J., Mateo, P., and Keller, G., 2014. Effects of Deccan volcanism on paleoenvironment and planktic foraminifera: A global survey, Geological Society of America Special Paper, v. 505, p. 91-116, doi:10.1130/2014.2505(04)

Quiron, P.C., and MacLeod, K.G., 2014. Oxygen isotopes from conodont apatite of the midcontinent, US: Implications for Late Ordovician climate evolution, Palaeogeography, Palaeoclimatology, Palaeoecology, v. 404, p. 57–66, doi.org/10.1016/j.palaeo.2014.03.036

Racki, G., 2020. A volcanic scenario for the Frasnian–Famennian major biotic crisis and other Late Devonian global changes: More answers than questions?, Global and Planetary Change, v. 189, doi.org/10.1016/j.gloplacha.2020.103174

Racki, G., 2005. Toward understanding Late Devonian global events: few answers, many questions, in Understanding Late Devonian and Permian-Triassic Biotic and Climatic Events; Towards an Integrated Approach, D.J. Over, J.R. Morrow, and P.B. Wignall (editors), Developments in Palaeontology & Stratigraphy, v. 20, p. 5-36, Elsevier, Amsterdam.

Rampino. M.R., 2020. Relationship between impact-crater size and severity of related mass extinction episodes (in press).

Rampino. M.R., Caldiera, K., and Prokoph, A., 2019. What causes mass extinctions? Large asteroid/comet impacts, flood-basalt volcanism, and ocean anoxia— Correlations and cycles, *in* Koeberl, C., and Bice, D.M., eds., 250 Million Years of Earth History in Central Italy: Celebrating 25 Years of the Geological Observatory of Coldigioco: Geological Society of America Special Paper 542, p. 1–32, https://doi.org/10.1130/2019.2542(14).

Rampino, M.R., and Self, S., 2015. Large Igneous Provinces and Biotic Extinctions, in The Encyclopedia of Volcanoes, second edition, H. Sigurdsson, B. Houghton, H. Rymer, J. Stix, and S. McNutt (editors), p.1049-158, Elsevier, Amsterdam.

Rampino. M.R., and Shen, S.-Z., 2019. The end-Guadalupian (259.8 Ma) biodiversity crisis: the sixth major mass extinction?, Historical Biology, doi: 10.1080/08912963.2019.1658096

Raup, D.M., 1979. Size of the Permo-Triassic bottleneck and its evolutionary implications. Science, v. 206, p. 217-218.

Raymo, M.E., Kozdon, R. , Evans, D., Lisiecki, L., and Ford, H.L., 2018. The accuracy of mid-Pliocene $\delta^{18}O$-based ice volume and sea level reconstructions, Geochimica et Cosmochimica Acta, Vol. 63, No. 7/8, pp. 1039–1048.

Raymo, M.E., and Ruddiman, W.F., 1992. Tectonic forcing of Late Cenozoic Climate, Nature 359:117-122.

Raymo, M.E., Ruddiman, W.F., & Froelich, P.N. 1988. Influence of late Cenozoic mountain building on ocean geochemical cycles. *Geology*, 16, 649–653.

Rea, D.K., Zachos, J.C., Owen, R.M., and Gingerich, P.D., 1990. Global change at the Paleocene-Eocene boundary: climatic and evolutionary consequences of tectonic events, Palaeogeography, Palaeoclimatology, Palaeoecology 79:117-128.

Rees, P.McA., Ziegler, A.M., and Valdes, P.J., 2000, Jurassic phytogeography and climates: new data and model comparisons, in Warm Climates in Earth History, BT. Huber, K.G. MacLeod, and S. Wing (editors), Cambridge University Press, Cambridge, p. 297-318.

Reichow, M.K., Saunders, A.D., White, R.V., Al'Mukhamedov, A.I., and Medvedev, A.Ya., 2005. Geochemistry and petrogenesis of basalts from the West Siberia Basin: an extension of the Permo-Triassic Siberian Traps, Russia. Lithos, v. 79, p. 425-452.

Reichow, M. K., Pringle, M. S., Al'Mukhamedov, A. I., Allen, M. B., Andreichev, V. L., Buslov, M. M., Davies, C. E., Fedoseev, G. S., Fitton, J. G., Inger, S., Medvedev, A. Y., Mitchell, C., Puchkov, V. N., Safonova, I. Y., Scott, R. A., and Saunders, A. D., 2009, The timing and extent of the eruption of the Siberian Traps large igneous province: Implications for the end-Permian environmental crisis, Earth and Planetary Science Letters, v. 277, no. 1-2, p. 9-20.

Renne, P.R., Sprain, C.J., Richards, M.A., Self, S., Vanderkluysen, L., and Pande, K., 2015. State shift in Deccan volcanism at the Cretaceous-Paleogene boundary, possibly induced by impact, Science 350 (6256):76-78.

Retallack, G., 2013. Permian and Triassic greenhouse crises, Gondwana Research, v. 24, p. 90–103, doi:10.1016/j.gr.2012.03.003.

Retallack , G.J., Sheldon, N.D., Carr,P.F., Fanning, M., Thompson, C.A., Williams, M.L., Jones, B.J., and Hutton, A., 2011. Multiple Early Triassic greenhouse crises impeded recovery from Late Permian mass extinction, Palaeogeography, Palaeoclimatology, Palaeoecology, v. 308, 233–251, doi: 10.1016/j.palaeo.2010.09.022

Richards, M.A., Alvarez, W., Self, S., Karlstrom,L., Renne, P.R., Manga, M., Sprain, C.J., Smit, J., Vanderkluysen, L., and Gibson, S.A., 2015. Triggering of the largest Deccan eruptions by the Chicxulub impact, Geological Society of America Bulletin, 127 (11-12):1507-1520,doi:10.1130/B31167.1

Rigo, M., and Joachimski, M.M., 2010. Palaeoecology of Late Triassic conodonts: constraints from oxygen isotopes in biogenic apatite, Acta Palaeontologica Polonica, v. 55, p. 471–478.

Rigo, M., Preto, N., Roghi, G., Tateo, F., and Mietto, P. 2007. A rise in the Carbonate Compensation Depth of western Tethys in the Carnian (Late Triassic): deep-water evidence for the Carnian Pluvial Event, Palaeogeography, Palaeoclimatology, Palaeoecology, v. 246, p. 188–205.

Roghi, G., Gianolla, P., Minarelli, L., Pilati, C., and Preto, N., 2010. Palynological correlation of Carnian humid pulses throughout western Tethys, Palaeogeography, Palaeoclimatology, Palaeoecology, v. 290, p. 89–106.

Rogner, H.H., 2012. Energy Resources and Potential, Chapter 7, in Yeager, Kurt, Dayo, Felix, Fisher, Brian, Fouquet, Roger, Gilau, Asmerom, Rogner, Hans-Holger, Haug, Marianne, Hosier, Richard, Miller, Alan, Schnitteger, Sabine, Lustig, Nora, Johansson, Thomas B., Nakicenovic, Nebojsa, Patwardhan, Anand and Gomez-Echeverri, Luis (2012) *Energy and economy.* In: Global Energy Assessment (Gea). Cambridge University Press, Cambridge, UK, pp. 385-422. ISBN 9780511793677

Rosenau, N. A., Tabor, N. J., and Herrmann, A. D., 2014, Assessing the paleoenvironmental significance of middle–late Pennsylvanian conodont apatite $\delta^{18}O$ values in the illinois basin conodont apatite $\delta^{18}O$ values, Palaios, v. 29, no. 6, p. 250-265.

Rowley, D.B., 1996. Age of inititation of collision between India and Asia: A review of stratigraphic data, Earth and Planetary Sciences, v. 145: 1-13.

Rowley, D.B., 1998. Minimum age of initiation of collision between India and Asia north of Everest based on the subsidence history of the Zhepure mountain section, Journal of Geology, v. 106: 229-235.

Rowley, D.B. and Currie, B.S., 2006. Palaeo-altimetry of the late Eocene to Miocene Lunpola basin, central Tibet, Nature, v. 439/9, p. 677-681, doi:10.1038/nature04506

Royer, D.L., Berner, R.A., Montañez, I.P., Tabor, N.J., and Beerling, D.J., 2004. CO_2 as a primary driver of Phanerozoic climate, GSA Today, v. 14, no. 3, p. 4-10, doi: 10.1130/1052-5173 (2004) 014<0004: CAAPDO>2.0.CO:2.

Royer, D., 2016. Climate Sensitivity in the Geological Past, Annual Review of Earth and Planetary Sciences, v. 44, pp. 277-293., https://doi.org/10.1146/annrev-earth-100815-024150.

Ruddiman, W.F., 2001. Earth's Climate: Past and Future, W.H. Freeman and Company, New York, NY, 465 pp.

Ruffell, A., Simms, M.J., and Wignall, P.B., 2015. The Carnian Humid Episode of the late Triassic: a review, Geological Magazine, v. 153, p. 271–284.

Sandberg, C.A., Morrow, J.R., Ziegler, W., 2000. Late Devonian events and mass extinc- tions. In: Catastrophic Events and Mass Extinctions: Impacts and Beyond. 1053. Lunar and Planetary Institute Contribution, Houston, Texas, pp. 188–189.

Sandberg, C.A., Morrow, J.R., Ziegler, W., 2002. Late Devonian sea-level changes, catastrophic events, and mass extinctions. In: Koeberl, C., MacLeod, K.G. (Eds.), Catastrophic Events and Mass Extinctions: Impacts and Beyond, Geological Society of America Special Paper 356, p. 473–487.

Sanei, H., Grasby, S., and Beauchamp, B., 2012. Latest Permian mercury anomalies. Geology, v. 40, p. 63-66.

Saunders, A.D., England, R.W., Reichow, M.K., and White, R.V., 2005. A mantle plume origin for the Siberian traps: uplift and extension in the West Siberian Basin, Russia, Lithos, 79:407-424.

Suarez, C.A., Edmonds, M., and Jones, A.P., 2019. Earth catastrosphes and their impact on the Carbon Cycle, Elements, v.15, p. 301-306.

Savin, S.M., Douglas, R.G., and Stehli, F.G., 1975. Tertiary marine paleotemperatures, Geological Sociaty of America Bulletin, v. 86, p. 1499-1510.

Savin, S.M., 1977. The history of the Earth's surface temperature during the past 100 Ma, Annual Reviews of Earth and Planetary Sciences, v. 5, p. 319-355.

Savitsky, A., and Golay, M.J.E., 1964. Smoothing and Differentiation of Data by Simplified Least Squares Procedures, Analytical Chemistry, v. 36, no. 8, pp. 1627-1639.

Scher, H.D., and Martin, E.E., 2006. Timing and Climatic Consequences of the opening of Drake Passage, Science, 312:428-430.

Schlanger, S.O., and Jenkyns, H.C., 1976. Cretaceous oceanic anoxic events: causes and consequences, Geol. Mijnbouw, 55:179-184.

Schmitz, M.D., and Davydov, V.I., 2012. Quantitative radiometric and biostratigraphic calibration of the Pennsylvanian–Early Permian (Cisuralian) time scale and pan-Euramerican chronostratigraphic correlation, Geological Society of America Bulletin, v. 124, no. 3/4, p. 549–577, doi: 10.1130/B30385.

Schobben, M., van de Schootbrugge, B., Wignall, P.B., 2019. Interpreting the carbon isotope record of mass extnctions, Elements, v. 15, p.331-337.

Scholle, P.A., 1995. Carbon and sulfur isotope stratigraphy of the Permian and Adjacent Intervals, in *The Permian of the Northern Hemisphere*, volume 1: Paleogeography, Paleoclimates, Stratigraphy, P.A. Scholle, T.M. Peryt, D.S Ulmer-Scholle (editors), Springer-Verlag, Berlin, p. 133-149.

Schouten, S., Hopmans, E.C., Schefuß, E., Sinninghe Damsté, J.S., 2002. Distributional variations in marine crenarchaeotal membrane lipids: a new tool for reconstructing ancient sea water temperatures? Earth Planet. Sci. Lett. 204, 265–274.

Schuchert, C.,1910. Palaeogeography of North America, Geological Society of America Bulletin, 20, 427-606.

Schuchert, C.,1955. (published posthumously), Atlas of paleogeographic Maps of North America, C. O. Dunbar & C. M. Levene (Eds.), John Wiley & Sons, New York, and Chap Mann & Hall, Ltd., London, 177 pp.

Schulte, P., Alegret, L., Arenillas, I., et al., 2010. The Chicxulub asteroid impact and mass extinction at the Cretaceous-Paleogene boundary, Science,327:1214-1218.

Scotese, C.R., Boucot, A.J., and McKerrow, W.S., 1999. Gondwanan paleogeography and paleoclimatology, in Gondwana 10: Event Stratigraphy, Journal of African Earth Sciences, v. 28, issue 1, pp. 99-114.

Scotese, C.R., 2009. Late Proterozoic plate tectonics and paleogeography: A tale of two supercontinents, Rodinia and Pannotia, in Global Neoproterozoic petroleum systems: The emerging potential in North Africa, J. Craig, J. Thurow, A. Whitman, and Y. Abutarruma (editors), Geological Society of London Special Publication 326, pp. 67-83.

Scotese, C.R., 2014. Atlas of Permo-Carboniferous Paleogeographic Maps (Mollweide Projection), Maps 53-64, volume 4, The Late Paleozoic, PALEOMAP Project Atlas for ArcGIS, PALEOMAP Project, Evanston, IL.

Scotese, C.R., 2016. A New Global Temperature Curve for the Phanerozoic, (abstract), Deological Society of America Annual Meeting, Sunday, September 25, 2016, Session no. 74, #287, Recent

Advances in Paleoclimatology and Paleoceanography (Posters). Exhibit Hall E/F (Colorado Convention Center), Geological Society of America Annual Meeting, Denver, CO.

Scotese, C.R., 2020. Global Warming during the next 300 years, A Global Warming Calculator (student exercise with Excel spreadsheet), PALEOMAP Project, Evanston, IL. 49 pp.

Sellwood, B.W., and Valdes, P.J., 2006. Mesozoic climates: General circulation models and the rock record, Sedimentary Geology 190:269–287, doi:10.1016/j.sedgeo.2006.05.013

Şengör, A.M.C., and Atayman, S., 2009. The Permian Extinction and the Tethys: An exercise in global geology, Geological Society of America Special Papers, v. 448, 96 pp.

Sepkoski, J.J., Jr., 1989. Periodicity in extinction and the problem of catastrophism in the history of life. Journal of the Geological Society of London, v. 146, p. 7-19.

Sepkoski Jr., J.J., 1996. Patterns of Phanerozoic extinction: a perspective from global data bases, in O.H. Walliser (editor), Global Events and Event Stratigraphy in the Phanerozoic, Springer-Verlag, Berlin, pp. 35–51.

Sheehan, P.M., 2001. The Late Ordovician Mass Extinction, Annual Reviews of Earth and Planetary Sciences, v. 29, p. 331–364.

Sheehan, P.M., and Coorough, P.J., 1990. Brachiopod zoogeography across the Ordovician – Silurian extinction event, in Palaeozoic Palaeogeography and Biogeography, W.S. McKerrow and C.R. Scotese (editors), Geological Society Memoir No. 12, p. 181-187.

Shi, G.R., 2001. Possible influence of Gondwanan glaciation on low-latitude carbonate sedimentation and trans-equatorial faunal migration: the Lower Permian of South China, Papers from IGCP Project No. 411 on the Geodynamic Processes of Gondwanaland-derived Terranes in Eastern Asia, Geosciences Journal, v. 5, no. 1, p. 57-63.

Simms, M.J., and Ruffell, A.H. 1989. Synchroneity of climatic change and extinctions in the Late Triassic, Geology, v. 17, p. 265–268.

Shell (2018), Shell Scenarios: SKY, Meeting the Goals of the Paris Agreement, https://www.shell.com/promos/business-customers-promos/download-latest-scenario-sky/_jcr_content.stream/1530643931055/eca19f7fc0d20adbe830d3b0b27bcc9ef72198f5/shell-scenario-sky.pd

Sloss, L.L., 1963. Sequences in the cratonic interior of North America, Geological Society of America Memoir 39, pp. 91-124.

Smit, J., 1999. The global stratigraphy of the Cretaceous Tertiary boundary impact ejecta, Annual Review of Earth and Planetary Sciences, 27:75-91, doi:10.1146/annrev.earth.27.1.75.

Song, H., Wignall, P.B., Chu, D., Tong, J., Sun, Y., He, W., and Tian, L., 2014. Anoxia/high temperature double whammy during the Permian-Triassic marine crisis and its aftermath, Scientific Reports, 4:4132, doi: 10.1038/srep04132

Song, H., Wignall, P.B., Song, H., Dai, X., and Chu, D., 2019. Seawater temperature and dissolved oxygen over the past 500 million years, Journal of Earth Sciences, v.30, no. 2, p. 236-243, doi:10.1007/s12583-028-1002-2.

Song, H., Huang, S., Jia, E., Dai, X., Wignall, P.B., Dunhill, A.M., 2020. Flat latitudinal diversity gradient caused by the Permian–Triassic mass extinction. Proceedings of the National Academy of Sciences, 117(30): 17578-17583.

Spicer, R.A., Ahlberg, A., Herman, A.B., Hofmann, C.C., Raikevich, M., Valdes, P.J., and Markwick, P.J., 2008. The Late Cretaceous continental interior of Siberia: A challenge for climate models, Earth and Planetary Science Letters, v. 267, p. 228-235, doi:10.1016/j.espl.2007.11.049.

Spray, J., 2020. Earth Impact Database (EID), http://passc.net/EarthImpactDatabase/New%20website_05-2018/Index.html

Stanley, G. D., 2003. The evolution of modern corals and their early history, Earth Science Reviews, v. 60, p. 195–225.

Stanley, S.M., 2016. Estimates of the magnitudes of major marine mass extinctions in earth history, Proceedings of the National Academy of Sciences, USA., v. 113, E6325–E6334.

Steffen. W., Rockstrom, J., Richardson, K., Lenton, T.M., Folke, C., Liverman, D., Summerhayes, C.P., Barnosk, A.D., Cornell, S.E., Crucifix, M., Donges, J.F., Fetzer, I., Lade, S.J., Scheffer, M., Winkelmann, R., and Schellnhuber, H.J., 2019. Trajectories of the Earth System in the Anthropocene, Proc. National Academy of Sciences, www.pnas.org/cgi/doi/10.1073/pnas.181014115, 8 p.

Stock, C.W., 2005. Devonian stromatoporoid originations, extinctions, and paleobiogeography: how they relate to the Frasnian-Famennian extinction, in Understanding Late Devonian and Permian-Triassic Biotic and Climatic Events; Towards an Integrated Approach, D.J. Over, J.R. Morrow, and P.B. Wignall (editors), Developments in Palaeontology & Stratigraphy, v. 20, p. 71 – 92, Elsevier, Amsterdam.

Sullivan,D.L., Brandon, A.D., Eldrett, J., Bergman, S.C., Wright, S., and Minisini, D., 2020. High resolution osmium data record three distinct pulses of magmatic activity during Cretaceous Oceanic Anoxic Event 2 (AOE-2), Geochimica et Cosmochimica Acta, v. 285, p. 257-273.

Summerhayes, C.P.,2015. Earth's Climate Evolution, Wiley-Blackwell, Chichester, UK, 394 pp.

Sun, Y., Joachimski, M.M., Wignall, P.B., Yan, C., Chen, Y., Jiang, H., Wang, L., and Lai, X., 2012. Lethally Hot Temperatures During the Early Triassic Greenhouse, Science, v. 338, p. 366-370.

Sun, Y.D., Wignall, P.B., Joachimski, M.M., Bond, D.P.G., Grasby, S.E., Lai, X.L., Wang, L.N., Zhang, Z.T., Sun, S., 2016. Climate warming, euxinia and carbon isotope perturbations during the Carnian (Triassic) Crisis in South China, Earth and Planetary Science Letters, v. 444, p. 88-100, doi:org/10.1016/j.epsl.2016.03.037

Swanson-Hysell, N.L., and Macdonald, F.A., 2017. Tropical weathering of the Taconic Orogeny as a driver for Ordovician cooling, Geology, v.45, p. 719-722., doi.org/10.1130/G38985.1

Tans, P. 2009. An accounting of the observed increase in oceanic and atmospheric CO_2 and an outlook for the future, Oceanography, v. 22,No.4, pp. 26 -35.

Taylor, B., 2006. The single largest oceanic plateau: Ontong Java–Manihiki–Hikurangi. Earth and Planetary Science Letters, v. 241, p. 372–380.

Taylor, E.L., Taylor, T.N.,and Cuneo, R., 2000. Permian and Triassic high latitude paleoclimates: evidence from fossil biotas, in Huber, B.T., MacLeod, K.G., and Wing, S.L., (editors), Warm Climates in Earth History, Cambridge University Press, p. 321-350.

Toggweiler, J.R., and Bjornsson, H., 2000. Drake Passage and palaeoclimate, Journal of Quaternary Science, 15:319-328.

Tollefsen, E., Balic-Zunic, T., Mörth, C. et al., 2020.

Torsvik, T.H., Svensen,H. H., Steinberger, B., Royer,D. L., Jerram, D.A., Jones, M.T, and Domeier, M., 2020. Connecting the Deep Earth and the Atmosphere, in Mantle Convection and Surface Expression S. Cottaar et al. (editors), AGU Monograph (in press).

Trotter, J., Williams, I.S., Barnes, C.R., Männik, P., and Simpson, A., 2016. New conodont $\delta^{18}O$ records of Silurian climate change: Implications for environmental and biological events, Palaeogeography, Palaeoclimatology, Palaeoecology, v. 443, p.34–48, doi.org/10.1016/j.palaeo.2015.11.011

Trotter, J.A., Williams, I.S., Barnes, C.R., Lécuyer , C., and Nicoll, R.S., 2008. Did Cooling Oceans Trigger Ordovician Biodiversification? Evidence from Conodont Thermometry, Science, v. 321, no. 5888, p. 550-554, DOI: 10.1126/science.1155814

Trotter, A.J., Williams, S.I., Nicora, A., Mazza, M., and Rigo, M., 2015, Long-term cycles of Triassic climate change: A new $d^{18}O$ record from conodont apatite, Earth and Planetary Science Letters, v. 415, p. 165–174.

Umbgrove, J.H.F., 1947. The Pulse of the Earth, Martinus Niijhoff, The Hague, Netherlands, 358 pp.

United Nations, 2019. United Nations Report on World Population, (https://www.un.org/development/desa/publications/world-population-prospects-2019-highlights.html).

Upchurch, G.R., Otto-Bliesner, B.L., and Scotese, C.R., 1999, Terrestrial vegetation and its effects on climate during the latest Cretaceous, in *Evolution of the Cretaceous Ocean-Climate System*, E. Barrera and C. Johnson, (editors), Geological Society of America, Special Paper 332, pp.407-426.

Upchurch, G.R., Kiehl, J., Shields, C., Scherer, J., and Scotese, C.R., 2015. Latitudinal temperature gradients and high latitude temperatures during the latest Cretaceous: Congruence of geologic data and climate models, Geology, v. 43, no. 9, p. 683-686.

Urey, H.C., Lowenstam, H.A., Epstein, S., McKinney, C.R., 1951. Measurements of paleotemperatures and temperatures of the Upper Cretaceous of England, Denmark, and the southeastern United States, Geological Society of America Bulletin, v. 62, p. 399-416.

Valdes, P.J., 1994, Atmospheric general circulation models of the Jurassic, in *Palaeoclimates and their modeling: with special reference to the Mesozoic Era*, J.R.L. Allen, B.J. Hoskins, B.W. Sellwood, R.A. Spicer, and P.J. Valdes (editors), Chapman and Hall, London, p. 109-118.

Valdes, P.J., Lunt, D.L., and Scotese, C.R., 2018. Modelling the Climate History of the Phanerozoic, (abstract), American Geophysical Union, Monday, December 10, 2018, Convention Center, Hall A-C (Poster Hall), Fall Meeting 2018, #PP11F-1031, Washington, D.C.

Valdes, P.J., Scotese, C.R., and Lunt, D.J., 2020. Deep ocean temperatures through time, Climates of the Past (in press).

Valdes, P.J. and Sellwood, B.W., 1992, A palaeoclimate model for the Kimmeridgian, Palaeogeography, Palaeoclimatology, and Palaeoecology, 95:47-72.

Vandenberghe, N., Hilgen, F.J., Speijer, R.P., 2012. The Paleogene Period, Chapter 28, in The Geologic Time Scale 2012, volume 2, F.M. Gradstein, J.G. Ogg, M.D. Schmitiz, and G.M. Ogg, (editors), p. 855-922, Elsevier, Amsterdam.

van der Meer, D.G., Zeebe, R.E., van Hinsbergen, J.J., Sluijs, A., Spakman, W., and Torsvik, T., 2014. Plate tectonic controls on atmospheric CO_2 levels since the Triassic, Proceedings of the National Academy of Sciences, v. 111, no. 12, p. 4380-4385, doi/10.1073/pnas.1315657111

van der Meer, D.G., van den Berg van Saparoea, A.P.H., van Hinsbergen, D.J.J., van de Weg, R.M.B., Godderis, Y., Le Hir, G., and Donnadieu, Y., 2017. Reconstructing first-order changes in sea level during the Phanerozoic and Neoproterozoic using strontium isotopes, Gondwana Research, v. 44, 22-34.

van de Schootbrugge, B., Tremolada, F., Rosenthal, Y., Bailey, T.R., Feist-Burkhardt, S., Brinkhuis, H., Pross, J., Kent, D.V., and Falkowski,P.G., 2007. End-Triassic calcification crisis and blooms of organic-walled ‘disaster species’, Palaeogeography, Palaeoclimatology, Palaeoecology 244:126–141, doi:10.1016/j.palaeo.2006.06.026

van de Schootbrugge, B., Quan, T.M., Lindström, S., Püttmann, W., Heunisch, C., Pross, J., Fiebig, J., Petschick, R., Röhling, H.-G., Richoz, S., Rosenthal,Y., Falkowski, P.G., 2009. Floral changes across the Triassic/Jurassic boundary linked to flood basalt volcanism, Nature Geoscience, v.2, p. 589-594.

van de Schootbrugge, B., Bachan, A., Suan, G., Richoz, S., and Payne, J.L., 2013. Microbes, mud and methane: cause and consequence of recurrent Early Jurassic anoxia following the end-Triassic mass extinction, Palaeontology, v. 56, p. 685–709.

van Gelderin, R., Joachimski, M.M., Day, J., Jansen, U., Alvarez, F., Yolkin, E.A., and Ma, X.-P., 2006. Carbon, oxygen and strontium isotope records of Devonian brachiopod shell calcite, Palaeogeography, Palaeoclimatology, Palaeoecology, v. 240, p. 47–67. doi:10.1016/j.palaeo.2006.03.045

Vaughan, A.P.M., 2007. Climate and geology – A Phanerozoic perspective, in Deep-Time Perspectives on Climate Change: Marrying the Signal from Computer Models and Biological Proxies, Williams, M., Haywood, A.M., Gregory, F.J., and Schmidt, D.N., (editors), p. 5-59, Micropalaeontological Society Special Publication, Geological Society of London, London.

Veevers, J.J., Conaghan,P.J., and Shaw, S.E., 1994. Turning point in Pangean environmental history at the Permian/Triassic (P/Tr) boundary, in Pangea: Paleoclimate, Tectonics, and Sedimentation during the Accretion, Zenith, and Breakup of a Supercontinent, George D. Klein (ed.), Geol. Soc. America Special Paper, 288: 187-196.

Veizer, J., Fritz, P., and Jones, B., 1986. Geochemistry of brachiopods – oxygen and crbon isotopic records of Paleozoic oceans, Geochemica et Cosmochemica Acta, v. 40, pp. 1387-1395.

Veizer, J., Ala, D., Azmy, K., Bruckschen, P., Buhl, D., Bruhn, F., Carden, G.A.F.,Diener, A., Ebneth, S., Godderis, Y., Jasper, T., Korte, C., Pawellek, F., Podlaha, O.G., and Strauss, H., 1999. $^{87}Sr/^{86}Sr$, $\delta^{13}C$ and $\delta^{18}O$ evolution of Phanerozoic seawater, Chemical Geology, v. 161, no. 1-3, pp. 59-88.

Veizer, J.T., Godderis, Y., Francois, L.M., 2000. Evidence for decoupling of atmospheric CO_2 and global climate during the Phanerozoic Eon, Nature, v. 408, no. 6813, p. 698-701, doi: 10.1038/35047044. 2000

Veizer, J., and Hoefs, J., 1976, The nature of O^{18}/O^{16} and C^{13}/C^{12} secular trends in sedimentary carbonate rocks, Geochimica et Cosmochimica Acta, v. 40, no. 11, p. 1387-1395.

Veizer. J.T., and Prokoph. A., 2015. Temperatures and Oxygen isotopic composition of Phanerozoic oceans, Earth-Science Reviews, v. 146: p. 92-104, doi: 10.1016/j.earscirev.2015.03.008.

Vellekoop, J., Sluijs, A., Smit., J., Schouten, S., Weijers, J.W.H., Sinninghe Damsté, and Brinkhuis, H., 2014. Rapid short-term cooling following the Chicxulub impact at the Cretaceous-Paleogene boundary, Proceedings of the National Academy of Science, v. 111, n. 21, pp. 7537-7541.

Vellekoop, J., Esmeraysenlet, S., Miller, K.G., Browning, J.V., Sluijs, A., De Schootbrugge, B.V., Damste, J.S.S., Brinkhuis, H., 2016. Evidence for Cretaceous-Paleogene boundary bolide “impact winter” conditions from New Jersey, USA. Geology, 44(8): 619-622.

Verard, C. and Veizer, J., 2019. On plate tectonics and ocean temperatures, Geology, v. 47, p. 881-885.

Vickers, M.L., Bajnai, D., Price, G.D., Linckens, J., and Fiebig, J., 2019. Southern high-latitude warmth during the Jurassic–Cretaceous: New evidence from clumped isotope thermometry, Geology, doi.org/10.1130/G46263.1

Walker, J.C.G., Hays, P.B., and Kasting, J.F., 1981. A negative feedback mechanism for the long-term stabilization of Earth’s surface temperature. Journal of Geophysical Research, 86, 9776–9782.

Wallace, D.R., 2004. Beasts of Eden, Walking Whales, Dawn Horses, and Other Enigmas of Mammal Evolution, University of California Press, Berkeley, 340 pp.

Wanless, H.R. and Shepherd, F.P., 1936. Sea level and climatic changes related to late Paleozoic cycles. Geological Society of America Bulletin, v. 47, p. 1177-1206.

Wanless, H.R. and Weller, J.M., 1932. Correlation and extent of Pennsylvanian cyclothems. Geological Society of America Bulletin, v. 43, p. 1003-1016.

Waterhouse, J.B., and Shi, G.R., 2013. Climatic implications from the sequential changes in diversity and biogeographic affinities for brachiopods and bivalves in the Permian of eastern Australia and New Zealand, Gondwana Research, v. 24, p. 139–147, doi:10.1016/j.gr.2012.06.008

Webby, B.D., Paris, F., Droser, M.L., and Percival, I.G., 2004. The Great Ordovician Biodiversification Event, Columbia University Press, New York, 884 pp.

Weirzbowski, H., and Joachimski, M., Reconstruction of late Bajocian–Bathonian marine palaeoenvironments using carbon and oxygen isotope ratios of calcareous fossils from the Polish Jura Chain (central Poland), Palaeogeography, Palaeoclimatology, Palaeoecology, v. 254, p. 523–540, doi:10.1016/j.palaeo.2007.07.010

Wenzel, B., LeCuyer, C., and Joachimski, M.M., 2000. Comparing oxygen isotope records of Silurian calcite and phosphate - $\partial^{18}O$ compositions of brachiopods and conodonts, Geochimica et Cosmochimica Acta, v. 64, no. 11, p. 1859–1872.

Wenzel, B., and Joachimski, M.M., 1996. Carbon and oxygen isotopic composition of Silurian brachiopods (Gotland/Sweden)" palaeoceanographic implications, Palaeogeography, Palaeoclimatology, Palaeoecology, v. 122, p. 143-166.

Westerhold. T., Marwan, N., Drury, A.J., Liebrand, D., Agnini., C., Anagnostou, E., Barnet, J.S.K., Bohaty, S.M., De Vleeschouwer, D., Florindo, F., Frederichs, T., Hodell, D.A., Holbourn, A.E., Kroon, D., Lauretano, V., Littler, K., Lourens, L.L., Lyle, M., Pälike, H., Röhl, U., Tian, J., Wilkens, R.H., Wilson, P.A., Zachos, J.C., 2020. An astronomically dated record of Earth's climate and its predictability over the last 66 million years, Science 369: 1383-1387.

Whiteside, J.H., and Grice, K., 2016. Biomarker Records Associated with Mass Extinction Events, Annual Review of Earth Planetary Sciences, v. 44, p. 581–612, doi: 10.1146/annurev-earth-060115-012501

Whiteside, J.H., Olsen, P.E., Eglinton, T., Brookfield, M.E., and Sambrotto, R.N., 2010. Compound-specific carbon isotopes from Earth's largest flood basalt eruptions directly linked to the end-Triassic mass extinction, Proceedings of the National Academy of Sciences, v. 107, p. 6721–6725.

Wierzbowski, H., and Joachimsky, M., 2007. Reconstruction of the late Bajocian-Bathonian marine paleoenvironments using carbon and oxygen isotope ratios of calcareous fossils from the Polish Jura Chain (central Poland), Palaeogeography, Palaeclimatology, Palaeoecology, v. 254, p. 523-540, doi: 10.1016/j.palaeo.2007.07.010.

Wignall, P.B., and Hallam, A., 1992. Anoxia as a cause of the Permian/Triassic mass extinction: facies evidence from northern Italy and the western United States. Palaeogeography, Palaeoclimatology, Palaeoecology, v. 93, p. 21-446.

Wignall, P.B., 2001. Large igneous provinces and mass extinctions. Earth-Science Reviews, v. 53, p.1-33.

Wignall, P.B., 2015. The Worst of Times, How life on Earth Survived Eighty Million Years of Extinctions, Princeton University Press, Princeton, NJ, 199 p.

Wilf, P., Johnson. K., and Huber, B.T., 2003. Correlated terrestrial and marine evidence for global climate changes before mass extinction at the Cretaceous – Paleogene boundary, Proceedings of the National Academy of Sciences, v. 100, no. 2, p. 599-604, doi /10.1073/pnas.0234701100

Willis, K.J., and McElwain, J.C., 2014. The Evolution of Plants, Oxford University Press, Oxford, UK, 378 pp.

Wing, S.L., Gingerich, P.D., Schmitz, B., and Thomas, E., 2003. Causes and Consequences of Globally Warm Climates in the Early Paleogene, Geol. Soc. America, Special Paper 369, Boulder, Colorado, 614 pp.

Wing, S., and Huber, B., 2019. Earth's Temperature History Workshop, Smithsonian National Museum of Natural History, March 30-31, 2018, Washington, D.C.

Wolfe, J. A. and G. R. Upchurch, 1987. North American nonmarine climates and vegetation during the Late Cretaceous, Palaeogeography, Palaeoclimatology, Palaeoecology 61: 33-77.

Wolfe, J.A., 1971. Tertiary climatic fluctuations and methods of analysis of Tertiary floras, Palaeogeog., Palaeoclim., Palaeoecol., 9:27-57.

Wolfe, J.A., 1978. A paleobotanical interpretation of Tertiary climates in the northern hemisphere, American Scientist, 66:694-703.

Wolfe, J.A., 1992. Climatic, floristic, and vegetational changes near the Eocene/Oligocene boundary in North America, in Eocene-Oligocene Climatic and Biotic Evolution, D.R. Prothero and W.A. Berggren (eds.), Princeton University Press, Princeton, 421-436. pp.

Wolfe, J.A., 1994. Tertiary climatic changes at middle latitudes of western North America, Palaeogeog., Palaeoclim., Palaeoecol., 108:195-205.

Worsley, T.R. & Kidder D.L., 1991. First-order coupling of paleogeography and CO_2, with global surface temperature and its latitudinal contrast. Geology, 19, 1161-1164.

Yancey, T.E., and Guillemette, R.N., 2008. Carbonate accretionary lapilli in distal deposits of the Chicxulub impact event: Geol. Soc. America Bulletin, 120:1105-1118.

Young, S.A., Saltzman, M.R., Foland, K.A., Linder, J.S., and Kump, L.R., 2009. A major drop in seawater $^{87}Sr/^{86}Sr$ during the Middle Ordovician (Darriwilian): Links to volcanism and climate?, Geology v. 9, no. 10, p. 951–954, doi: 10.1130/G30152A.1

Zachos, J., Pagani, M., Sloan, L., Thomas, E., and Billups, K. 2001. Trends, rhythms and abberations in global climate 65 Ma to present, Science, v. 292, p. 686-693.

Zachos, J.C., Dickens, G.R., and Zeebe, R.E., 2008. An early Cenozoic perspective on greenhouse warming and carbon-cycle dynamics, Nature, v. 45117, p. 279-283.

Zeebe RE, Zachos JC, Dickens GR. 2009. Carbon dioxide forcing alone insufficient to explain Palaeocene- Eocene Thermal Maximum warming. *Nat. Geosci.* 2:576–80

Zeng, J., Cao, C.-Q., Davydov, V.I., and Shen, S.-Z., 2012. Carbon isotope chemostratigraphy and implications of palaeoclimatic changes during the Cisuralian (Early Permian) in the southern Urals, Russia, Gondwana Research, v. 21, p. 601–610, doi:10.1016/j.gr.2011.06.002

Zhang, L., Chen, D., Huang, T., Yu, H., Zhou, X., Wang, J., 2020. An abrupt oceanic change and frequent climate fluctuations across the Frasnian–Famennian transition of Late Devonian: constraints from conodont Sr isotope. Geol. J. https://doi.org/10. 1002/gj.3657. (in press).

Zhang, R.M.J., Follows, Grotzinger, J., and Marshall, J., 2001. Could the Late Permian deep ocean have been anoxic? Palaeocenography, v. 16, p. 317-329.

Zhu, M.-Y., Babcock, L.E., and Peng, S.-C., 2006. Advances in Cambrian stratigraphy and paleontology: Integrating correlation techniques, paleobiology, taphonomy and paleoenvironmental reconstruction, Palaeoworld, v.15, p. 217–222, doi:10.1016/j.palwor.2006.10.016

Ziegler, A.M., Eshel, G., Rees, P.Mc., Rothfus, T.A., Rowley, D.B., and Sunderlin, D., 2003. Tracing the tropics across land and sea: Permian to present, Lethaia, v. 36, p. 227-254.

Ziegler, A.M., Hulver, M.L., Rowley, D.B., 1997, Permian World Topography and Climate, in *Late Glacial and Postglacial Environmental Changes: Quaternary, Carboniferous-Permian, and Proterozoic*, I. Peter Martini (editor), Oxford University Press, Oxford, p. 111-146.

Ziegler, A.M., Parrish, J.M., Jiping, Y., Gyllenhaal, E.D., Rowley, D.B., Parrish, J.T., Sahngyou, N., Behher, A., and Hulver, M.L., 1994. Early Mesozoic phytogeography and climate, in Allen, J., Hoskins, B.J., Sellwood, B.W., Spicer, R.S., Valdes, P.J. (editors), Paleoclimates and Their Modelling: with Sprecial Reference to the Mesozoic Era, Chapman and Hall, London, pp. 89-97.

Ziegler, A.M., Rowley, D.B., Lottes, A.L., Sahagian, D.L., Hulver, and Gierlowski, T.C., 1985. Paleogeographic Interpretation: With an Example from the Mid-Cretaceous, Annual Reviews of Earth and Planetary Sciences, v. 13, p. 385-425

Figure Captions

Figure 1. Estimates of Phanerozoic Global Average Temperature (GAT). Sources: Wing and Huber (2019), Valdes et al. (2018), Mills et al. (2019), and This study.

Figure 2. “Double Hump” pattern of Phanerozoic Climate (Fischer, 1981; 1982), I = icehouse, G = greenhouse.

Figure 3. Modern Köppen belts and the average temperature of each belt.

Figure 4. Early Permian (280 Ma) lithologic indicators of climate and continental paleo-Köppen Belts (Boucot et al., 2013).

Figure 5. Mid-Cretaceous (100 Ma) lithologic indicators of climate and continental paleo-Köppen Belts (Boucot et al., 2013).

Figure 6. Long-Term Phanerozoic temperature trend calculated by estimating the changing area of paleo-Köppen belts (see Supplementary Materials for data and details of calculations).

Figure 7. Raw and mean values of oxygen isotopes from phosphatic and carbonate fossils for reconstructing sea surface temperatures over the past 500 million years (modified after Song et al., 2019). The scale of $\delta^{18}O_{Phos}$ is used for phosphatic fossils, i.e., phosphatic brachiopod, conodont, and fish. The scale of $\delta^{18}O_{Carb}$ is used for carbonate fossils, i.e., belemnite, bivalve, brachiopod, planktonic foraminifer, and others. Magenta curve represents the mean values of sea surface temperatures per million years. Shaded area represents 95% confidence intervals.

Figure 8. Phanerozoic Isotopic Temperature (Song et al., 2019). A. = Each dot represents the average of all temperatures that fall within a given one million year interval. The best-fit curve was obtained using the Savitsky-Golay smoothing technique (window 11-15, degree 4). B. Change in Tropical Temperature (ΔT°_{trop}). The black dots along the x-axis are the times when no data are available.

Figure 9. Modifications to the Phanerozoic Isotopic Temperature Curve. The dashed line is the isotopic temperature curve (see Figure 8). The colored lines represent modifications and adjustments made to that curve based on geological and paleontological constraints.

Figure 10. Comparison of isotopic temperature data from the late Pennsylvanian of South China (open dots) and the USA (black dots) (Song et al., 2019).

Figure 11. Comparison of Cenozoic deep ocean isotopic temperatures and tropical temperatures A. gray line = low resolution Tropical Temperatures (this study), and the black line = high resolution Δ Tropical Temperatures for the Cenozoic. B. isotopic temperatures from deep ocean, benthic foraminifera (Zachos et al., 2001, 2008; Westerhold et al., 2020).

Figure 12. Phanerozoic Global Average Temperature (GAT), blackline = Global Average Temperature, dashed line = Long-term temperature change derived from changes in the pole-to-Equator

temperature gradient calculated from the changing area of Köppen Climatic Belts (see Figure 6). When the Global Average Temperature is below 18˚C large polar icecaps can form. When the Global Average Temperature is above 18˚C large polar icecaps are unlikely to form.

Figure 13. Timing and magnitude of Large Igneous Provinces (rectangles) eruptions and bolide impacts (circles). The size of the rectangles indicates the relative eruptive intensity (10^6 km^2/my) (left-hand scale). See Table 1 and 2 for abbreviations. Sources: Ernst (2014), Spray (2020).

Figure 14. Comparison of the timing of LIPS (black squares, Table 1), large bolide impacts (circles with dots, Table 2), and putative large impact events (light gray circles with x's) with the changes in Tropical Temperature (ΔT°_{trop}). The size of the lettering is roughly proportional to the size of the LIP or bolide imapact. See Table 1 and 2 for abbreviations. Sources: Ernst (2014), Spray (2020).

Figure 15. Phanerozoic Ice Ages. gray = global area of snow and ice cover (10^6 km^2), dotted line = snow and ice predicted by Global Average Temperatures (GAT < 18˚C, Figure 12), numbers = number of glacial deposits (tillites, dropstones, and glendonites). Note inverted temperature scale (left side).

Figure 16. Tropical, Global Average, Deep Ocean, and Polar Temperatures. (a) red line = tropical temperature (15 N - 15 S), (b) black line = global average temperature (GAT), (c) blue line = deep ocean temperatures (after Valdes et al., 2020) (d) light blue line = polar temperature (> 67 N&S). The chronological resolution of this diagram, ~ 5 million years, matches the chronological resolution of the paleo-Köppen maps (see Supplementary Materials).

Figure 17. The polar temperature and the Pole to Equator temperature gradient for different Global Average Temperatures (GAT). Polar Temperature = average temperature above 67˚ latitude (N&S), Deep Sea = the average temperature at the bottom of the oceans (after Valdes et al., 2020). Pole to Equator Gradient = the average change in temperature for every one degree of latitude measured between 30˚ and 60˚ latitude. The Pole to Equator temperature gradient is shallow near the Equator and steepens rapidly near the Pole. The plus signs are the combined average temperatures for the present-day northern and southern hemispheres. Frequency = the percent of the time during the Phanerozoic characterized by this Pole-to-Equator temperature gradient. All of these calculations are based on an average tropical temperature of 26˚C (15 N – 15 S).

Figure 18. Comparison of Phanerozoic global average temperatures (black line) with strontium flux ratio relative to the present-day flux (dashed line). Red line highlights when the trends are coincident.

Figure 19. A Paleozoic Paleotemperature Timescale. white = warm time intervals, black = cool time intervals. Solid black line = Global Average Temperatures (GAT), < 18˚C = large permanent, icecaps, > 18˚C = no large, permanent icecaps. Light gray jagged lines = a schematic representation of >50 glacial/interglacial cycles during the Permo-Carboniferous. Timescale = International Chronostratigraphic Chart v2020/01. Refer to Table 3 for more information about each chronotemp and abbreviations.

Figure 20. A Mesozoic Paleotemperature Timescale. white = warm time intervals, black = cool time intervals. Solid black line = Global Average Temperatures (GAT), < 18˚C = large, permanent icecaps, > 18˚C = no large, permanent icecaps. Timescale = International Chronostratigraphic Chart v2020/01.Refer to Table 3 for more information about each chronotemp and abbreviations.

Figure 21. A Cenozoic Paleotemperature Timescale. white = warm time intervals, black = cool time intervals; Light gray jagged lines = a schematic representation of >50 glacial/interglacial cycles during the Plio-Pleistocene. Solid black line = Global Average Temperatures (GAT),), < 18˚C = large, permanent icecaps, > 18˚C = no large, permanent icecaps. Timescale = International Chronostratigraphic Chart v2020/01. Refer to Table 3 for more information about each chronotemp and abbreviations.

Figure 22. IPCC Estimates of Global Warming compared to the Results Predicted by the Carbon Budget Model (this study). The blue curve represents the projected increase in atmospheric CO_2 based on the continued burning of fossil fuels at the "modern rate" (1970 – 2020). The black curves are the CO_2 levels used in the IPCC models RCP 2.5, RCP 4.5, RCP 6.0, and RCP 8.5. The red curve is the projected CO_2 levels obtained in our model (between 750 ppm and 800 ppm at 2200 CE). Estimates from RCP 2.5 and RCP 4.5 are too low. The estimate of CO_2 used in RCP 8.5 is much too high. Estimates of CO_2 used in RCP 6.0 are about right.

Figure 23. Projection of Future Global Warming onto Phanerozoic Temperature Time Scale. The likely amount of Post-Anthropogenic Warming (PAW) (red line). The boxes indicate times in the geological past when global temperatures were within the range of predicted PAW. When the Global Average Temperature is below 18˚C large polar icecaps can form. When the Global Average Temperature is above 18˚C large polar icecaps are unlikely to form.

Figure 24. Paleogeographic maps for the early Oligocene (30 Ma) and early Miocene (15 Ma). These past time periods are a good climatic match for world after Anthropogenic Warming.